# The Effect of the Agulhas Current on Synthetic Aperture Radar Derived Wind Fields




**Daniel E. Schilperoort**

Department of Oceanography

University of Cape Town

**Supervisors:**

Dr Marjolaine Krug

Assoc. Prof. Mathieu Rouault

Dr Morten Hansen

This dissertation is submitted for the degree of

*Master of Science*

2015

# Declaration

I, Daniel Eric Schilperoort, hereby declare that the following thesis is of my own work and I have not used the ideas, concepts, writing and data of others and claimed it as my own. I understand that all ideas and text, copied verbatim, must be properly acknowledged and I have used the Harvard Method of referencing. To the best of my knowledge, all previous research, methods, techniques, data and work which I have utilised in this document have been correctly referenced.

Daniel E. Schilperoort
2015

# Acknowledgements

Behind this thesis is not only my own hard work, but the hard work, dedication and support of others without whom I would not have been able to do what I have done.

First and foremost I would like to sincerely thank my supervisors: Marjolaine, Mathieu and Morten for giving me the guidance, motivation, knowledge, data and technical support in order to complete this. To Marjolaine especially, without all of your effort this thesis would be nothing. Thank you for all of your knowledge both technically and scientifically. And thank you for your patience with me when I was struggling to find my feet in the beginning or any time that I faltered. ADHD related or otherwise!

Thank you also to Johnny Johannessen and Alexis Mouche for their input, knowledge and ideas in the early stages of my project.

To all my friends fellow scientists in the oceanography department. I thank you all for the company and empathy. It's always great to know that you are not the only one going through strife. Obstacles are best overcome with company. Thank you for the, far too many, coffee breaks and scintillating conversations about many important world and philosophical issues (Let's be honest it was mostly about the different ways we were going to get people to bring cake, coffee, beer or pizza more often). A special thanks must go to Neil, my Norway roomie and fellow night/rain hiker. Thanks for making the morning and afternoon walks in rain and dark, not so terrible. Also for being my swimming buddy, and for being forever complementary of the food I put up even when I wasn't so sure what it was!

To my friends outside of the world of science, thank you for the support, motivation and thousands of, "So are you done yet?/ Why the heck are you still writing?!" questions. Nothing helps with motivation more like wanting to stop your friends moaning at you. Thank you for being (mostly) understanding when I missed important events and dropped off the radar every now and then. Thanks to Lorne for being a champ and proof reading when no one else wanted to!

To my parents. Mom, Dad. Thank you So SO SO much for you support during the tough times I've had over the last two years. Mom, for being there to just sit with me when I was in one of my many dark spaces. I think 90% of my worrying was done by you more than me. I made it though. Dad, thank you for providing guidance with the tough choices

and situations I found myself in every now and then. Your mentality of, “Do the best you can with the time you have.” has helped me to no end and will stay with me always.

Lastly, to my beautiful Tiny. I know I am by far not the easiest character to deal with, nor do my choices and methods often make sense to you. But thank you for accepting and loving me for who I am. Idiosyncrasies, downright craziness and all! Your had work, determination and dedication to whatever you do is amazing and has always been something for me to aspire to. Thank you for the moral support in the final stages when I was starting to doubt my abilities. Love you too the moon and back!

For Funding, primarily, I would like to thank the Nansen-Tutu Centre of Marine Environmental Research for supporting my masters project financially for the duration of the two years as well as for providing travel funding for my attendance at the Ocean Remote Sensing Synergy summer school at Telecom Bretagne, Brest, France in 2014. And thank you for giving me a space in the cool office. Secondly I would like to thank UCT for providing additional support in the form of a merit based award for achievement in my previous academic studies. I would like to thank the Nansen Tutu Centre and Norway South Africa bilateral SANCOOP-SCAMPI project for providing opportunity for me to travel to Bergen, Norway and work at NERSC for 6 weeks. I gained invaluable knowledge during this time. Special thanks go to NERSC for providing accommodation. Lastly, I would like to the SCAMPI-NRF bilateral agreement for providing funding for my attendance at the South African Symposium for Atmospheric Science.

# Contents

# List of Figures

# Acronyms

AMMA: African Monsoon Multidisciplinary Analyses

AMOC: Atlantic Meridional Overturning Circulation

AMSR: Advanced Microwave Scanning Radiometer

ASAR: Advanced Synthetic Aperture Radar

AVHRR: Advanced Very High Resolution Radiometer

CFSR: Climate Forecast System Reanalysis

CFSv2: Climate Forecast System Version 2

CMOD5.n: C-Band Model 5 for Neutral Winds

CWD: Collocated Wind Differences

ECMWF: European Centre for Medium-Range Weather Forecasts

ERA40: ECMWF reanalysis 40

ESA: European Space Agency

EUMETSAT: European Organisation for the Exploitation of Meteorological Satellites

GMF: Geophysical Model Function

IOHP: Indian Ocean High Pressure

MABL: Marine Atmospheric Boundary Layer

MODIS: Moderate Resolution Imaging Spectroradiometer

NERSC: Nansen Environmental and Remote Sensing Centre

NCEP: National Centres for Environmental Prediction

NRCS: Normalised Radar Cross Section

NWP: Numerical Weather Prediction model

OSI SAF: The Ocean and Sea Ice Satellite Application Facility

OSTIA: Operational Sea Surface Temperature and Sea Ice Analysis

RAR: Real Aperture Radar

SAR: Synthetic Aperture Radar

SCARC: The Subtropical Convergence Agulhas Retroflection Cruise

SCAT: Scatterometer

SEVIRI: Spinning Enhanced Visible and Infrared Imager

SST: Sea Surface Temperature

SWIO: South West Indian Ocean

TAO: Tropical Atmosphere-Ocean

WSM: Wide Swath Mode

# Abstract

In this study, 5 years (987 swaths) of high resolution wind speeds, derived from Advanced Synthetic Aperture Radar data collected over the Agulhas Current region, are studied to investigate the effect of warm, high intensity currents on the ocean's surface roughness and resulting derived wind fields. The wind data are derived using the CMOD5.n GMF with CFS reanalysis wind data as direction input. The CFS direction data are validated using ASCAT derived wind observations

Globcurrent ocean current velocity data is used to investigate the difference between the satellite derived wind speeds compared to surface velocities of the current and the true wind speed. The, so called, current-relative effect is investigated for different wind direction regimes, namely: upcurrent, downcurrent, crosscurrent west and crosscurrent east. Our analyses are conducted for 6 locations of interest, evenly spaced along the Northern Agulhas Current. MODIS, SEVIRI and OSTIA SST data are used as proxy for locating the core of the Agulhas and it's temperature fronts, as well as to investigate wind speed modifications as a result of ocean-atmosphere energy transfer.

It is found that higher resolution SAR derived winds have a greater ability to represent higher intensity and smaller scale wind features in comparison to winds derived from Scatterometers. A combination of the current relative effect and SST-atmospheric heating for upcurrent wind directions results in a sharp increase in mean wind speeds over the inshore boundary of the current of between $5m/s$ and $7m/s$ $(50-60\%)$. Individual events can reach as high as $15m/s$ $(100\%)$ over $10's$ of kilometres. For downcurrent winds, the expected current relative effect is overridden by increased wind speeds of up to $5m/s$ $(40\%)$ across the entire current due to the influence of SSTs. The mean effect of SSTs on wind speeds has a stronger effect than the current relative effect on wind speed changes over the current. The wind speed differences are best represented under moderate wind speeds, between $5-15m/s$.

This investigation will contribute to future satellite wind speed derivations to identifying new wind speed and surface roughness altering effects. It will also serve to increase understanding of high resolution wind features and sharp changes over ocean features.

# Chapter 1

# Introduction

The use of satellite remote sensing of wind speed and direction over large spatial scales has revolutionised the way weather patterns and wind features can be viewed, surveyed and investigated. Up until the 1970's, the study of the wind patterns and collection of wind data was primarily a qualitative exercise, undertaken by individuals at a point source. The amount of effort and resources needed to collect sufficient data for an accurate analysis of mean spatial wind field patterns was too great a task to warrant effort. Thus the ability to understand and study wind and weather patterns and events relied on the subjective knowledge of individuals and their experience rather than in quantitative proof (Taub, 2004). However, since the launch of the first vector scatterometer (SCAT) on board the Skylab satellite in 1973, satellite remote sensing data collection technology have evolved to the point where accurate and precise data can be collected autonomously in large volumes and over high spatial resolutions. This has enabled scientists to more effectively study and understand complex weather patterns and events over a range of spatial scales. Where satellites have excelled most is in collecting data over the ocean which historically has been an even greater undertaking than on land due to the sheer vastness and inaccessibility of what is effectively the largest surface area of the Earth. Satellites such as Synthetic Aperture Radar (SAR) and scatterometers are able to accurately represent wind and weather patterns of the like which have never been investigated before. This unique perspective has allowed for an expansion in both the scientific and industrial uses for wind data. Scientists are able to utilise SAR and SCAT to investigate ocean-atmosphere interactions and teleconnections as well as to understand specific processes such as tropical cyclones, polar lows, katabatic or coastal winds, atmospheric and oceanic gravity waves and myriad other processes (Dagestad et al., 2013). Industrial uses of satellite derived wind data are just as valuable for: wind farm planning and placement or in construction, planning and optimisation in design of structures, as well as in disaster management such as the identification of oil slicks and surfactants and track-

ing their spread and development (Dagestad et al., 2013). Finally a combined use for both scientific and industrial benefit is the assimilation of the satellite derived wind data into numerical weather prediction (NWP) models, in conjunction with other in situ data, in order to improve the model output, better interpolate areas of low data acquisition and increase predictive capabilities (Dagestad et al., 2013). Numerical models are limited in the accuracy of the data that they can produce; as they are based on the Navier-Stoke equations which describe the natural fluid dynamic processes taking place. The equations cannot completely describe the complexity of the ocean and atmosphere and all its interactions because of the massive complexities involved, thus they have to be simplified using approximations. These are themselves based on assumptions that are fundamentally flawed due to the lack of complete knowledge about the properties and physical processes involved in atmospheric circulation. These errors and flaws can be mitigated by using in situ and satellite data to reduce error in the models through statistical comparison and correction, but there is still much to be improved. Thus, although in situ data collection and numerical modeling both fill vital gaps in the furthering of knowledge and understanding of the wind and other environmental forces and processes, both have weakness and gaps which can partially be filled with satellite data.

One issue with investigating the effect of a western boundary current such as the Agulhas on satellite derived wind speeds, however, is the fact that there are other significant ocean-atmosphere interactions which result in similar effects on the wind speed signature over the current to the current relative effect. These roughness modifying factors are not necessarily a relative effect but can include include physical forcings such as: an increase in the wind speed due to changes in atmospheric properties, or the general turbulence and shear within a fast flowing current which results in increased surface roughness at the current surface. One such known influence on physical wind speed is the increase in velocities over sharp sea surface temperature gradients as a result of the changes in the overlying atmospheric stability. This is due to heat transfers between the ocean and atmosphere causing an unstable marine atmospheric boundary layer. This effect has been previously shown to occur over the Agulhas through in situ data collection exercises (Jury and Courtney, 1991; Rouault et al., 2000) as well as elsewhere in the world with similar remote sensing techniques (Park et al., 2006; Xie et al., 2010). The influence of turbulent flow on the surface roughness over a current has also been shown (**?**). Thus, the challenge lies in separating the different effects on the derived wind speeds from each other in order to determine which effects result form a genuine increase in wind speed and which effects merely cause an apparent increase in wind speed due to relative motion.

To date, the majority of satellite derived winds are collected using scatterometers even

though the ability of SARs to observe surface winds has been amply demonstrated (Gerling, 1986). SARs however are increasingly being used in synergy with atmospheric numerical model outputs to provide surface wind observations over the ocean at much higher resolutions (500m and 1km compared to typical resolutions of 25km) (Dagestad et al., 2013). But there are still major errors the SARs and remote sensing in general have to contend with. For SAR and Scatterometers alike, a major limitation is the fact that the wind speeds are derived using an empirical relation algorithm in the form of a Geophysical Model Function (GMF). The physical limitations which inhibit SARs from observing exceptionally high ($> 35m/s$) and low ($< 2m/s$) wind speeds are also an issue. In high wind speeds, the surface roughness of the ocean becomes saturated with foam and breaking waves which poorly reflect a signal and during low wind speeds there is not enough surface roughness generated to reflect a return signal.The fact that the surface off which the satellite rebounds its signal is in constant motion also presents a major problem. Due to the fact that satellites such as SAR and Scatterometers survey the roughness coefficient from the surface of the ocean generated by friction between the wind stress and the ocean below, a relative motion component between the wind speed and direction and the motion of the ocean is introduced. This creates an "error" in the satellite derived wind speed versus the true wind speed which is dependent on the direction of the wind in relation to the moving ocean (Bourassa et al., 2010; Chelton et al., 2004; Dagestad et al., 2013; Plagge et al., 2012). This relative motion effect, commonly referred to as "current-relative wind" or the "current relative effect" (Plagge et al., 2012) , is most prevalent over strong western boundary currents such as the Agulhas Current. According to previous investigations, discrepancies in wind speeds in the order of up to $20-50\%$ have previously been recorded (Kelly et al., 2001, 2005; Plagge et al., 2012). The current-relative effect was first highlighted by (Kelly et al., 2001) who noted wind speed difference between Scatterometer derived wind speeds and in situ wind measurements in the tropical Pacific. Since then, similar investigations have been undertaken in order to quantify the current relative effect, however the majority of studies have only used the lower resolution scatterometer data and not SAR. The majority of investigations conducted were also over regions of the ocean with low velocities such as equatorial flow and diurnal tidal flows. The low resolution of SCAT does not resolve the sharply varying, intense features which occur in the ocean as effectively as is needed. Especially changes which might occur over the narrow, intense Agulhas Current, which can reach speeds of up to $2.6m/s$ over areas as narrow as $30km$ (Lutjeharms, 2006b; Rouault et al., 2010). The much higher resolution of SAR would allow for investigation into far greater detail of the small and rapid changes which occur over such an intense boundary current.

Correcting for errors such as the relative motion effect, as well as increasing the accuracy

of satellite wind measurements over the ocean is of paramount importance for both the advancement of scientific knowledge and understanding. It is also vital for nonscientific uses such as for commercial use, disaster risk assessment and management and even recreation.

## 1.1 Research Objectives

This study analyses 5 year of high resolution oceanic winds derived from ASAR Wide Swath mode images. The dataset was derived for the purpose of this study and provides the 1st ever observation of surface ocean winds at a much higher resolution (1km versus 25km or lower) over South African waters. Since the Agulhas Current is one of the strongest western boundary currents in the world, a unique opportunity presents itself to better understand the impact of strong oceanic currents on satellite-derived wind observations

- The primary objective of this study is to investigate and attempt to quantify the effect that strong western boundary currents, such as the Agulhas, have on the speed and direction of their overlying wind patterns and regimes. In order to achieve this objective, the different effects which influence the ASAR derived wind speed need to be identified and isolated. The primary three effects are namely:
  - The effect of the speed and direction of the wind relative to the flow of the current. Depending on the relative direction differences, the derived wind speed would differ from the true wind speed.
  - The geophysical modification of the true wind speed over the current as a result of energy transfer between warm sea surface temperature and the overlying marine atmospheric boundary layer.
- The effect of initial wind speed intensities on the relative wind speed increases will also be investigated in order to identify the wind speed thresholds which are most affected by the different effects. This will be done by categorising and assessing different wind intensities in relation to each other and the Agulhas Current.
- Ultimately the aim is to produce a quantifiable rule for the different derived wind modified effects with the intention of improving future SAR wind processing endeavours.

# Chapter 2

# Literature Review

## 2.1 Geographic Context

### 2.1.1 Oceanographic Setting

The Agulhas Current is the western boundary current of the greater, Southern Indian Ocean subtropical gyre (Beal et al.; Gordon, 1986). It is a deep and narrow, warm-cored current with typical depths ranging between $1000m$ and $2200m$ and a mean width of approximately $100-200km$. The current is the most intense western boundary current in the Southern Hemisphere and can reach speeds in excess of $2.5m/s$ with strong velocity gradients on either side of its core and an estimated total poleward transport of $69.7Sv$ (Bryden et al., 2005; Cásal et al., 2009; Lutjeharms, 2006b). The Agulhas Current has three major source regions. These are namely; the southern branch of the East Madagascar Current, Mozambican Channel flow and recirculated Agulhas water from the South West Indian Ocean (SWIO) subgyre. Past research suggests that most of the Agulhas Current's water originates in the SWIO sub-gyre, with the East Madagascar Current and the Mozambican Throughflow contributing to the mesoscale variability of the Agulhas Current through the injection of intense cyclonic and anti-cyclonic eddies (de Ruijter et al., 2005; Lutjeharms, 2006b).

The Agulhas Current can be separated into three major regions: The Northern Agulhas, Southern Agulhas and the Agulhas Retroflection.

#### The Northern Agulhas

The Northern Agulhas, located between $26^\circ - 34^\circ S$, is the most intense and least variable of the three regions and exhibits flow speeds between $1.5-2.6m/s$ (Bryden et al., 2005;

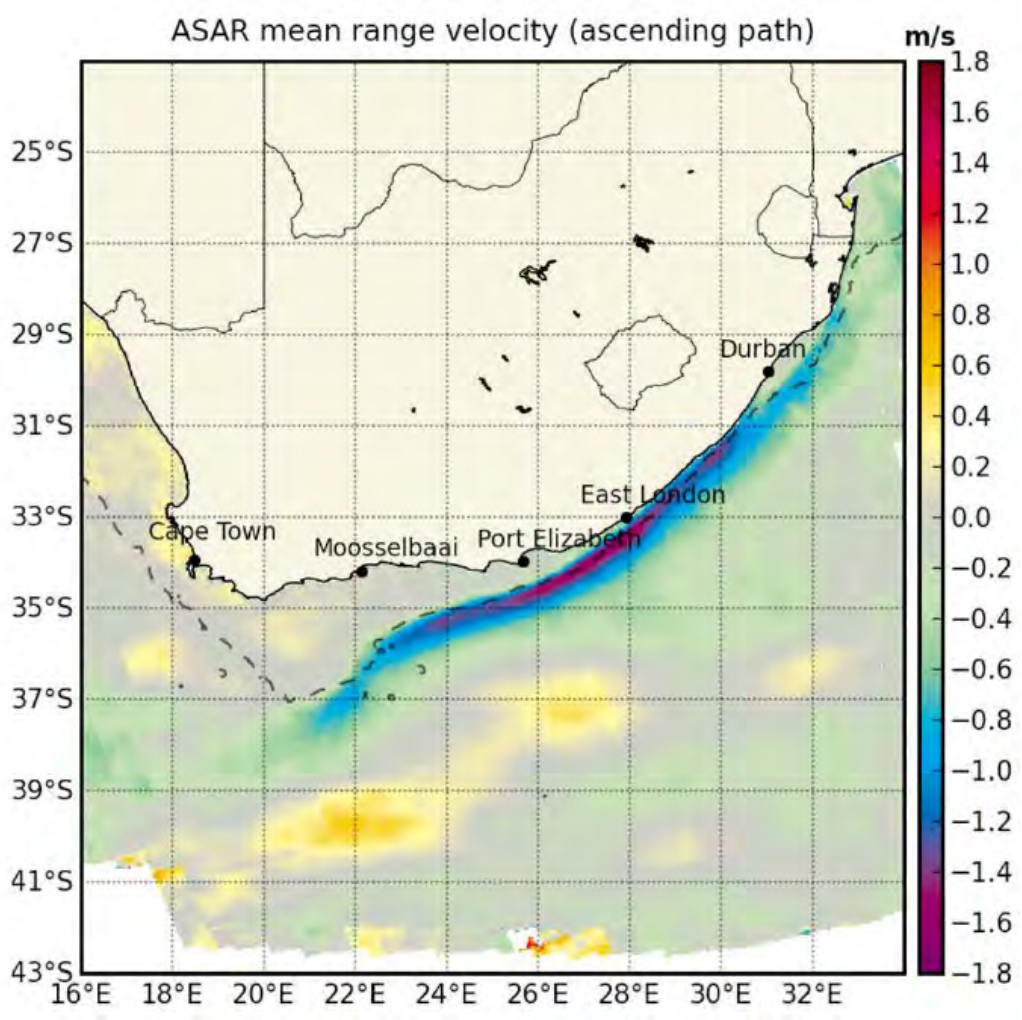


**Figure 2.1:** The mean range directed surface current velocity (m/s) for ASAR in the ascending path configuration from Rouault et al. (2010). Positive values denote an east-north-easterly flow (Approx. 75° from north). The black dashed line indicates the 1000m isobath.

Gründlingh, 1983). The current has a cross-sectional velocity gradient that is asymmetrically biased towards the coast. Mean velocities emanate from the coast at close to $0m/s$ and increase sharply towards peak flow velocities and then decrease at a more gradual rate out to sea (Rouault, 2011). The current flows in close proximity to the coast, topographically steered by the steep continental shelf for the majority of its length with relatively low variability until it reaches Port Elizabeth where the continental shelf widens to form the Agulhas Bank and the current manifests into its Southern region (Rouault et al., 2010). Figure 2.1 depicts a high resolution map of the time averaged surface velocities for the Agulhas Current as derived by Rouault et al. (2010), using information derived from Envisat ASAR data. The map depicts the intense flow speeds and topographic steering that is typically representative of western boundary currents.

Although the Northern Agulhas shows little variability in speed and direction (Gründlingh, 1983), large, solitary meanders known as Natal Pulses are known to periodically propagate downstream from their location of origin. Natal Pulses have been so named as they originate near the Natal Bight ($28°S$) as a result of barotropic instability and propagate downstream at phase velocities of approximately $10-20km/day$ (Lutjeharms, 2006b; van der Vaart and de Ruijter, 2001). They are associated with cold cores and cyclonic circulation on the inshore side of the current. Natal pulses occur at irregular intervals and can occur anytime between 50 to 240 days apart with an average frequency of 4 to 6 meanders per year. However, only approximately 1.6 Natal Pulses reach as far south as Port Elizabeth ($34°S$) and propagate in to the Southern Agulhas (Bryden et al., 2005; de Ruijter et al., 1999; Lutjeharms, 2006b; Rouault and Penven, 2011). This is mostly like due to the growth and interaction of the Pulses with the inshore topography which results in the generation of secondary, smaller meanders and a "cascade of energy" dissipation (Rouault and Penven, 2011).

### The Southern Agulhas

The Southern Agulhas is less stable than its northern counterpart as a result of the widening of the continental shelf. Decreased topographic steering from the change in the continental shelf configuration results in an increase in the number of current meanders, inshore cyclonic eddies and plumes (Speich et al., 2006).

The Southern Agulhas continues to follow the southwestward curve of the Agulhas Bank until it reaches the most southerly point at approximately $36°S$ where it retroflects and forms the Agulhas Retroflection (Lutjeharms and Van Ballegooyen, 1988; Lutjeharms, 2006b).

### The Agulhas Retroflection

The Agulhas Retroflection is characterised by a large anticyclonic loop with a mean diameter of $342km$ which reverses the flow of the current from a southwesterly flow to an easterly flow. The location of the retroflection is not fixed and can range in position from between $36^\circ - 40^\circ S$ and $16^\circ - 20^\circ E$ (Lutjeharms, 2006a,b). Although the majority of warm, salty water of the Agulhas follows the Retroflection and forms the Agulhas Return Current, large eddies and filaments do periodically detach from the main flow and propagate into the Southern Atlantic Ocean. This phenomenon has been termed Agulhas Leakage and plays a major role in the global thermohaline circulation through the transport of heat and salt into the Atlantic Meridional Overturning Circulation (AMOC) and, by extension the global climate (Beal et al.; Hall and Lutjeharms; Lutjeharms and Cooper, 1996; Schouten et al., 2002).

## 2.1.2 Atmospheric Setting

The greatest atmospheric influence on the east coast of Southern Africa and the greatest driver of the Agulhas system is the South Indian Ocean High Pressure (IOHP), a large anticyclonic feature which spans the entirety of the Southern Indian ocean, generally centered around $20^\circ - 35^\circ S$ (Driver, 2014; van Heerden and Taljaard, 1998).

A global climatology derived by (Risien and Chelton, 2008) from eight years of QuikSCAT data, as seen in Figure 2.2, shows the northerly shift of the IOHP from January to June. The centre of the cyclone is represented by the location of considerably lower mean wind speed and circulating wind vectors. The increase in wind velocities can be seen to the south of Madagascar with a mean increase in wind speeds of approximately $3m/s$.

The northeast, southwest polarity in wind direction remains relatively constant throughout the year, however a north to south shift of the IOHP, from winter to summer does result in a change in frequency of southwesterly events. During summer, the IOHP strengthens and moves further south. This coupled with a greater teleconnected influence of the summer monsoon over the northern Indian Ocean and an increase in subtropical cyclones results in predominantly northwesterly wind regimes over the greater Agulhas region (Ffield et al., 1997; Grundlingh and Largier, 1991; Matano et al., 2002; van Heerden and Taljaard, 1998). During the winter months, the IOHP shifts further north and allows the continuous, circumpolar low pressure band known as the westerly wind belt to interact with the African continent. This northerly shift allows low pressure, mid-latitude cyclones which detach from the westerly wind belt to come in to contact with the continent and move further north along the Agulhas' coastline. In turn, this increases the frequency of southwesterly wind

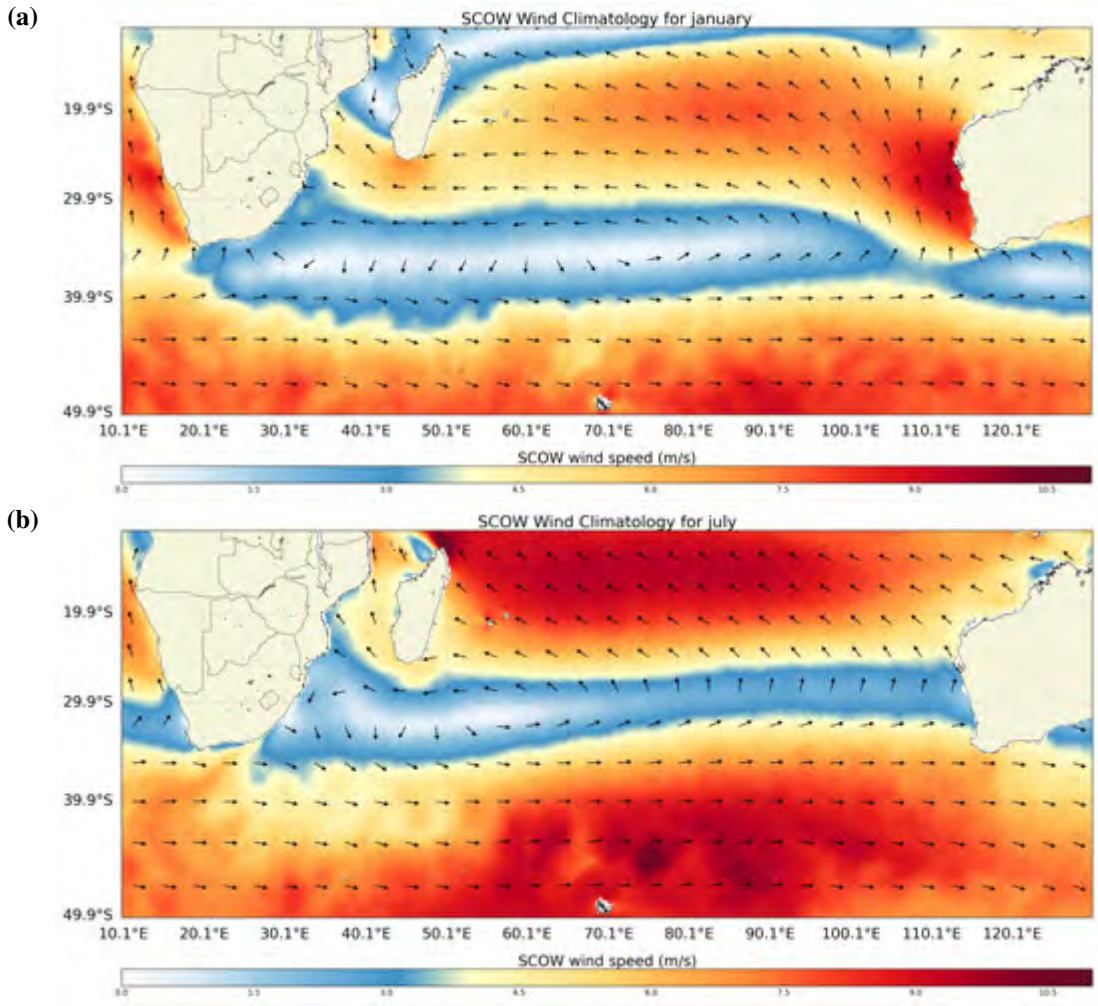


**Figure 2.2:** Global climatology of surface winds derived over the period September 1990 to August 2007 representing the typical austral summer (a) and winter (b) conditions. Colour scheme represents scalar wind speed. Black arrows represent wind direction and are standardised in length.

events in the regimes over the Agulhas (Ffield et al., 1997; Grundlingh and Largier, 1991; Matano et al., 2002; van Heerden and Taljaard, 1998). The anticyclonic IOHP drives a dominant wind regime of northeasters over the Agulhas throughout the year, interspersed with predominantly southwesterly events (Hunter, 1988). As a result, winds over the Agulhas Current are generally alongcurrent throughout the year. Wind speeds for both the northeasterly and southwesterly regimes depend on the intensity of the cyclonic events from which they originate, and tend to have a high range from approximately $5m/s$ to $30m/s$ with mean wind speeds centering at approximately $5-8m/s$ annually (Hunter, 1988).

### 2.1.3 Ocean-Atmosphere Interactions

The Agulhas Current is a dynamic region both oceanographically and atmospherically due to sharp temperature gradients, strong physical forcing and an abundance of moisture and energy. Not only do the strong current flows and steep temperature gradients of the current affect the surrounding ocean, but mesoscale ocean-atmosphere interactions over the Agulhas Current have been shown to have a strong influence on the properties and dynamics of the overlying atmosphere as well as the adjacent coastline (Jury and Courtney, 1991; Jury et al., 1993; Mason and Jury, 1997; O'Neill et al., 2005; Park et al., 2006; Rouault et al., 2000).

The marine atmospheric boundary layer (MABL) is the relatively thin layer of atmosphere ($1-2km$) that comes into direct contact with the surface of the ocean and is the boundary across which all energy, moisture and heat exchanges between the ocean and atmosphere take place (Chelton and Xie, 2010). As such, the MABL is a highly dynamic and well mixed layer which reacts almost instantaneously to outside influences, particularly in the form of energy fluxes from the ocean surface.

A study conducted by Rouault et al. (2000) during a ship borne meteorological and oceanographic survey found that the specific humidity and potential temperature of the MABL were greatly influenced by the sharp SST gradients across the Agulhas Current. Rouault et al. (2000) found that the characteristically stable boundary layer overlying the cooler shelf waters was replaced by a much more unstable, convective boundary layer. In a different analysis of the same study, Lee-Thorp et al. (1998) observed the formation of cumulus clouds directly above the Agulhas Current, in contrast to otherwise clear conditions. Both Rouault et al. (2000) and Lee-Thorp et al. (1998) concluded that the strong ocean to atmosphere heat fluxes from the much warmer Agulhas were resulting in convergence, convection and mixing in the atmosphere, thereby redistributing heat and moisture. Additionally, Rouault et al. (2000) found that wind events which contained alongcurrent velocity components displayed an increase in magnitude as well as wind stress over the current which resulted in changes to the overlying MABL and the creation of an internal boundary layer; a boundary layer that was stable for winds blowing from warm to cold water and convective for winds from cold to warm. This represents an increase in the overall kinetic energy over the Agulhas system. Similarly, on the Subtropical Convergence Agulhas Retroflection Cruise (SCARC) in 1987, Mey et al. (1990) documented an increase in air temperature, dew point temperatures and, most importantly, wind speeds above the Subtropical Convergence-Agulhas SST front. During aircraft observations over the inshore front of the Agulhas south of George, South Africa ($34.0°S$, $22.45°E$), Jury and Courtney (1991) noted that, "air flow accelerated towards the SST front and, at times, decelerated downstream, causing convergence of the order of $-4\times10^{-4}S^{-1}$", and concluded that a major

contribution of the Agulhas Current to weather systems over South Africa is the increase in surface wind stress.

The study of the teleconnections between ocean-atmosphere dynamics and properties is a well established field globally. Thus, similar research has been conducted for several other locations and phenomena, around the world, using both remote sensing and in situ observational methods (Chelton et al., 2001; Liu, 2002; O'Neill et al., 2003; Park et al., 2006; Vecchi et al., 2004; Wentz et al., 2000; White and Annis, 2003; Xie, 2004; Xie et al., 1998, 2001). All these investigations on ocean-atmosphere interactions point to similar trends which are summarised in Xie (2004)'s comparative study.

Xie (2004) investigated different ocean-atmosphere coupling analyses and noted that over "cool oceans", such as the extratropics, the direct effects of SST variation on the atmosphere are likely to be contained within the narrow boundary layer. This is due to the lack of warm water-induced convection resulting in a temperature inversion which caps any major energy transfer with the upper atmosphere. Secondly, Xie (2004) found that a positive SST-wind speed correlation could be noted in satellite data collected over key regions similar to that of the Agulhas Current, such as the Kuroshio and its extension and Gulf Stream Rings, where warmer temperatures lead to faster wind speeds. In the cooler wakes of tropical cyclones, marked wind decreases were observed. The resulting conclusion by Xie (2004) was that the transition from colder to relatively warmer SST's results in a destabilisation of the near-surface atmosphere which causes intensified turbulence and mixing. This then leads to an increase in wind shear between the colder ocean and overlying atmosphere and a resulting increase in wind speed. Importantly, Xie (2004) notes that the lateral advection mechanism is such that the vertical mixing and resultant wind speed changes should only occur on the downwind side of the front.

Finally, a study conducted by Park et al. (2006) on scatterometer derived surface wind field modifications over Gulf Stream rings found that near surface wind speed and direction modifications of $10-15\%$ and $5-10^{\circ}$ respectively, can occur. The effect is valid for warm and cold core eddies which means that either a drop or rise in wind speeds of equal magnitude is apparent depending on the temperature change.

## 2.2 Satellite Wind Measurement

Wind speed and direction observations from satellites started in 1973 when the first vector scatterometer flew aboard the Skylab satellite. The more sophisticated operational scatterometer SEASAT in 1978 was then used to predict wind speeds toward an accuracy of $1.6 m/s$ (Dagestad et al., 2013; Mccandless and Jackson, 2004; Monaldo and Beal, 2004). The SEA-

SAT scatterometer was accompanied by an L-band synthetic aperture radar which was not originally intended to be used to measure wind properties, but in 1986, (Gerling, 1986) illustrated that wind related features were evident in the SAR data and that wind direction could be estimated using Fourier transform techniques. Eventually, wind speeds could be estimated using the directional input from these surface features in the derivation process (Fetterer et al., 1998; Monaldo and Beal, 2004; Vachon and Dobson, 1996; Wackerman et al., 1996). Since then many scatterometers and SAR's have flown aboard satellites and have proven useful for both the scientific and industrial communities especially as the long wavelengths within which they operate allow for the penetration of weather systems and cloud formations with almost no atmospheric attenuation (Mccandless and Jackson, 2004). Satellite wind measurements have been used to study oceanic and atmospheric circulations as well as ocean atmosphere interactions and resulting teleconnections. Satellite wind measurements are also widely used by industry, to improve numerical weather prediction models and in the planning of offshore wind farms (Dagestad et al., 2013).

### 2.2.1 Normalised Radar Cross Sections (NRCS)

Although technically and mechanically quite different, both SCAT and SAR operate using the same physical principles. Both Scatterometers and Synthetic Aperture Radars are based on side looking, low frequency ($6cm$), active radars and emit microwave pulses at varying beam widths and angles. They then record the properties of the returning signal, which has rebounded off the Earth's surface (Bentamy and Fillon, 2012; Desnos et al., 2000; Holt, 2004; Mccandless and Jackson, 2004). The properties of the return signal such as the magnitude, polarisation and emittance-recapture time are directly related to the nature and shape of the surface from which they rebound and so can be used to determine the surface roughness over the ocean. The measure of the recaptured backscattered electromagnetic energy is called the Normalised Radar Cross Section (NRCS) or Sigma0 ($\sigma^0$). The higher the $\sigma^\circ$value, the more rough the surface. The NRCS is determined through the principle of Bragg Scattering whereby the strength of the return signal is dependent on the radar wavelength being in phase with the short, wind driven surface waves. The relationship between the radar frequency and surface wavelengths can be described by equation 2.1 (Holt, 2004; Mccandless and Jackson, 2004; Wright, 1966).

$$\lambda_B = \lambda_r / 2 \sin\theta \tag{2.1}$$

Where $\lambda_B$is the wavelength of the surface waves, $\lambda_r$is the radar wavelength and $\theta$ is the incidence angle of the radar (ie: the angle between the radar line of sight and nadir).

Bragg scattering is most prevalent between incident angles of 15°-70° (Monaldo and Beal, 2004; Wright, 1966). In equation 2.1 it is evident that an increase in $\theta$ requires an increase in radar frequency ($\lambda^r$) in order to resolve the same Bragg wavelength ($\lambda_B$) thus, different SAR sensor frequencies, such as X-band ($\sim 3cm$), C-band ($\sim 5.5cm$) and L-Band ($\sim 23cm$) have different wavelength detectability. This means that a threshold for wind speed and the resulting wind generated waves must be reached in order for the radar to receive a detectable return signal. As a result, a wind speed threshold of approximately between $2-3.5m/s$ is required in order to estimate wind speeds from scatterometers and SAR observations of sea surface roughness (Hersbach, 2010; Monaldo and Beal, 2004). Bragg scattering and therefore the NRCS signal can be influenced by a multitude of oceanic, atmospheric and physical roughness modifying effects. These roughness modifiers can range from anything between variable wind speed, atmospheric boundary layer stratification, ocean waves, films and surfactants, moving ship wakes, and principally, ocean current. Each of these signals will theoretically present a unique signature in the retrieved NRCS signal and can thus ideally be identified (Holt, 2004; Mccandless and Jackson, 2004). The key challenge in SAR processing to date is to adequately separate each signal from each other (Rouault, 2011).

### 2.2.2 Geophysical Model Functions

The NRCS obtained from SAR and Scatterometry is merely a measure of the surface roughness of the ocean. Thus, in order to derive a wind speed and direction, an empirical or modelled relation needs to be applied to the NRCS. To date, the best relations are empirically developed (Hersbach et al., 2003). The empirically derived models, referred to as Geophysical Model Functions (GMF), were developed through the collocation of in-situ measurements and numerical weather prediction models with NRCS data. GMF's which were designed specifically for use with C-band scatterometers and SAR's are called CMOD. A general relational formula for all CMOD's is displayed by equation 2.2 which illustrates the dependency of $\sigma^0$on three key variables: wind speed $v$, wind direction $\chi$, and radar incidence angle $\theta$.

$$\sigma_0 = CMOD(c,v,\phi,\theta) = B0(c_0,v,\theta)[1+B1(c_1,v,\theta)cos(\phi)+B2(c_2,v,\theta)cos(2\phi)]^p \quad (2.2)$$

From the above formula it is evident that given a specific wind speed and direction at a known radar incidence angle, a unique NRCS can be predicted. This is not the case

however in the reverse. Any given NRCS can correspond to multiple combinations of wind speed, direction an incidence angle. Thus, in order to determine a surface wind speed, the wind direction and incidence angle are needed in conjunction with the NRCS signal (See Figure 2.3). One of the main challenges in deriving wind speeds from NRCS data lies in the determination of the wind direction variable. Wind directions from scatterometers can be somewhat estimated by increasing the number of simultaneous look directions over a region in order to reduce the number of potential solutions. This technique has been employed to great effect in scatterometer wind derivations but cannot however, be used for SARs to date due to the mechanical impracticalities of mounting two, much larger, SAR's on one satellite. As a result, SAR derived winds require wind direction inputs from sources such as numerical weather models, estimates from Fast Fourier transforms from wind streaks and shadows, or through Interferometry and Doppler (Hansen, 2011; Rouault et al., 2010).

None of the aforementioned techniques are, however, capable of generating wind direction data at as great a resolution or accuracy as SAR for varying reasons. For example, Fast Fourier Transforms from wind streaks have a much lower resolution and are subject to an 180° ambiguity. Numerical models might be able to reach a comparable resolution, but it is only for small regions or with massive computing power and the data is not considered "real" due to the nature of numerical models. Numerical Models are also particularly limited near coastal regions and over western boundary currents due to the difficulties in computing such intense and dynamic features and lack of knowledge for adequate parameterisation (Speich et al., 2006).

The most recent CMOD to be developed is CMOD5.n, a GMF which is designed to determine the equivalent "neutral" wind speed at 10 meters above sea level. "Neutral" wind can be defined as: "the wind at a 10-metre height for given surface stress in case the marine boundary layer were neutrally stratified" (Hersbach, 2008). Most in situ wind observations are generally standardised at 10m above the surface, thus the Neutral wind variable is more compatible with conventional data sets Hersbach (2008).

### 2.2.3 Scatterometry

Scatterometers are real aperture radar (RAR) remote sensors whose principal uses are to measure the surface wind speed over the open ocean. Since the flight of the Seasat-A scatterometer in 1978 many different scatterometers have gone into operation each with different technical specifications and scanning characteristics in attempts to increase the accuracy and resolution of the data collected (Falcon and Lewis, b; Long et al., 2001). One of the currently operational scatterometers is the Advanced Scatterometer (ASCAT) on board the Metop satellite system (Eumetsat, 2015). The satellite employs a fan-bean geometry for its

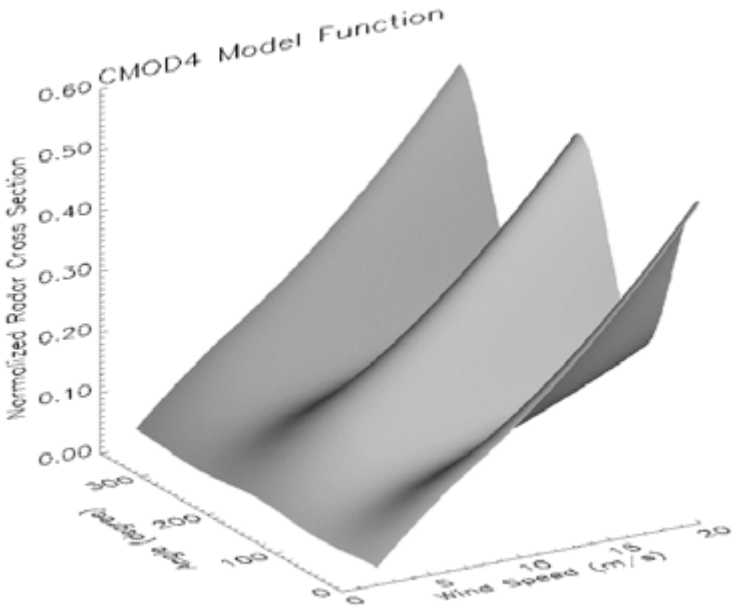


**Figure 2.3:** A three dimensional visualization example of the CMOD4 geophysical model function, taken from Monaldo and Beal (2004), which relates the normalised radar cross section to multiple corresponding wind speeds and directions at a specified radar incidence angle of 25° from Nadir. The x-axis represents the wind speed (m/s), the y-axis represents the wind direction angle in degrees from north and the z-axis represents the NRCS values.

antennas with two sets of three antennas - each spaced 45° from the other - on either side of the satellite, which collect data in two 500*km* wide swaths on either side of the satellite's ground trajectory. The satellites operate within the Bragg range at between 25° to 65° from NADIR (Eumetsat, 2015; Figa-Saldaña et al., 2002). The employment of three different antennas at different look angles over the same swath allows for the scatterometer to eliminate some of the ambiguity in the NRCS signals relating to wind speed and direction and thus enables a wind speed and direction to be derived using the GMF with no external input. This eliminates any errors and caveats which occur due to inaccurate wind direction inputs (Bentamy and Fillon, 2012; Figa-Saldaña et al., 2002). However, due to the nature of the antennas and their operating range of frequencies, scatterometers are severely limited in resolution to only the kilometre scale. Currently the best operational resolution that scatterometers can produce are ASCAT and RapidScat which operate at a maximum approximate resolution of 30 and 15 kilometres respectively (Eumetsat, 2015; Falcon and Lewis, a,b).

### 2.2.4 Synthetic Aperture Radar

The basic principle of Synthetic Aperture Radar was developed in the early 1950's as a solution to increase the azimuthal resolution of the already operational Real Aperture Radars (RAR). RAR were severely limited due to physical constraints in both physical size and radar wavelength (Chan and Koo, 2008; Mccandless and Jackson, 2004).

As illustrated in equation 2.3, for RAR's and scatterometers to increase in azimuthal resolution the length of the antenna would need to increase substantially to the point of impracticality (a resolution in the 10s of meters would require an antenna size in the order of 10s of kilometres in size (Mccandless and Jackson, 2004)). Alternatively, the radar would need to employ such a high frequency beam that atmospheric attenuation becomes a major issue (Chan and Koo, 2008). To solve the problem, signal processing was used in order to enable a relatively small sensor to operate at a much larger aperture. The process of synthesising the aperture relies on the principle that, for radar that has an orthogonally directed beam to its direction of travel, the larger beam width will result in the region of the earth's surface to be scanned for an extended period. This increase in illumination time combined with phase and Doppler measurements simultaneously collected by the satellite allows for the return signal to be retrieved by the moving satellite and adjusted for the time and position change. This results in a theoretical aperture length much longer than that of the true size of the sensor (Mccandless and Jackson, 2004; Tomiyasu, 1978).

$$L = \frac{\lambda R}{D \sin\theta} \; and \; \rho_g = \frac{c\tau_p}{2\sin\theta} \tag{2.3}$$

Equation 2.3 represents the formulae for the azimuthal and range resolutions of SAR respectively. $R$ is the distance between the satellite and the ocean's surface, $\lambda$ is the radar's wavelength, $D$ is the length of the antenna, $\theta$ is the radar incidence angle,$\tau_p$ is the pulse length and $c$ is the speed of light.

Similarly, the range resolution is able to be improved on in both SAR and RAR devices through a technique known as "pulse chirping" where the radar emits a pulse which varies the frequency of the radar pulse linearly for a specific frequency range. This variation is known as linear frequency modulation and determines the radio frequency bandwidth within which the satellite operates (Mccandless and Jackson, 2004).

It is through these two techniques, specifically aperture synthesis, that SAR is able to obtain the much higher resolutions of hundreds of meters over scatterometry which is limited to the kilometre scale. This results in SAR seemingly being the perfect choice for mesoscale and sub-mesoscale processes such as the ocean atmosphere interactions over current boundaries and close to the shore. A prime example is the effect that the Agulhas Current

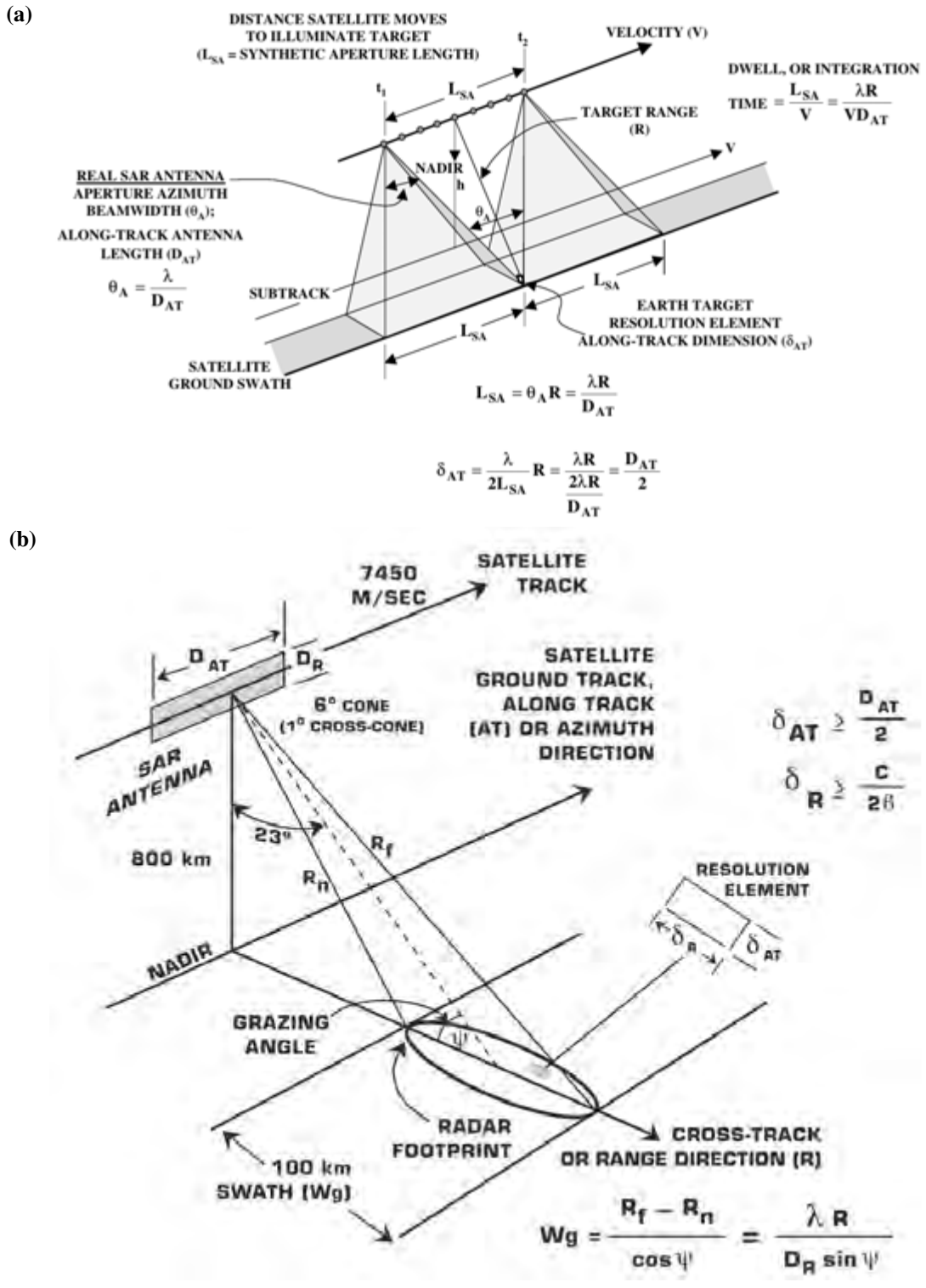


**Figure 2.4:** Representation of the basic principles (a) and geometry (b) of synthetic aperture radar with regards to the synthesis of real aperture beam azimuthal width into a larger synthetic aperture (Mccandless and Jackson, 2004).

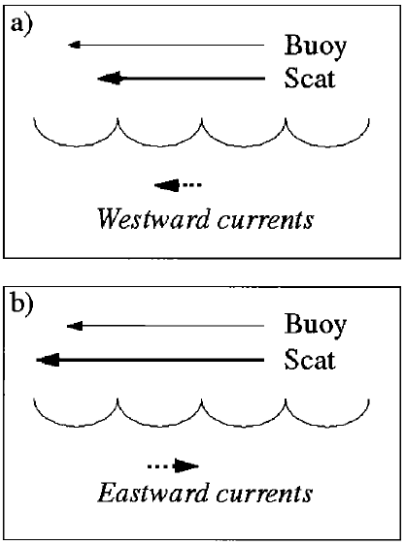


**Figure 2.5:** Schematic created by Kelly et al. (2001) illustrating the relative decrease (a) or increase (b) in scatterometer derived wind speed for winds flowing with (a) or against (b) the flow of the current

might have on wind speed and direction in the boundary layer and atmosphere above it.

There are, however key limitations to the SAR system which create substantial technical and usage difficulties. Firstly, the SAR antenna is energy demanding and thus cannot be employed on a continuous basis. Therefore specific regions of interest must be selected for investigation over a specified time period. SAR also has a lower temporal resolution than that of scatterometers at one full orbit every 35 days which translates to approximately 3 to 5 days between each repeat measurement. This means that SAR is not effective for studying the temporal evolution of mesoscale and sub-mesoscale events particularly those related to atmospheric interactions which operate on an hourly timescale. Once it was proven that SAR could be utilised to derive wind speed, the higher resolution of SAR made it a potentially viable supplement to - if not a replacement of - scatterometer derived wind fields.

### 2.2.5 Effect of currents on SAR wind data

One of the major issues affecting the accuracy of the SAR wind output is the fact that the SAR and scatterometry measure the backscatter of the centimetre scale waves which result from the *relative* motion of wind over the surface of the ocean. This means that the wind speed derived from SAR will contain a component that is influenced by the movement of the water above which the wind is blown (i.e. a current or other larger scale waves) (Bourassa et al., 2010; Chelton et al., 2004; Dagestad et al., 2013; Plagge et al., 2012).

In 2001, Kelly et al. (2001) illustrated that large scale, equatorial ocean currents were

evident in scatterometry derived wind data. The study used NSCAT scatterometry data in comparison to in situ measurements from the Tropical Atmosphere-Ocean (TAO) array in the equatorial pacific.

Kelly et al. (2001) established that there could be a significant disparity of up to nearly 50% in some areas between scatterometry data and in situ measurements over the equatorial region. Kelly et al. (2001) states that, although in most of the ocean the speed of the movement is negligible in comparison to that of the wind, over fast flowing current boundaries and areas of high current shear and steep velocity gradients, there could be a significant influence in the wind measurement derived from Scatterometry. Kelly et al. (2001) believed that wind blowing in the opposite direction to the currents direction of flow would manifest in a faster wind speed derivation from the scatterometry data and, conversely, a slower wind speed would be derived from winds blowing in the same direction as the current.

Kelly et al. (2001) concluded by stating that scatterometry derived wind speed measurements should be referred to rather as a relative wind speed and that relative wind derived stress could potentially help to improve understanding of vital air-sea interactions and fluxes.

In a later study, Kelly et al. (2005) compared QuikSCAT scatterometer data with absolute wind measurements from the same TAO array. Collocated wind differences (CWD's) were calculated between the scatterometry derived relative wind and the absolute wind from TAO. The resulting monthly averaged differences were compared with near surface derived geostrophic current measurements. An overall good agreement was found between the CWD's and areas of strong current data, particularly between $2°N$ and $2°S$, thus further affirming Kelly et al. (2001)'s notion of scatterometer derived *relative* winds.

The most recent investigation of the influence of ocean current on scatterometry derived wind fields was conducted by Plagge et al. (2012) when five years of data collected from 2 separate meteorological and surface current moorings was compared to QuikSCAT, ASCAT and altimeter derived winds for varying wind resolutions over the Gulf of Maine: a region known for strong semi-diurnally reversing tides and resulting current.

The study found a near one to one correlation between ocean surface velocities and the along current wind speeds products, particularly for moderate wind speeds and neutral atmospheric conditions. The combined analysis of all satellite products found differences in the order of 10% between the current-relative and earth-relative wind speeds. Thus Plagge et al. (2012) reaffirmed Kelly et al. (2001)'s conclusions that satellite derived wind speeds should be referred to as a relative wind stress rather than a true wind speed

Finally, Chelton et al. (2004) produced a similar study to that of Kelly et al. (2001, 2005) and Plagge et al. (2012) using four year averaged, $25km$ resolution QuikSCAT near surface

wind speed and direction. The study revealed ocean currents persistently altered the wind speed measurements to a point where the currents were clearly visible in the temporally averaged data, despite the fact that wind variability is over a much shorter scale and was expected to be smoothed out.

Chelton et al. (2004) also demonstrated that the faster flowing narrow currents persistently altered the wind curl directly over the current in crosscurrent wind regimes. Chelton et al. (2004) did find, however, that the currents did not have nearly as great an effect on the wind stress divergence.

Although Chelton et al. (2004); Kelly et al. (2001, 2005) and Plagge et al. (2012) used scatterometry data in their studies, the relative wind concept remains true for SAR derived winds as they both operate on the same principles of Bragg Scattering and NRCS (Stoffelen and Anderson, 1993, 1997). In fact, the GMF's used in SAR wind derivations were in fact designed for scatterometry and have been retrofitted to SAR outputs.

To date, little research has been conducted using such high resolution SAR derived winds to determine the effect the strong western boundary current have on the derived product. Temperature fronts in regions such as the Agulhas have much smaller spatial variation scales than in the open ocean. The high resolution of SAR means that it excels at resolving such small scale features. To date this study is the only one to use SAR over such strong a western boundary current. The strong persistent nature of the current means that it is an ideal location for such a study however, the results will most likely be applicable to other western boundary currents around the world.

Thus is it important to further investigate the effect that a strong current such as the Agulhas might have on the high resolution derived wind speeds from SAR.

# Chapter 3

# Data and Methods

## 3.1 Data

### 3.1.1 Envisat Advanced Synthetic Aperture Radar

The Advanced Synthetic Aperture Radar (ASAR) wind fields used in this study are derived from a 5-year archive of ASAR images collected over the Southern African region. ASAR was the SAR sensor used as part of the European Space Agency (ESA) driven, Envisat based mission which ran from 2002 to 2012. From July 2007 the Agulhas Current became a region of systematic data acquisition in order to test the feasibility of extracting surface current information from satellite-borne SARs, as part of the SAR ocean wind-wave-current project funded by ESA (Collard et al., 2008; Johannessen et al., 2008).Most SAR acquisitions during the 2007-2012 period are in the Wide Swath Mode (WSM) mode, with a sampling frequency of one ascending and one descending image every three to 5 days. As a result, a large number of SAR images are available over the Agulhas Current making it an ideal study region.

In total, 987 Wide Swath Mode images over the Southern African region are used with a maximum per-point data density of 297 readings. The area with the highest density of repeat measurements is located off shore of the east Coast of South Africa, to the north East of Algoa Bay. For the investigation, I selected the region with the highest number of observations, which is marked by the blue square in Figure 3.1. The blue square encompasses the majority of the Northern Agulhas Current and extends from just south of Port Shepstone to Port Elizabeth along the coast. The region does not include the Agulhas or the Agulhas Return Current.

The Normalised Radar Cross Section was extracted from the raw N1 ASAR files using the open-source NanSat (https://github.com/nansencenter/nansat) python module. The Wide

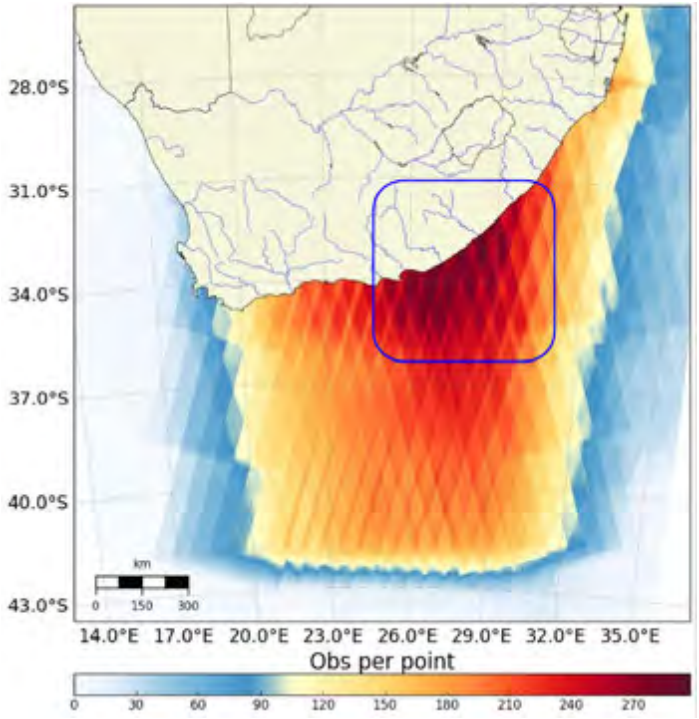


**Figure 3.1:** Data density plot showing 987 swaths (colour) of Envisat ASAR data over the Southern African region for the period 2007-2012.

Swath Mode Normalised Radar Cross Section swaths which have a range-azimuth resolution of $150m \times 150m$ were then down sampled to a regular geographic grid with a resolution of $1km \times 1km$ using Lanczos spatial interpolation. Wind directions were sourced from the CFSR and CFSv2 reanalysis models described in Section 3.1.3. Wind speeds were derived using the open-source NanSat openwind (https://github.com/nansencenter/openwind) python package which is based on the CMOD5.n GMF. All data pre-processing was undertaken by Dr M. Krug (Council for Scientific and Industrial Research, Cape Town, South Africa) with additional support from Dr M. Hansen (Nansen Environmental and Remote Sensing Centre, Bergen, Norway) and using the computer resources provided by the ACE Lab at the Centre for High Performance Computing (CSIR-CHPC).

### 3.1.2 CMOD5.n

The Geophysical Model Function (GMF) used in the derivation of the wind speed is the CMOD5.n model, a C-Band specific GMF first published as CMOD5 in 2007 by Hersbach et al. (2007). The CMOD5 GMF was then later fine tuned for the derivation of equivalent neutral surface winds at a 10m height in order to be more compatible with other observational data sets (Hersbach, 2010).

CMOD5.n is the preferential Geophysical Model Function for wind speed derivation. It delivers a $0.7m/s$ increase in the derived wind speed over the previous CMOD5 versions, and is thus a better representation of the winds at 10m. CMOD5.n also has a reduction in the seasonally dependent biases present in comparison with operational wind products such as the European Centre for Medium-Range Weather Forecast's (ECMWF) model output (Hersbach, 2010).

There are well known limitations to using the CMOD5.n GMF. Firstly, the model function is only considered reliable for wind speeds between $2m/s$ and $35m/s$ due to constraints in the return signals received from a lack of surface roughness at low speeds and breaking waves at extreme wind speeds (Hersbach et al., 2007; Portabella and Stoffelen, 2006). Secondly, it is acknowledged that, although CMOD5.n is corrected for neutral wind conditions, other roughness influencing factors that have been neither determined nor catered for, but could contribute to wind speed derivation errors. For Example, the sea state or, most importantly, ocean currents (Hersbach, 2010) could result in an unstable boundary layer and thus non-neutral conditions Rouault et al. (2000) which the GMF is not calibrated for.

Finally, like all other GMF's, CMOD5.n requires a wind direction input in order to extract the wind fields from the Normalised Radar Cross Section. For this purpose wind directions from the CFSR and CFSv2 global reanalyses were used.

### 3.1.3 Climate Forecast System Models

The wind direction data used in the derivation of the SAR wind speeds is sourced from two separate reanalysis data sets over different time periods. Namely the Climate Forecast System Reanalysis (CFSR) and the Climate Forecast System Version 2 (CFSv2) (Saha et al., 2010, 2014).

#### CFSR

The CFSR is a global reanalysis and is a precursor to the CFSv2 forecast model. It was primarily developed to generate sufficient initial conditions for its successor's planned atmosphere-ocean-land-sea ice coupled forecasts from 1982 to present day (Saha et al., 2010). CFSR is still considerably more accurate than any previous global reanalyses generated by NCEP in the 1990's Saha et al. (2010) such as NCEP, NCEP2 and ERA40 (Kistler et al., 2001; Ma et al., 2008).

The reanalysis covers the period from 1979 to 2010 and assimilates data from a multitude of cross platform observations, each spanning different time spans according to their availability. A brief summary of the atmospherically relevant assimilated observations in-

clude: Reprocessed Scatterometer derived wind data from the ERS1 and ERS2 satellites (1991-2007); QuikSCAT derived surface wind data (2001-2009); Windsat derived wind data (2007-2010); SSM/I passive microwave imaging derived surface wind speed (1997-2010); Global Atmospheric radiosondes and PIBALs (1948-2010) as well as special radiosondes from the AMMA (2001-2010); aircraft and surface observations (1992-2010 and 1976-2010 respectively) among other data sets Saha et al. (2010).

Important ocean assimilations include data from: Optimally Interpolated products from the currently operational AVHRR infrared SST sensors (1981-2002) as well as a combined AVHRR and AMSR optimally interpolated product (2002-2010). Both satellite derived products have a 0.25°resolution and are supplemented with available observational data from ships and ocean buoys in order to correct for any satellite induced biases. The in situ data was also analysed using optimal interpolation (Saha et al., 2010). Although the SST data is assimilated into the atmospheric model in CFSR, the core of the Agulhas and the SST effect on wind speeds is inadequately resolved. The CFSR model is also known to decrease in reliability towards the coast as a majority of the assimilated data such as the scatterometer is unreliable toward the coast (Saha et al., 2010).

The coupled reanalysis is compiled of multiple numerical models representing different facets. This allowed for, at the time of release, a relatively fast production of an unprecedentedly high spatial and temporal resolution of $0.3^\circ \times 0.3^\circ$, horizontally (latitude dependent), as well as 37 atmospheric and 40 oceanographic levels at an hourly time step (Saha et al., 2010).

### CFSv2

The Climate forecast System Version 2 (CFSv2) is the currently operational global ocean-atmosphere-land-sea ice couple forecast model operated by NCEP. The model was developed as an upgrade to the first CFS global model retroactively named CFSv1 (Not to be confused with the CFSR) and features substantial improvements in all of the modeling and assimilation components utilised in the CFSv1 with the addition of several new features such as an upgraded soil model and the inclusion of an interactive sea ice model (Saha et al., 2014).

Most of the major upgraded features and data assimilations in the CFSv2 model were executed in the CFSR during the development of the initial conditions, however, changes were made to the atmospheric and land models in order to improve physical parameterisations and fine tune other parameters.

The most important difference between the CFSR and the CFSv2 is undoubtedly the increase in the horizontal spatial resolution from $0.3^\circ \times 0.3^\circ$ to $0.2^\circ \times 0.2^\circ$. The remainder

of the dimensional resolutions remained effectively the same. Both the CFSR and the CFSv2 data were interpolated on to a $1km \times 1km$ grid using Lanczos spatial interpolation in order to allow for high resolution wind derivation.

From this point further the combined CFSR and CFSv2 dataset will be referred to as the CFS dataset in order to eliminate ambiguity.

### 3.1.4 Advanced Scatterometer Derived Winds

The scatterometer derived wind speeds used in the validation of the CFS model data as well as in a comparison with the ASAR derived wind speeds are derived from NRCS data captured by the Metop-A satellite based Advanced Scatterometer (ASCAT). The Metop-A satellite has been in operation since October 2006 and is a lower polar-orbiting satellite. The ASCAT scatterometer is a dual swath, fan beamed scatterometer with 3 antennas on either side 45°apart. The scatterometer operates in the same C-band ($5.255GHz$) as the ASAR antennas and also uses the CMOD5.n GMF for wind derivation (Esa, 2007; Saf, 2012). Thus the ASCAT data is subject to many of the same roughness influencing factors as the ASAR, however the ASCAT is able to collect its own wind direction data in the data collection process due to the multi-antenna approach.

The wind speed and direction data used in this investigation were derived by EUMETSAT and KNMI and are referenced as a level 2b product. The data can be downloaded from the EUMETSAT website (http://www.eumetsat.int/Home/Main/Satellites/Metop/ Resources/index.htm?l=en) and from the Ocean Sea Ice Satellite Application Facility (OSI SAF) web site (http://www. knmi.nl/scatterometer/) (Bentamy and Fillon, 2012). The data has a temporal resolution of two measurements per day and a spatial resolution of 0.25°.

### 3.1.5 Sea Surface Temperature

#### MODIS

The level 3 processed Sea Surface Temperature (SST) data used for the geolocation of the mean Agulhas Current, and thus mapping of the locations of interest and transects, is from the Terra satellite based MODIS (Moderate Resolution Imaging Spectroradiometer). A temporally averaged composite for the entire mission, from 2000 to 2014, was acquired from the OceanColor Web data portal as supplied by the NASA Goddard Space Flight Centre, Ocean Ecology Laboratory, Ocean Biology Processing Group NASA Goddard Space Flight Center, Ocean Ecology Laboratory.

MODIS is a multi-spectral band, high radiometric sensitivity satellite with a spectral

range from $0.4\mu m$ to $14.4\mu m$. It has scanning dimension pf $2330km$ cross track width and $10km$ along track width. And a global repeat cycle of 1 to 2 days NASA Goddard Space Flight Center, Ocean Ecology Laboratory.

The wide spectral range of MODIS allows for a multitude of remote sensing uses which result in variable resolutions. The bandwidth used for SST remote sensing is the 23rd band at approximately $4\mu m$. This results in an approximate, post processed, gridded resolution of $4km \times 4km$ NASA Goddard Space Flight Center, Ocean Ecology Laboratory.

#### SEVIRI

The high-resolution SST data used in the transect analysis of each of the locations of interest is the $0.05^{\circ}$spatial resolution, level 3 pre-operational SEVIRI derived SST data set. The SEVIRI dataset is at an hourly temporal resolution and is derived using MSG/SEVIRI brightness temperatures. The SEVIRI dataset is available from OSI SAF under the European Organisation for the Exploitation of Meteorological Satellites (EUMETSAT). The data used in this study is accessible through OSI-SAF's homepage: http://www.osi-saf.org. Hourly SST maps were aggregated to generate daily composites.

#### OSTIA

The level 4 SST product used for the collocation of Natal Pulses with mesoscale atmospheric feature in the ASAR derived wind fields is sourced from the OSTIA Sea Surface Temperature and Sea Ice Analysis dataset as produced by the UK Met office (C) 2010, published by the Met Office. The data analysis is comprised of a multitude of input data including satellite observation data from AMSRE, ATS_NR_2P, AVHRR18_G, AVHRR17_NAR, AVHRR18_NAR, OSISAF_ICE, SEVIRI and TMI, in situ ship measurements and numerical reanalyses Martin et al. (2015).

The SST data has an effective gridded spatial resolution of $6km \times 6km$ and is a daily averaged product.

### 3.1.6 Ocean Current Velocities

#### Globcurrent

The ocean current data used in the comparative analysis of the wind speeds relative to the ocean current are sourced from the Globcurrent project website NERSC et al. (2013). Globcurrent is an ESA funded project that aims to reduce deficiencies in, and improve the final

estimate of ocean surface currents through optimisation and assimilation of multiple data sources combined with advanced processing tools and numerical simulations.

For this investigation we're using the Globcurrent Total Hs Currents. The Globcurrent Total Hs Currents is representative of surface ocean currents. It is the most relavant dataset for an investigation into the relative wind speeds motions induced by surface currents due to the fact that it is representative of the ocean dynamics and currents and its signature on the ocean surface. The total current represents the simple vector sum of the geostrophic and Ekman drift components. The geostrophic component of a current is derived from the simple balance between the pressure gradient force and and the Coriolis effect and the ekman component is net 90° offset of wind driven flow due to the interaction between wind driven inertial flow, the Coriolis effect and friction (Stewart, 1997). The Globcurrent Total Hs Currents is provided at a 0.1 spatial resolution and a 3-hourly temporal resolution which was averaged into a daily product.

More data will be added, in order to improve accuracy, in due time but for the purposes of this investigation all of the data available is used. An important caveat that must be considered when using the Globcurrent data is the fact that, during the process used to create the global current data, interpolation and filtering of the products during the assimilation process would result in a loss of accuracy in the data. It has been acknowledged by the creators of the Globcurrent dataset that, particularly for the Agulhas Current, the overall magnitudes of current flow can be as much as $1m/s$ slower than the true speeds of the current. There is also a notable widening in the current structure. This must be taken into consideration when using the Globcurrent data in a comparative nature (Danielson et al., 2014).

## 3.2 Method

### 3.2.1 Data Evaluation and Identification of Study Region

In order to adequately represent the ability of the ASAR dataset to capture the mean wind fields and thus investigate the mean effects of the Agulhas current on the various wind regimes, sufficient data must be used. As previously shown in Figure 3.1, the spatial coverage of the ASAR dataset varied greatly, from as low as 30 readings in peripheral areas, to as high as 297 readings in the central region off of the East Coat of South Africa. As a result, major discrepancies between the mean CFS and ASAR winds are found in the regions of low data coverage (Figure 3.2). For this investigation, only regions in which the number of valid observations per pixel exceeded 150 are selected. The resulting domain of study is

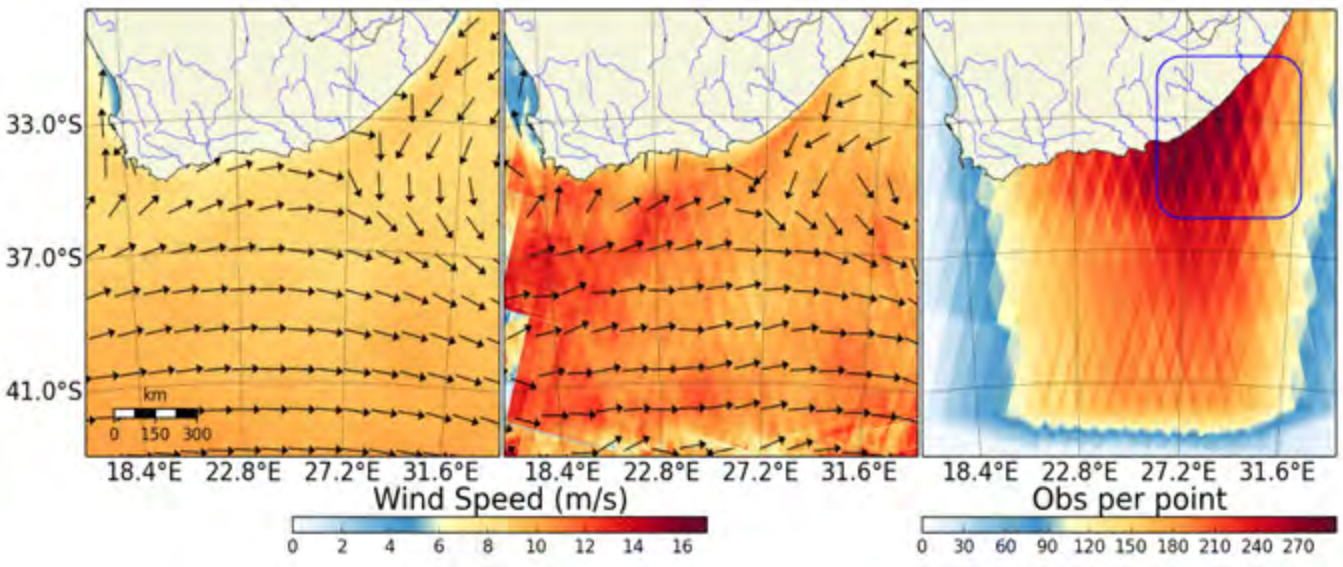


**Figure 3.2:** Scalar wind speed of CFS (left) and ASAR (middle) and data density (right) temporally averaged for the entire study period. Wind direction is represented by the black arrows (Not to scale). Blue square represents the chosen study location with the highest data density.

thus reduced to the area represented by the Blue Square in the third panel of Figure 3.2.

### 3.2.2 Locating locations of Interest

Within the location of highest data density, demarcated by the blue square in Figure 3.1, six locations (White, labelled boxes in Figure 3.3) are selected as key locations of interest in order to improve our estimation of the impact of the Agulhas Current on wind speeds along the coast of South Africa. This is done by selecting the regions with both the strongest current signature and the highest volume of reliable ASAR data. The locations, depicted in Figure 3.3, are located directly above the core of the Agulhas Current (estimated to be located at the maximum SST values) and are set at evenly space intervals along the entire east coast. This ensures that the entirety of the Northern Agulhas' varying properties were represented in the most efficient way possible. The designated regions for each location are set at a standard size of $0.4°lat \times 0.4°lon$.

A plot of the mean MODIS SST, averaged over a 14 year period from 2000-2014, is used as a general proxy of the mean location of the core of the Current (Represented by the blue line in Figure 3.3). MODIS data is used because the long period of high resolution data available allows for accurate identification of the core of the Agulhas Current.

The data within each location of interest for each swath is spatially averaged for the entire study period. The mean wind direction for each swath at each location of interest

is then calculated and grouped, according to its mean direction, into one of four direction regimes. The upcurrent and downcurrent regimes are parallel to the core of the current and perpendicular to the transects (Black lines in Figure 3.3). The crosscurrent east and crosscurrent west regimes are perpendicular to the core of the current and parallel to the transects. The data are grouped into the four direction regimes in order to isolate the along current conditions required to investigate the current relative effect as described by (Kelly et al., 2001, 2005) and (Plagge et al., 2012). Secondly the regimes are used to investigate the cross current effects off SST changes as suggested by (Jury and Courtney, 1991) and (Rouault et al., 2000). The specific bearing of the direction regimes for each location are set individually so as to ensure that the along current regimes are parallel to the mean current flow at the exact location of each location and consequently the crosscurrent regimes are perpendicular to the flow. Grouping the winds also enables winds of similar directions to be investigated in comparison to each other so that a mean effect is identified. The grouping also eliminates the temporal variation in wind events as the events are classified by their directional properties and not time of occurrence.

An accuracy threshold of $\pm 15^{\circ}$ on either side of the bearing of the direction regimes is used in order to maximise the amount of data used whilst reducing the ambiguity of having wind directions with too great a deviation from one of the four regimes. The qualifying events are then further refined using vector component geometry in order to extract the component which is exactly parallel to the regime direction. This serves to standardise the wind directions and reduce high inter-event variability. All wind directions which fall outside of the regime thresholds are discarded as their regime specific component does not show a true regime specific effect.

### 3.2.3 Identification Ocean features in the Wind Signature

In order to assess the viability of the full study, it is necessary to conduct an initial investigation into the post processed ASAR data to detect whether any sign of visually obvious mesoscale ocean features and patterns within the individual swaths are identifiable (Figure 4.3). The appearance of such features will suggest that there is indeed evidence of an influence of oceanic forcing on the surface roughness of the ocean and, in turn, an effect on the NRCS signatures and resulting derived wind speed. In order to qualitatively assess the occurrence of mesoscale atmospheric features within the data and their possible connection to the underlying ocean features, individual swaths of the ASAR derived scalar wind speed and wind direction vectors are plotted in comparison to the corresponding daily averaged OSTIA level 4 interpolated product. OSTIA SST contours are then overlaid on the ASAR data in order to visually identify any similarities between the mesoscale oceanic features

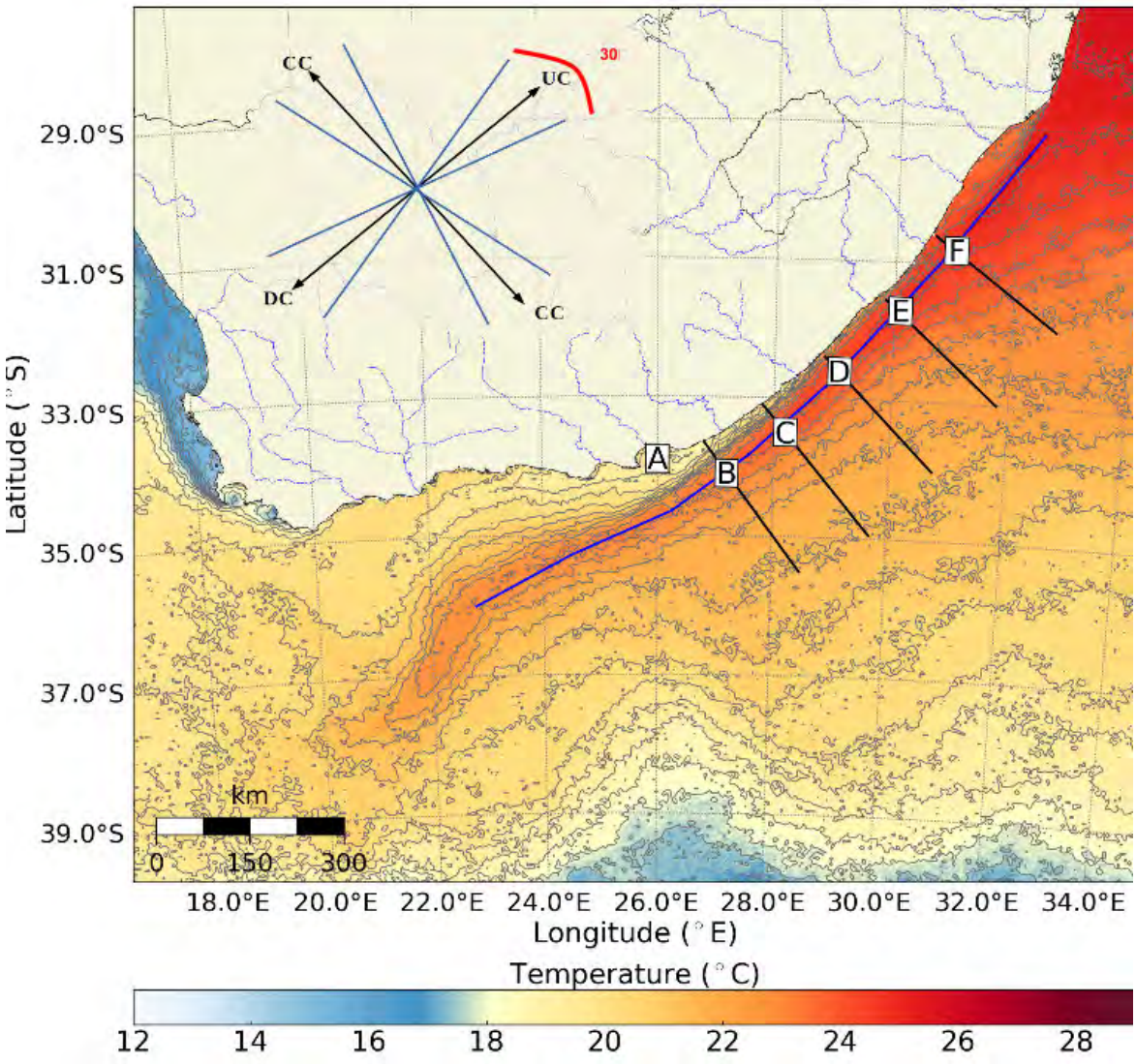


**Figure 3.3:** Mean MODIS SST over the greater Agulhas region for the period 2000-2010. (filled contours). Blue line represents a general proxy for the location of the core of the Agulhas Current. Black lettered squares (A to F) mark the locations of interest. The red lines indicate the location of the transects. Black arrows of the inset represents and indication of the four direction regimes within which the spatially averaged wind data was grouped. Angles of the direction regimes vary with each location so that the along current regimes are always parallel to the current. Blue wedges represent the threshold with which each direction regime was assessed.

present and visible features in the wind speeds or direction. Secondly the CFS data were co-plotted with the overlying OSTIA SST product in order to serve as a comparative reference of ASAR's superior feature resolving ability.

### 3.2.4 Wind Speed and Direction Frequency Wind Roses

To assess the validity of the model directions input into the CMOD5.n model during wind speed derivation, the CFS model data is compared to that of the ASCAT derived wind speed and direction for the same locations of interest (Figures 4.1 a and b). Once the data are sufficiently refined to reduce all unnecessary variability as described in section 3.2.2, the spatial mean from each location of interest is plotted as a wind rose of the frequency of intensity grouped wind velocities for the entire study period. The wind roses are split into 16 compass directions and 7 intensity categories ranging from $0m/s$ to $\geq 18m/s$ and plotted as a percentage frequency.

In addition to verifying the reliability of the mean direction regimes of the CFS model data against ASCAT, wind roses are plotted of the ASAR derived wind speeds in order to facilitate a comparison between the apparent mean wind speed differences between the ASAR derived data over the current and the CFS model (Figures 4.1 b and c). Comparisons are also made between the ASAR derived wind speeds and direction and the ASCAT derived data (Figures 4.1 a and c).

### 3.2.5 Total Wind Speed Intensity Frequency Assessment

To investigate the ability of ASAR to better resolve more realistically intense wind speeds over the Agulhas Current, the overall scalar wind speed intensities for all locations of interest are calculated as a percentage of the total number of observations for each location. The wind speed intensities from each of the ASAR, CFS and ASCAT datasets, are grouped into 7 bins of wind speeds from 0m/s to >18m/s and plotted as bar graphs for each location of interest (see Figure 4.2).

### 3.2.6 Spatial Variation Transects

The spatial variation of wind speed over the current is investigated through constructing transects which runs perpendicular to the current and intersects each location of interest. Each transects bearing is set so that the transect intersects the core of the current (Blue line in Figure 3.3) at 90°. This serves to ensure that the previously classified direction regimes are compatible with the transect. The transects for each location varied in length in order to

accommodate the widening in the Agulhas current further North and still include a significant area of open water, free from the Agulhas's influence, for the purpose of comparison.

Initially, the scalar wind speed is plotted for each direction regime as individual case studies of the scalar wind speeds. This facilitates a case by case qualitative investigation and comparison. A temporal mean is then calculated to illustrate the average spatial change in wind speed over the current versus open water (see Figure 4.8). Error bars indicating the average temporal standard deviation from the mean for the entire study period are included to show the high variation in wind speed throughout the study period.

All mean and individual transect data are plotted against corresponding SEVIRI SSTs for the same period as a proxy for the location of the core of the Agulhas Current and its boundaries. The individual case studies which are selected are co-plotted against the Globcurrent surface current velocity components perpendicular to each transect in order to facilitate a better comparison of the effects of current velocity and SST changes on wind speeds over the current.

Secondly, to try to reduce the standard deviation of wind speed intensity and to investigate the relative effect of varying wind speed on the wind speed changes over the current the wind regimes are further grouped into 4 wind speed intensity categories. These categories ranged from less than 5m/s; 5-10m/s; 10-15m/s and greater than 20m/s. The wind intensity categories are averaged and co-plotted against the SEVIRI SST data as well.

# Chapter 4

# Results

## 4.1 Time Averaged ASAR Wind Field Properties

### 4.1.1 ASAR wind directions:

As stated in Section 3.1.3, wind directions in the ASAR dataset are externally sourced from the CFS wind reanalysis. To evaluate the CFS wind directions, and hence the ASAR wind directions, comparisons were made between the CFS dataset and those from the ASCAT which derives its own direction.

The CFS winds show a distinct bipolar pattern for all locations (Figure 4.1b) with the two dominant wind directions flowing along a northeast-southwest axis parallel to the current. The only exception is the location furthest south (location F) where a shift to a more Westerly direction is observed. For all locations, including location F, the winds are aligned with the current flow 43% and 52% of the time. The ASCAT wind roses (Figure 4.1a) show similar characteristics to that of the CFS data. The dominant directions for locations C, D, E and F also show a strong Northeast, Southwest pattern but locations A and B display a clockwise shift to a more east-west pattern.

### 4.1.2 ASAR wind speeds:

The strongest wind speeds for ASAR fall mostly in the $6-9m/s$ ($27.94\pm2.78\%$) intensity range, with a near equal amount falling between $3-6m/s$ ($21.76\pm6.01\%$) and $9-12ms$ ($17\pm2.49\%$)

The CFS winds at the selected sites are generally moderate to weak with most wind speeds below $10m/s$ (Figure 4.2). Wind speeds greater than $12m/s$ only make up less than 20% of the observations with rare occurrences (less than 1%) of gale force winds (Fig-

ure 4.2). The frequency of the higher intensity winds is much lower than other intensity brackets, particularly the $< 18m/s$ regime which only occurred a total of $0.53 \pm 0.59\%$ of the time. (Figure 4.2). Similar wind distributions are seen in the ASCAT dataset, with a predominance of moderate to weak winds and even less occurrences of high winds. In the ASCAT dataset, wind speeds greater than $18m/s$ occur only make up $0.16 \pm 0.24\%$ of the dataset.

The major differences between ASAR and CFS is the higher frequency of higher intensity events, for example in the $15-18m/s$ bracket ($6.54 \pm 2.71\%$ Avg) and greater than $18m/s$ bracket ($6.12 \pm 3.97$) which are $4-5\%$ higher overall. More importantly, the increased frequency of high wind speeds is along both the northeast and southwest dominant direction regimes. The upcurrent and downcurrent regimes which are both parallel to the current. This illustrates that the NRCS signal captured by ASAR and the resulting derived wind speed is, on average greater than that of the CFS data.

The ASAR dataset also had a much greater frequency of high intensity winds than the ASCAT dataset, despite the fact that both datasets were derived using the same the same Bragg scattering principle and similar GMF's. The only notable difference between the two datasets is the spatial resolution and wind directions used as inputs before applying the GMF.

The ability of SAR over ASCAT to better detect more intense events with greater accuracy due to the increased resolution is illustrated by the wind rose plots and bar graphs. This ability however, is dependent on the accuracy of the wind direction inputs used in the SAR wind speed derivation. The wind direction inputs used in the SAR derivation are shown to be representative of the observations and thus appropriate for use in the wind processing. The increase in wind speed intensities detected by the SAR data itself does not provide any further knowledge as to the nature of the cause of the wind speed increases investigate in section 4.2. Thus further investigations into the spatial variations in wind speed across the current are needed. The spatial variation of winds speed in different directions relative to the current are presented in section 4.3

Before continuing with the investigation, it was decided that locations A and F were to be excluded from the remainder of the investigation as location A was centred inside Algoa bay, which was poorly resolved in both the CFS and ASCAT data, and location F contained insufficient data.

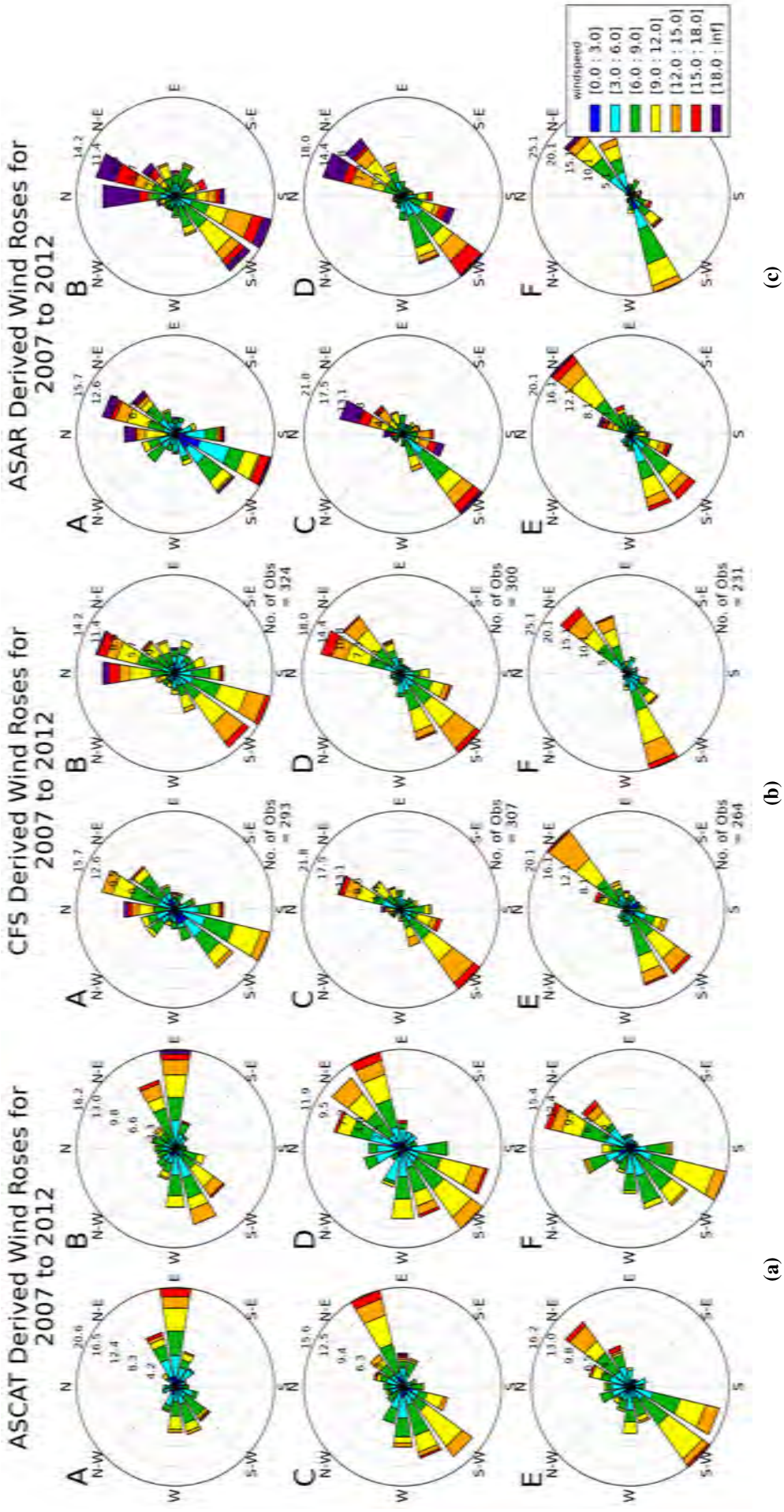


**Figure 4.1:** Percentage Frequency wind roses of the spatially averaged wind speed and direction from ASCAT (a), CFS (b) and ASAR (c) for the 6 locations of interest (Labelled A-F) over the period 2007-2012. The number of observations per wind rose is annotated to the bottom right of each plot. The colour bar denotes the intensity of each the wind event (See legend) and the rings denote the frequency of each event. Note, the wind directions for CFS and ASAR are the same as the direction input for CMOD is from CFS. **Coordinate positions of Locations of Interest: A.** 33.9°S, 26.0°E; **B.** 34.1°S, 27.2°E; **C.** 33.5°S, 28.2°E; **D**. 32.6°S, 29.1°E; **E.** 31.7°S, 30.1°E; **F.** 30.8°S, 31.0°E

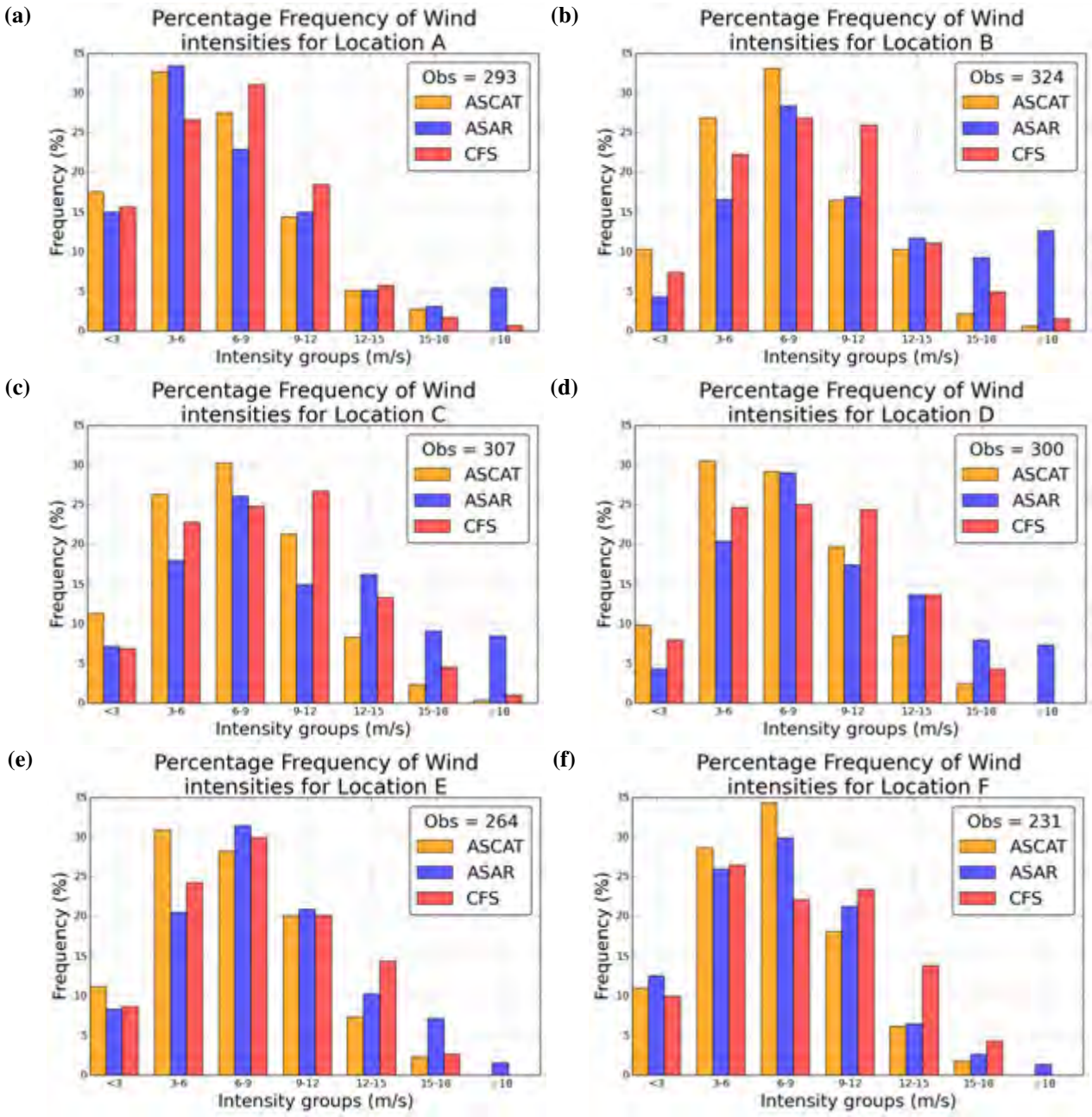


**Figure 4.2:** Percentage frequencies of overall scalar wind speed intensities from ASCAT (green), ASAR (blue) and CFS (red) for the 6 locations of interest (Labelled A-F) over the period 2007-2012. Wind speed intensites are grouped into 7 bins of 3m/s intervals. **Coordinate positions of Locations of Interest: A.** 33.9°S, 26.0°E; **B.** 34.1°S, 27.2°E; **C.** 33.5°S, 28.2°E; **D**. 32.6°S, 29.1°E; **E.** 31.7°S, 30.1°E; **F.** 30.8°S, 31.0°E

## 4.2 Ocean current signatures in the ASAR wind fields

The primary objective of the research presented in this thesis is to investigate the signature that strong ocean current features, such as the Agulhas Current leave in surface wind fields derived from satellite observations. The following figures represent three individual case studies selected in order to illustrate how satellite derived wind field observations vary in the presence of strong ocean mesoscale features. The three plots follow the southward progression of a single Natal Pulse in the Northern Agulhas over a period of 25 days and under various wind speed and direction conditions.

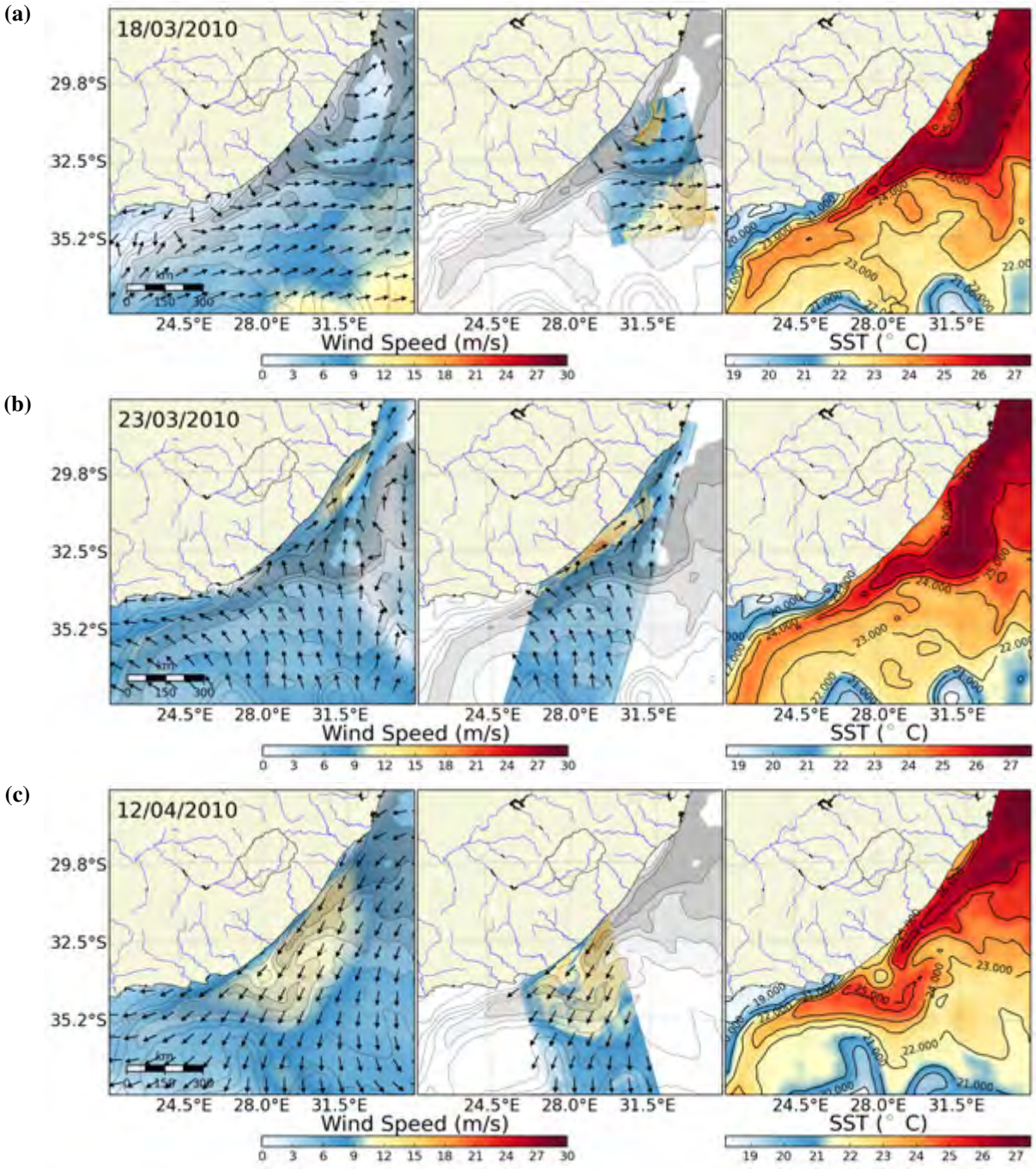


**Figure 4.3:** CFS (left) and SAR (middle) derived scalar wind speed versus OSTIA daily averaged SST product (right) for 18/03/2010 (a), 23/03/2010 (b) and 12/04/2010 (c). Grey and black contours represent the 1°C isotherms for the OSTIA data. The grey overlay highlights the area between the 24°C and 26°C isotherms. Black standardised arrows represent wind direction and are not to scale.

The influence of the oceanic mesoscale circulation on the estimated wind speeds is clearly seen in all of the plots in Figure 4.3. In all instances, increases and decreases in wind speeds occur near regions of strong SST gradient. These accelerations follow the shape of the Agulhas Current as it meanders offshore during the Natal Pulse but the response of the winds to the SST distribution are complex and nonlinear. The direction of the wind event does however, to have an influence in the nature of the increase in wind speed as well as where it increases over the current.

ASAR Winds on 18 March 2010 (Figure 4.3a) vary between about $15m/s$ and $8m/s$ with the strongest winds observed offshore over the open ocean and at the Agulhas Current's inshore boundary. The wind is blowing predominantly offshore with a northwesterly direction directly at the coast and a shift to a more westerly direction over the current and further out to sea, and then a more southwesterly direction further offshore. The wind speeds are moderate at approximately $8m/s$. In the western region of the ASAR swath, the Agulhas Current is "hugging" the coastline and the magnitude of the winds changes little as one moves from the coast, over the Agulhas Current and into the open ocean. Further north, between 31°S and 31.6°S however, we observe a strong wind intensification from the cooler coastal waters to the warm waters of the Agulhas Current, and with a near doubling increase to approximately $14-16m/s$ over the current. This increase in wind speed occurs on the inshore boundary of the current as the wind crosses it in a primarily crosscurrent direction and coincides with a rapid change in SST from approximately $24°C$ to over $26°C$. Interestingly the wind speeds decrease again to approximately $8m/s$ past the region of strong SST gradient at the Agulhas Current's inshore front and while still over the current proper. The increase evident in the ASAR data is not seen at all in the accompanying CFS wind plot. Further offshore, it is also underestimated.

In Figure 4.3b, the predominant wind direction over the current is southeasterly with a shift to a more south-southwesterly further north. The wind speeds over the entire ASAR swath are again, moderate at approximately $7m/s$. Closer to the coast and between latitudes of 33.5°S and 30.3°S the wind speeds up significantly to around $17-18m/$s over the current. The greatest change in wind speed also occurs over the inshore boundary of the current, mainly to the south of the meander where the current's southwest flow direction is directly against the wind direction. Again, the CFS data underestimates the wind speed increase over the current. However the location is correct.

The most significant signature of an influence on wind speed in relation to the meander in the current is observed in Figure 4.3c, where the spatial distribution of wind increases reveals the shape of the Agulhas Meander. Wind speeds away from the current range around approximately $8-9m/s$ with an increase over the current to approximately $13-15m/s$.

The wind regime of the event is almost entirely northeasterly and thus downcurrent over the Agulhas. The wind speed increase over the current are not entirely restricted to the inshore boundary of the current but rather appears to span over the entire current width. Over the core of the Agulhas meander, the wind speed decreases to between $11m/s$ and $9m/s$. This corresponds to a drop in SSTs from $26°C$ to $23°C$ in the core of the meander. The accompanying CFS wind data does represent the wind speed values relatively well although still with a minor underestimation. The small scale wind speed troughs are not evident at all. In the wind data, the region of weaker winds within the cold Agulhas Meander core is not symmetrically rounded, as portrayed in the SST data. Meanders in the Agulhas Current are often associated with warm water plume at their leading edge flowing towards the northeast (Lutjeharms, 2006b). It is likely that the region of intensified winds near the shore in Figure 4.3c highlights the region of warm waters associated with the Agulhas Current warm water plume. That such a feature is not picked up in the daily merged SST product is hardly surprising. Both infrared and microwave SSTs observed from satellites are severely challenged in the coastal region of the Agulhas Current (Krug et al., 2014) and the spatial and temporal interpolation required to produce cloud free merged SST products such as that used in Figure 4.3 can smooth or misrepresent oceanic features near the coast.

The case studies presented here highlight the complexity of categorising ASAR wind speed signatures based on the SST surface fields. What the selected case studies suggest however is that the response of the wind speed to specific ocean features appears to be dependent on wind direction. In order to adequately assess how the oceanic mesoscale circulation may affect derived SAR wind fields through either geophysical air-sea interaction processes and/or roughness modifications, it is therefore necessary to study the separate impact of different wind directions regimes. The output of this further research is presented in the section below.

## 4.3 Impact of the Agulhas in Different Wind Direction Regimes.

For each wind direction regime, three ideal case studies were selected from the pool of 987 swaths. The case studies displayed the most constant bearing over the entire Agulhas cross-section to better isolate the effect of changing SST values and the relative motion of the current might have.

The mean wind speed for each wind direction, at each location was then assessed in order to ascertain whether a general average relationship between any wind speed changes

in the transect and the location of the core of the Agulhas Current could be found. This was executed for each wind direction regime. For the mean wind variability, only the SST data was used as the Globcurrent data was not available for the entire study period and thus would result in a biased mean.

### 4.3.1 Case Studies

#### 4.3.1.1 Upcurrent

Three individual case studies were selected to illustrate the impact of upcurrent winds on the ASAR derived wind speeds. It was at locations B (Figure 4.4a and b) and C (Figure 4.4c), where the current is narrowest and most intense, that the influence of the Agulhas Current on the ASAR wind speeds in an upcurrent wind configuration was most striking. Figures 4.4a and c are relatively intense wind events, displaying peak wind speeds close to $20 m/s$ whereas Figure 4.4b is of moderate intensity with the maximum wind speeds reaching only $13 m/s$. All three transects displayed a sharp increase in wind speed on the shoreward boundary of the current.

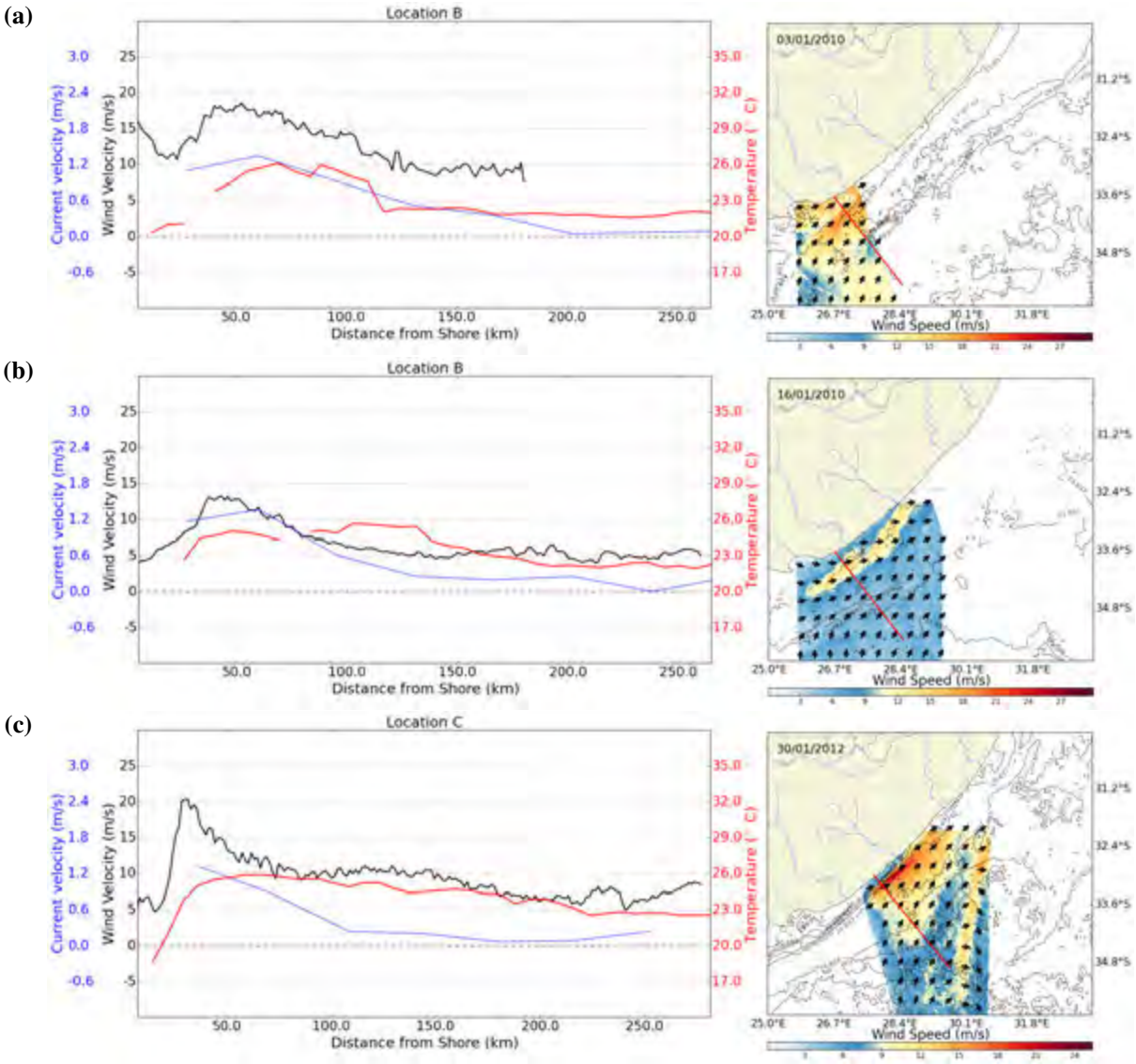


**Figure 4.4:** Transects of individual case studies of the upcurrent scalar wind speed component (Black) versus distance offshore over locations B (a and b) and C (c) co-plotted against the underlying SEVIRI SST (Red) and Globcurrent surface current speed (Blue). Current speed is a scalar value of the ocean current perpendicular to the transect in a south westerly flow direction. Accompanying map represents the scalar wind speed (color) and scaled directional arrows (Black) for the region containing the transect co-plotted above the SEVIRI SST contours (grey).

The wind speeds change patterns for each of the transects do differ comparatively, however, the two transects from location B (Figure 4.4a and b) do exhibit a more similar pattern of increase to each other than in comparison to Location C (Figure 4.4c). This is characterised by a sharp increase in wind speed on the inshore side of the core of the Agulhas at approximately 40$km$ offshore, directly over an increase in the SST values of approximately $4-5°C$ and current speeds of only approximately $0.3m/s$. The wind speed increases to a distinct but rounded peak of approximately $18m/s$ for Figure 4.4a and $13m/s$ for Figure 4.4b. The wind speeds then decreases more gradually further offshore. The underlying current velocities decrease more rapidly than the wind speed values in both 4.4a and b. Figure 4.4b has a steeper, more concave gradient of roughly $0.24m/s$ per 10$km$ compared to Figure 4.4a which displays a more linear $0.09m/s$ per 10$km$ decrease. The corresponding pattern of decrease between the wind speed and current speed is similar for each transect. The wind speeds in Figure 4.4a appear to decrease more linearly whereas the wind speeds in Figure 4.4b have a more exponentially curved shape decrease.

The SST values do not appear to decrease further offshore in the same pattern as either the current speeds or the wind speeds (Figures 4.4a and b). For Figure 4.4a, the SSTs drop fairly rapidly from $26°C$ to $22°C$ and then begin to even out around 130km offshore. Figure 4.4b however exhibits an increase in SSTs from $24.6°C$ over the core of the current to nearly $26°C$ a further 100km offshore. This lesser decrease in SST values can be seen to manifest slightly in the wind speed values further offshore, where the wind speed values begin to diverge from the current speeds, however the increase in SSTs in Figure 4.4b does not seem to elicit a corresponding increase in the wind speeds.

The transect from location C (Figure 4.4c) exhibits a different pattern in wind speed changes from the previous two transects, and is is characterised by a much sharper peak to approximately $20m/s$ but much closer to shore (Approximately 20$km$). This sharp increase in wind speed is located directly over a sharp increase in SST values, from $19°C$ to $26°C$ in 40$km$, as well as the current speed maxima for the transect. The current speed does not appear to increase from the coast at all, but rather starts off at a higher value of $1.2m/s$ and then decreases concavely to $0.2m/s$ in approximately 80$km$. On the immediate oceanward side of the wind speed maxima, the wind speeds drop relatively sharply in comparison to the two previous transects, however the gradient of decrease is still not as extreme as the inshore increase. This is then followed by a much more gradual decrease in wind speed further offshore. The sharp decrease in wind speed appears to associate with the decrease in current velocities on the oceanward side of the current as current speeds drop to nearly $0m/s$ about 130$km$ offshore. Conversely, the SST values offshore remain relatively high and only gradually decrease from their maxima at the current core in a convex pattern to a low

of 22.8°$C$ over 220$km$ offshore. The more gradual wind speed decreases, away from the sharp peak, appear to follow the changing SST values better that the current velocities as they decrease in a convex fashion as well.

Importantly, all three winds speed patterns seem to relate well to a combination of the shape of the SST gradients and the current speeds over different parts of the current cross-section. Over the core of the current and the inshore boundary, the wind speed increases are more dependent on the relative motion of the current than on the influence of SSTs on the overlying atmosphere. Further offshore where the influence of the current is less strong, the wind speeds appear to be more affected by the changing SST values.

#### 4.3.1.2 Downcurrent

The three best individual case studies for the downcurrent wind direction regime were selected from locations B (Figures 4.5a and b) and D (Figure 4.5c).

Unlike the upcurrent regime, the wind speed patterns for the three downcurrent case studies do not appear to display sharp peaks in wind speed values on the inshore boundary of the current. Each of the case studies from location B (Figures 4.5a and b) exhibit a more flat tabletop like structure. The transect from location D (Figure 4.5c) displays a more irregular pattern. Each transect also ranges in the moderate mean wind speed range of between 10 to 15$m/s$.

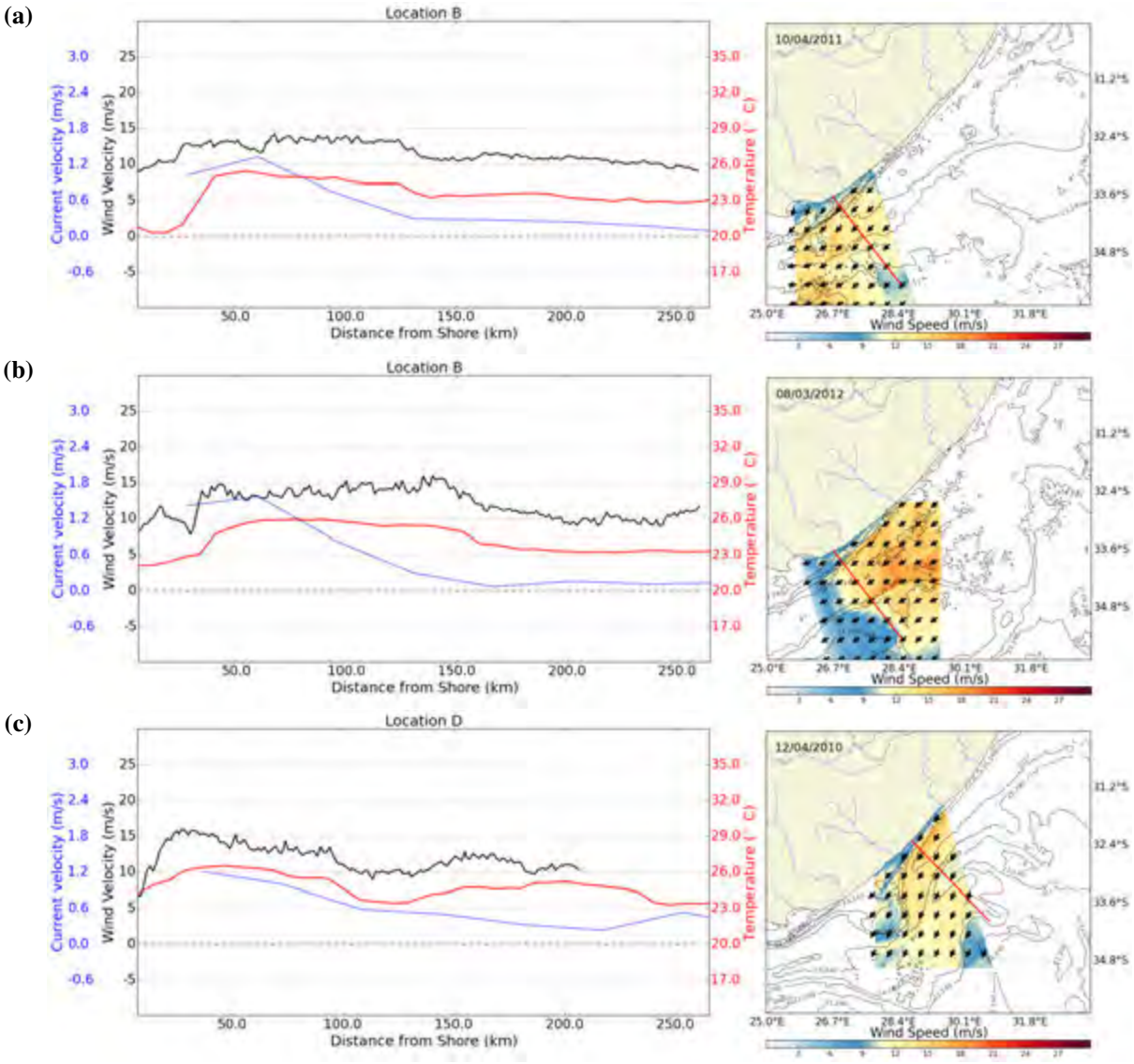


**Figure 4.5:** Transects of individual case studies of the downcurrent scalar wind speed component (Black) versus distance offshore over locations B (a and b) and D (c) co-plotted against the underlying SEVIRI SST (Red) and Globcurrent surface current speed (Blue). Current speed is a scalar value of the ocean current perpendicular to the transect in a south westerly flow direction. Accompanying map represents the scalar wind speed (color) and scaled directional arrows (Black) for the region containing the transect co-plotted above the SEVIRI SST contours (grey).

The transects all show a distinct inshore and offshore front of wind speed changes. These fronts are associated with wind speed changes of up to $6m/s$ in some cases with the wind speeds between the inshore and offshore fronts appearing relatively constant.

The strongest inshore to offshore gradients in wind speeds are observed in Figure 4.5a. The change in wind speed is approximately $4m/s$ on both sides with a further decrease in wind speed closer to the coast after a slight flattening out. The most noticeable similarities between the wind speed and the current properties is the much closer pattern of change in the SST values. Changes in SST coincide with those in wind speed with a similar tabletop like structure. Temperatures range between $25.4°C$ and $24.5°C$ and increase and decrease in nearly the exact same places as the wind speed changes ($30km$ and $130km$ offshore). The inshore decrease in SST is, however much greater than the offshore changes as it decreases to $20.2°C$. from $25.5°C$ in $40km$. The offshore decrease in SST is only by $1.4°C$.

Surprisingly, the shape of the current speed changes does not appear to be similar to the wind speed changes at all. In fact, when the current speed decreases in much the same concave way as in the upcurrent regime (with a gradient of $0.13m/s$ per $10km$), the wind speeds do not appear to react to the change at all.

The same wind speed pattern and relation to the SST and current property changes is true for Figure 4.5b. The wind speeds values exhibit a distinct table top like pattern, albeit slightly more irregular. The distinct relation between the wind speed changes and the SST pattern is also evident as the wind speeds increase by $7m/s$ in $15km$ on the inshore boundary and decrease by $5.1m/s$ in $50km$ directly over the sharpest SST gradients again ($35km$ and $150km$ offshore). The SST decrease on the inshore boundary is not as intense as in Figure 4.5a, and the SSTs decrease by less than $4°C$ but over a greater distance of over $50km$. The offshore SST decrease is similar to Figure 4.5a with a $1.1°C$ over approximately $7km$. Again, the rapidly changing current speeds appear to have no relation to the wind speed values.

For Figure 4.5c, the wind speed change pattern is quite substantially different from the two previous transects, however the SST patterns are also different in shape. The underlying SSTs for this transect do not display one single increase but rather two gradually sloping dome like features. The first dome corresponds to a increase of $2.5°C$ over $30km$ and peak SSTs of $26.5°C$. The second dome has a lesser increase and a shallower gradient, only reaching $25°C$ from $23.5°C$ over $70km$. This twin-dome like increase is also evident in the wind speed values which appear to closely follow the SST pattern along the entirety of the transect. A minor exception is the fact that on the shore side of the first wind speed and SST peak, where the inshore boundary of the Agulhas is located ($20km$ offshore), the peak wind speeds display a much greater increase than their corresponding SST values of 12m/s

from the coast to the maximum at 35$km$ offshore. Over the core of the current, between 30$km$ and 100$km$ offshore, the SST values are high with distinct fronts on either side of the current and an increase of nearly 2.8°$C$ on each front. This increase in SSTs is congruent with a similar increase pattern in wind speeds of up to 6$m/s$ over the same location. Further offshore, between 100$km$ and 150$km$ the SSTs dip back to 23.5°$C$ before rising again by 1.5°$C$ to 25°$C$. The wind speed increases clearly correspond with a similar dip in wind speeds of nearly 3$m/s$ before increasing again to 12$m/s$.

Finally, as with the previous two transects, the current speeds do not appear to have any effect on the changes in wind speed. The gradient of decrease in speed is shallower than the previous transects at 0.07$m/s$ per 10$km$ and there is a step in data at 120$km$ offshore

The spatial distribution of the wind speed to temperature correlation is best illustrated in the accompanying maps for all three figures but especially in Figure 4.5b. It can be clearly seen that a band of faster wind speeds is evident which closely follows the patterns of the underlying isotherms in grey.

Thus it appears that the influence of changing SST values on the overlying atmospheric boundary layer and the resultant influence on wind speeds is the primary driver of wind speed increases over the current. There appears to be little influence on the wind speeds by the relative motion of the current to the wind speed.

#### 4.3.1.3 Crosscurrent West

The case studies extracted for the crosscurrent west regime were selected from locations B (Figure 4.6a and b)and D (Figure 4.6c).

The shape of the wind speed increases and patterns in comparison to each other for all three case studies are much more irregular and dissimilar than each of the three case studies selected for the upcurrent and downcurrent regimes. This is due in part to the much lower data availability which limited the choice of ideal situations. The three transect also have variable mean wind speeds although they are all moderate to low-none of them range above 10$m/s$ on average.

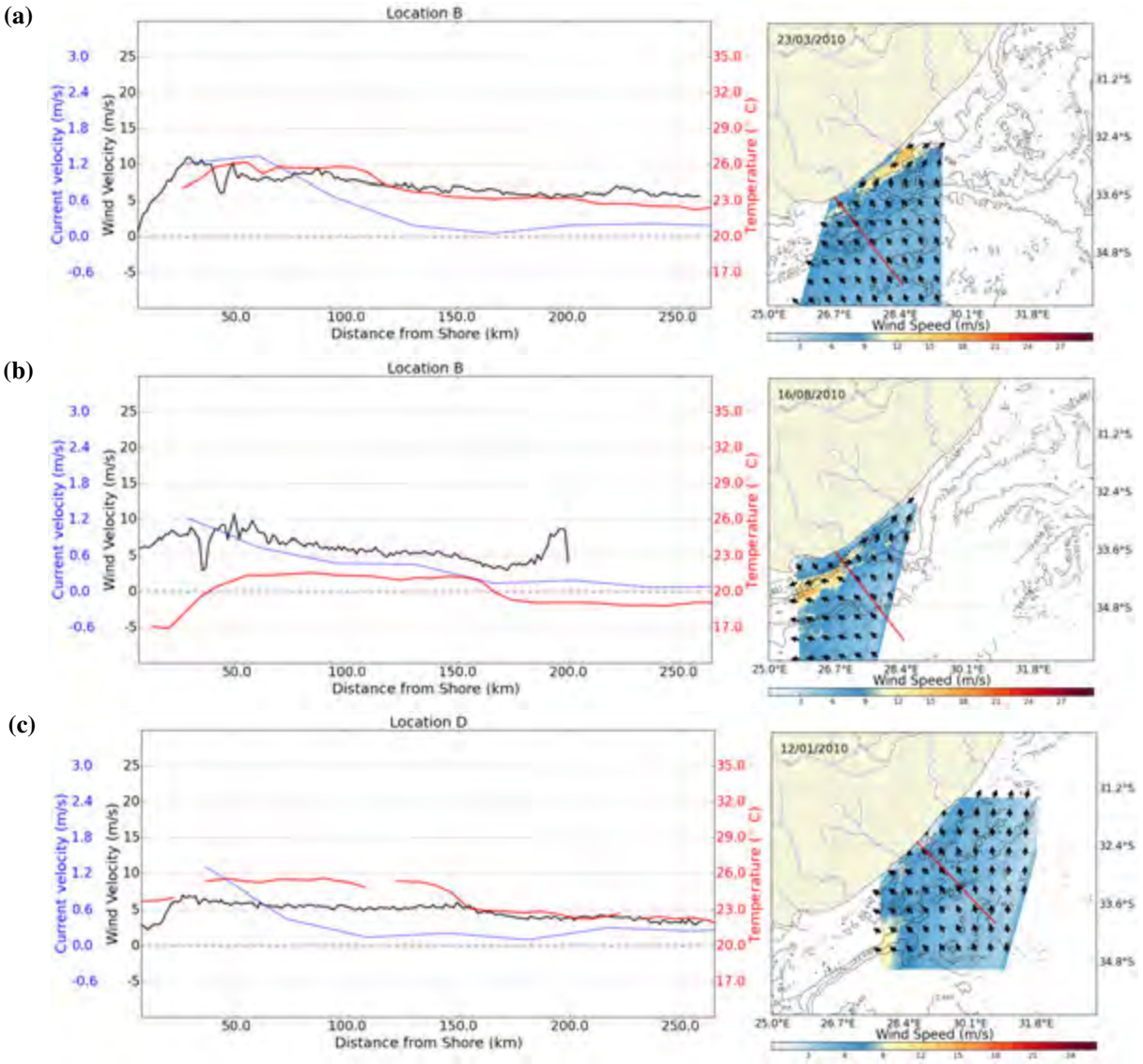


**Figure 4.6:** Transects of individual case studies of the crosscurrent west scalar wind speed component (Black) versus distance offshore over locations B (a and b) and D (c) co-plotted against the underlying SEVIRI SST (Red) and Globcurrent surface current speed (Blue). Current speed is a scalar value of the ocean current perpendicular to the transect in a south westerly flow direction. Accompanying map represents the scalar wind speed (color) and scaled directional arrows (Black) for the region containing the transect co-plotted above the SEVIRI SST contours (grey).

All three case study transects in Figure 4.6 appear to exhibit minor spikes in wind speed along the transect with little apparent relation to either the SST data or the ocean current data.

Figure 4.6a exhibits a sharp wind speed gradient on the inshore boundary of the Agulhas with an increase from nearly $0m/s$ at the coast to just above $10m/s$ at $25km$ offshore. The peak wind speeds are not however located over the maximum current speeds or SST values which are located further offshore at $65km$. Further east of the peak the wind speeds do not appear to decrease drastically when the current values decrease nor do the wind speeds change when the SST values fluctuate. Rather they gradually decrease over a long distance far offshore. There is a minor increase in wind speed from $8m/s$ to $10m/s$ $80km$ offshore, in a region of high but decreasing current speeds. In the accompanying map plot (Figure 4.6a) the lack of noticeable wind speed change over the transect is apparent. Interestingly, a definite increase in wind speed can be seen further north. This increase in wind speed is also associated with a change in the wind direction of almost 90°to a southwesterly direction.

The wind speed gradient on the inshore boundary of the current is not as sharp in Figure 4.6b, with an increase of approximately $4.5m/s$ over $50km$, however, there is still definite increase to a wind speed maxima of approximately $10m/s$. The wind speed peak does not appear over the maximum current speeds but it does occur at the climax of the steep inshore SST gradient of the current where the inshore increase of SSTs is over $4.5°C$ in $45km$. Further offshore, the wind speeds do decrease in magnitude although quite gradually. At between$140-165km$ offshore, a wind speed change of $3m/s$ does appear to coincide with both a drop in SSTs of $3°C$ and a decrease in current speeds of nearly $0.6m/s$, however the decrease is not as substantial as either of the ocean properties. Similar to Figure 4.6a, the lack of wind speed change is apparent in the accompanying map plot of Figure 4.6b. Also similar to Figure 4.6a, but to the south of the transect this time, a definite increases in wind speed can be seen. This, again, is associated with a change in the wind direction to the northeast this time.

The final transect in Figure 4.6c, displays the weakest wind speeds with a maximum of approximately $7m/s$. It is also the least irregular transect with little sharp or substantial increases in wind speed with the exception of the sharp wind speed increase of $4m/s$ right at the coast. The wind speed remains relatively constant across the entire transect, with almost no apparent influence of current speed changes, until approximately $150km$ offshore where a substantial decrease in SSTs values of $2.5°C$ does appear to coincide with a minor decrease in winds speed of approximately $1-2m/s$. The accompanying map plot for Figure 4.6c does not show any increase or dramatic wind speed changes across the entire region.

The wind speed changes presented in the crosscurrent west case study did not show any

significant increases in wind speed. Although there appears to be a minor influence of SST values on the wind speed changes over the current in certain of the case studies, the results are not as clear as those in sections 4.3.1.1 and 4.3.1.2.

#### 4.3.1.4 Crosscurrent East

The three case studies for the final wind regime, the crosscurrent east regime, were selected from the smallest dataset due to the low occurrence of a northwesterly wind over the Agulhas region. The best results were chosen from locations B (Figure 4.7a) and C (Figures 4.7b and c). All three wind events experience moderate to low wind speeds at between $5-8m/s$. The wind speed patterns for all three wind events display no distinguishing features and no real pattern can be discerned. The lack of the sharp wind speed change at the coast is especially notable.

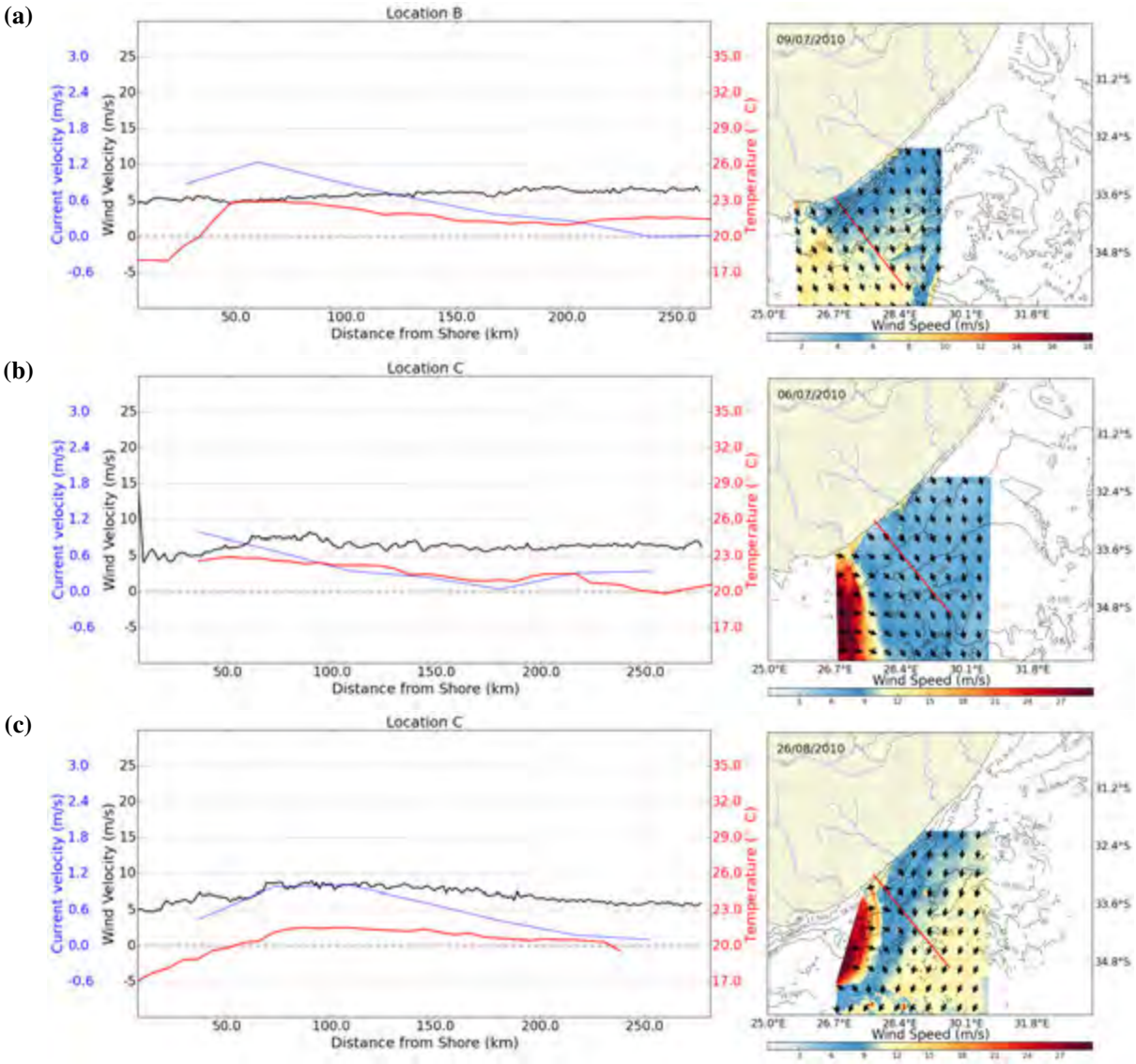


**Figure 4.7:** Transects of individual case studies of the crosscurrent east scalar wind speed component (Black) versus distance offshore over locations B (a) and C (b and c) co-plotted against the underlying SEVIRI SST (Red) and Globcurrent surface current speed (Blue). Current speed is a scalar value of the ocean current perpendicular to the transect in a south westerly flow direction. Accompanying map represents the scalar wind speed (color) and scaled directional arrows (Black) for the region containing the transect co-plotted above the SEVIRI SST contours (grey).

The wind speed shape of Figure 4.7a exhibits a surprising result in that it does not increase over the current but rather appears to be relatively constant from the coast, over the current. It then appears to increase marginally, further offshore away from the current (From 5 to $7m/s$ over $200km$). The wind speed increase appears to originate from the core of the current at $50km$, where the SST values are highest at $23°C$, and then mirror the decreasing SSTs with an increase. The SST values inshore of the core of the current increase sharply again from $18.5°C$ to $23°C$ over $30km$. There appears to be no significant relationship between the current speed values and the wind speed changes as the current increases gradually from the coast to a maximum of $1.2m/s$ at $60km$ offshore and then decreases with a similar gradient to $0m/s$ at $245km$ offshore. The increase in wind speeds can best be seen in Figure 4.7a's accompanying map plot where, again, the wind speed appears to increase gradually across the majority of the region. The high wind speeds to the south indicate that the transect is only capturing the edge of a stronger wind event.

Figure 4.7b shows the least relationship of all the three figures for the crosscurrent east study. The Wind speed does appear to increase moderately from the coast to $90km$ offshore (from $5m/s$ to approximately $8m/s$) but the increase does not appear to be related to either the SST values or the current speeds. The SST values do not show any increase at the location of wind speed increase and the current speed maxima are relatively low at $1.1m/s$ and located closer to shore at $50km$. Further offshore the wind speeds do not increase or decrease significantly but rather fluctuate around 6 and $7m/s$. The regularity in wind speed is evident in the accompanying wind speed map where it is clear that the wind speeds doe not fluctuate much.

The final transect for the crosscurrent west case study, Figure 4.7c, is the transect that exhibits the greatest increase in wind speeds as well as the closest relationship to the SST and current values. The wind speed values increase from $5m/s$ to approximate $8m/s$, further offshore than usual (Approximately $100km$). The wind speeds then gradually begin to decrease again further offshore. The wind speed changes do appear to follow the fluctuations in SST quite well, especially closer inshore where a relatively steep SST gradient from $17°C$ to $21.5°C$ over $80km$, follows the wind speed changes. The peak current speeds are also found further offshore with a maximum of only $1.1m/s$ at approximately $105km$.

Interestingly, the accompanying wind speed map of Figure 4.7c displays a different scenario from what the transect appears to exhibit. The map displays an increase in wind speed further offshore where the transect displays a decrease in wind speed. What the map also displays is a dramatic change in wind direction from a northwesterly direction to a northeasterly direction, half way along the transect. Thus the apparent decrease in wind speed is not a true decrease in wind speed but rather a shift from the crosscurrent component

to a more downcurrent component. This is possible due to the refining of the wind speeds in the original grouping process. The transect in Figure 4.7c cannot be considered an accurate representation of the wind speed changes over the current. The change in directions and wind speed depicted in the map are still of great importance. This is a unique occurrence amongst all of the previous case studies for all of the direction regimes and is a result of such a small pool of choice.

The crosscurrent case studies exhibited results with the least impact, with little to no evidence of wind speed changes as a resultant of either SST influences or from the relative motion of the current. In fact, little to no genuine increase in wind speed was detected.

The case study results presented in the sections above (Section 4.3.1) served as an important indication of the variable influences that can affect the wind speed over a strong western boundary current such as the Agulhas. Especially under different wind direction regimes. The two most important results derived were the fact that the upcurrent wind regime exhibits the greatest increase in wind speed of all directions. The wind speed increase is in close relation with the relative speed of the current underlying the wind although, surprisingly, the greatest wind speed increases are not directly above the core of the current but slightly to the inshore side of the maximum current velocities. Secondly, the downcurrent wind regime also, surprisingly, displayed a notable increase in wind speeds over the current. The increase in wind speed was different from the upcurrent regime in that the increase was not as great and also relative uniform over the entire width of the current. The wind speed increase appear to, therefore be more dependent on the SST influences on the atmospheric boundary layer.

Although highly enlightening and indicative of the potential forcing and influences on wind speeds over ocean currents, the individual case studies are singular examples of ideal conditions under which the forces may act. Thus it is necessary to investigate the influences of the Agulhas on the mean wind directions regimes in order to determine if the effects are a constant occurrence. The following section (4.3.2) addresses the mean effects of the current on the wind speed regimes.

### 4.3.2 Impact of the Agulhas on Time Averaged Winds

For the mean wind speed spatial variability investigation, all four of the locations of interest still included in the study, from B to E were investigated and assess in comparison to each other as well as to their corresponding mean SST values. For all wind direction regimes more similar results to their corresponding individual case studies were found.

#### 4.3.2.1 Upcurrent

In the upcurrent regime a definite, sudden increase in mean wind speed, much like those in the individual case studies for all the locations was observed. The increases were somewhat dampened however due to the influence of the averaging process. The transects which displayed the greatest influence were from locations B (Figure 4.8a) and C (Figure 4.8b). Locations D (Figure 4.8c) and E (Figure 4.8d) also exhibited a shift closer to shore of the peak wind speeds along with a shallower inshore SST gradient. The number of observations for each location remains approximately at 40 with location B having the lowest number of observations at 33 and location D the highest at 44.

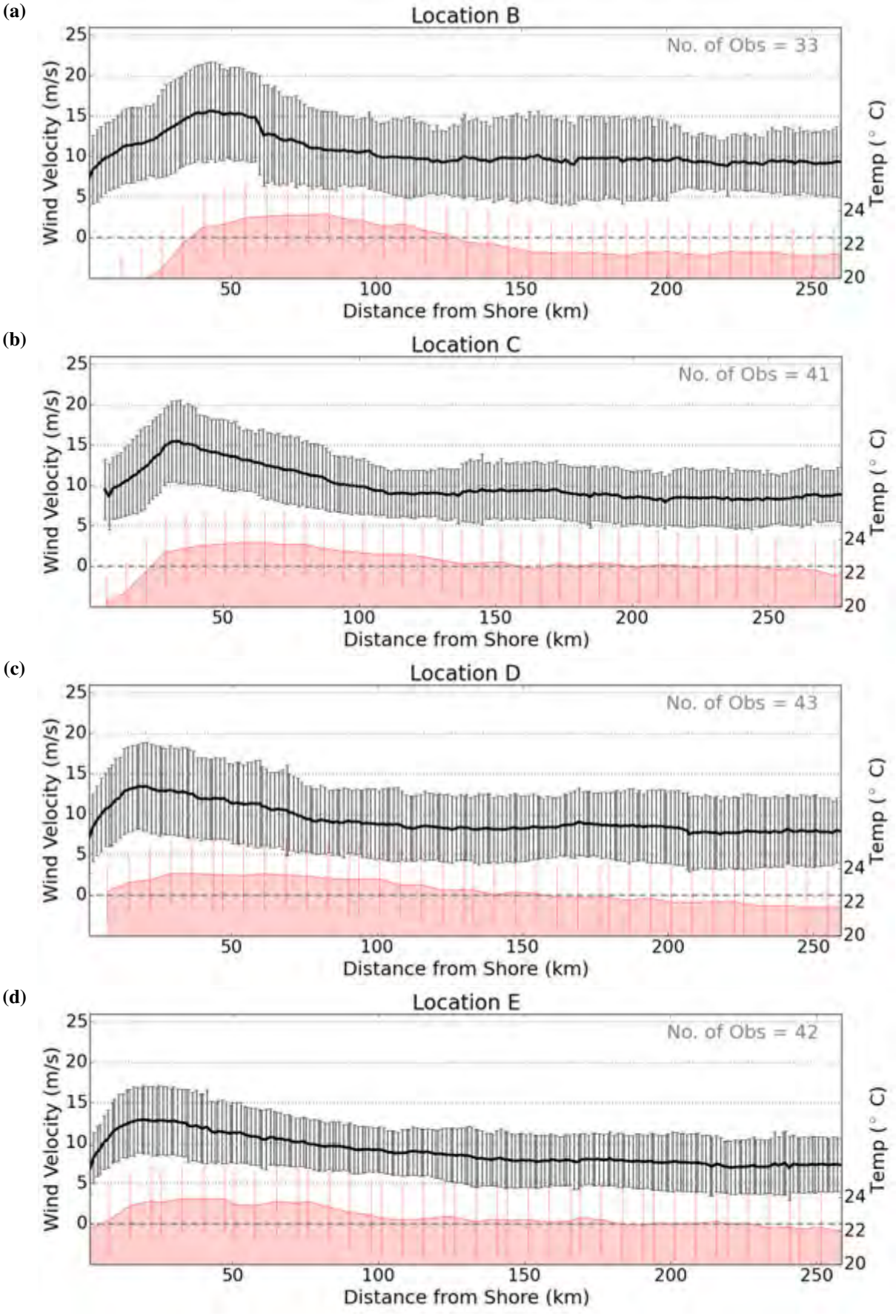


**Figure 4.8:** Mean upcurrent wind speed components plotted as perpendicular transects over the Agulhas Current for the locations B (a), C (b), D (c) and E (d). Data is co-plotted with the underlying SEVIRI SST (Red) as a representation of the location of the core of the Agulhas Current. Error bars show the standard deviations of each dataset along the transect.

The mean wind speeds in location B, (Figure 4.8a) increased by approximately $8.5m/s$ from the inshore boundary of the current to the maximum mean wind speed peak of approximately $16m/s$. The mean wind speed gradient on the inshore side of the peak is characterised by a sharp increase in wind speed from coast to the mean wind speed maximum. This sharp increase is located directly over the region of greatest mean SST change, between $10-50km$ offshore and not the actual peak mean SST values. Although no current data is available, it is reasonable to assume using information from the individual case studies that the peak current speeds would be located directly below the peak wind speeds, closer to shore. The oceanward gradient of mean wind speed change, from the maximum, is characterised by a shallower, slightly concave gradient where the mean wind speed gradually decreases out to sea from a high of $16m/s$ to a low of $9m/s$. The majority of wind speed change occurs over $50km$ from $50km$ to $100km$ offshore. This is similar to the case study of Figure 4.4b. There is no distinct marking of the outer edge of the Agulhas in either the mean wind speed increase or in the offshore SST mean gradient of decrease. The SSTs increase rapidly from $20°C$ at $20km$ offshore to a maximum of $24°C$, $80km$ offshore and then decrease convexly to $21.5°C$, $150km$ offshore.

Location C, (Figure 4.8b) displays a similar pattern of mean wind speed increase to that of Location B, with the exception that the wind speed peak is more defined and moderately closer to shore, at approximately $35km$ offshore. The mean wind speed increase on the inshore boundary is also similar to Location B with and increase of approximately $6.5m/s$ to a maximum of $15.5m/s$. Finally, the offshore gradient of mean wind speed change does not appear concave but is more linear, reaching a minimum of $7.5m/s$. This is more like the transect from Figure 4.4a of the case study. The SST values are similar to those in Figure 4.8a in that they rapidly increase to a maximum of $23.8°C$. This time close to shore at $50km$. The decrease in SSTs is also not as great to only $22°C$ at approximately $150km$ offshore.

Figures 4.8c and d, although quite different from the previous two transects, exhibit similar traits to each other. The wind speed maxima for both transects are located closer to shore at approximately $20km$ offshore for Location D (Figure 4.8c) and $15km$ offshore for Location E (Figure 4.8d). The mean wind speed maxima are also both lower than the previous two transects. Location D has a maximum of approximately $13m/s$ whereas Location E has a maximum of $12.5m/s$. The minimum wind speeds on the offshore side of the transect are similar with Location D dropping to $7m/s$ and Location E to $6.5m/s$ The mean SST values for both Location are less defined than those for Locations B and C with similar maximums of $23°C$ and $23.4°$ respectively, but no sharp inshore gradients.

The high standard deviation values (approx. $\pm 4-5m/s$), across the entire transect, indicate the generally high variability in the wind speed at each location.

A noticeable shift in the peak of maximum wind speeds is evident in the progression northward, from location B to E, as the peak appears to shift closer to the coast along with a less defined SST structure.

The distinct peak in wind speeds which was characteristic of the upcurrent cases is still evident in all of the locations of interest, especially in locations B and C. The increase in wind speeds are dampened by the averaging process and the increase is not as great as in some of the case studies, but it is still greater than 50% for all locations. Although the current data is not available for comparison with the mean, the relationship with the mean wind speed increase and the SST values is the same as it is with the individual case studies especially on the inshore edge of the current where the peak wind speeds are above the SST gradient. Thus it is reasonable to assume that the peak wind speeds are also slightly on the inshore side of the current core.

#### 4.3.2.2 Downcurrent

An increase in the mean wind speed over the core of the current was, like the upcurrent regime, found in the mean downcurrent regime. Also like the upcurrent regime, the two locations which displayed the greatest wind speed increase were Locations B (Figure 4.9a)and C (Figure 4.9b). Unlike the upcurrent regime, the peak wind increase is not as distinct, but rather represented by a gradual sloping dome-like shape. Thus the peak increase is also not located over the sharp gradient of the inside front of SST values but rather further offshore of the maximum SST's. The coastward gradient of wind speed is still, however steeper than the oceanward gradient and the lowest mean wind speed values are still at the coast. The number of observations per location for the downcurrent regime is greater in both locations B and C than their corresponding upcurrent regimes at approximately 50 observations per location whereas location D is principally the same (44 observations) and location E is substantially less (35 observations).

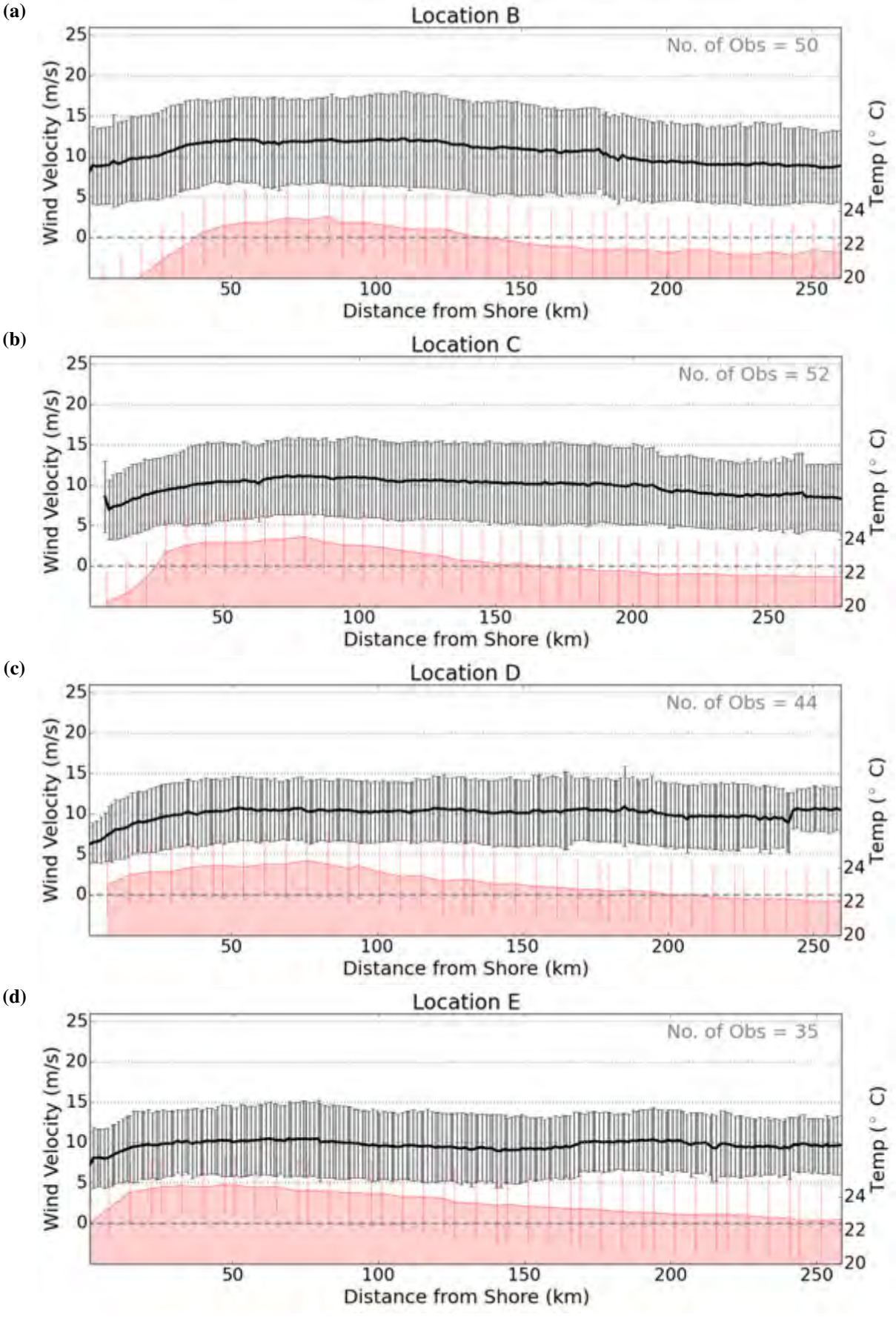


**Figure 4.9:** Mean downcurrent wind speed components plotted as perpendicular transects over the Agulhas Current for the locations B (a), C (b), D (c) and E (d). Data is co-plotted with the underlying SEVIRI SST (Red) as a representation of the location of the core of the Agulhas Current. Error bars show the standard deviations of each dataset along the transect.

The mean increase for Location B, (Figure 4.9a) is approximately $4m/s$ from $8m/s$ directly at the coast to $12m/s$ further offshore. The Exact wind speed maximum is much further offshore than the upcurrent regimes at $115km$ offshore. The gradually sloping dome-like pattern of the transect means that the wind speed features its greatest increase of $4m/s$ between the shore and approximately $45km$ offshore. The wind speeds then level off and do not vary much until $175km$ offshore where they decrease more noticeably again. The offshore minimum in wind speed is as low as the upcurrent regime transects at $8m/s$ but much further offshore. The pattern of change in the SST values does appear to follow a similar trend to that of the wind speeds with the sharpest gradient closest to shore and a more gradual decrease further offshore. The sharp inshore gradient is more intense than the wind speed however, at an increase of $3°C$ over $30km$ The peak SST values are centred in approximately the same position, albeit more skewed toward the coast with a maximum value of $23°C$ approximately $80km$ offshore.

Location C, (Figure 4.9b) exhibits a similar pattern of change to that of Location B with the sharpest increase occurring from the coast at $7m/s$ to a maximum of $11m/s$ $80km$ offshore. The true maximum is much closer to shore than location C, however a similar dome-like structure means that the maximum values do not vary much from $50km$ offshore to $200km$ offshore where a more noticeable decrease is visible and returns closer to the original wind speed at the coast at $7.5m/s$. Interestingly, the peak SST values are higher at $24°C$ and also closer to shore for Location C (Figure 4.9b) than for Location B (Figure 4.9a)

Locations D (Figure 4.9c) and E (Figure 4.9d) are, again, different from the two previous locations, but similar to each other in shape and magnitudes of change. Both locations have lower peak mean wind speeds at only just above $10m/s$. Location D still exhibits an increase in wind speed closer to shore, over the steepest SST gradients of $4m/s$, however the decrease in wind speed further offshore is not as great as Locations B and C where the wind speed appears to level out across the entire transect and does not drop back to its original speed at the coast. The SST values are actually higher than the previous two locations at $24.5°C$ and $25°C$ respectively, but there is little sharp variation with the exception of Location E (Figure 4.9d), where the SSTs drop to $22.4°C$ at the coast.

Location E exhibits close to zero increase in wind speed along the transect with the exception of a minor decrease in wind speed between $120km$ and $170km$ offshore. The sharp increase in wind speed at the coast is still evident although not as great as $3m/s$

The standard deviation in total mean wind speed along all the transects is again, constant at approximately $\pm 3-5m/s$ although it does appear to decrease in locations D and E. The coastward shift visible in the upcurrent direction regime is, again, visible in the downcurrent regime. As the core of the Agulhas SST's becomes less prominent and shifts coastward, the

peak wind speed increase shifts likewise and the coastward gradient decreases.

Thus, much like the mean upcurrent regime, the downcurrent wind speeds exhibit the same wind speed change patterns as their corresponding individual case studies. The effect is dampened but there is a clear relationship between the SST temperature change and the wind speed changes with the wind speed peak much further offshore, and more gradual gradients of change. Although there is no current for comparison, it is reasonable to assume that, like the individual cases, the wind speeds are more greatly affected by the SST changes than the relative motion of the current.

#### 4.3.2.3 Crosscurrent West

Little to no significant common pattern of increase over the core of the Agulhas was found between any of the locations of interest for the crosscurrent-west regime means. Locations B (Figure 4.10a) and C (Figure 4.10b) did appear to exhibit a minor increase in wind speed comparable to the patterns visible in the upcurrent regime, however Locations D (Figure 4.10c) and E (Figure 4.10d) do not. The most interesting result is that the wind speed changes, although irregular, do appear to still follow the pattern of change in the SST values to a degree. The number of observations for all locations are much smaller than both alongcurrent regimes. In fact, in all cases but location C, the number of observations do not reach higher than 10 observations.

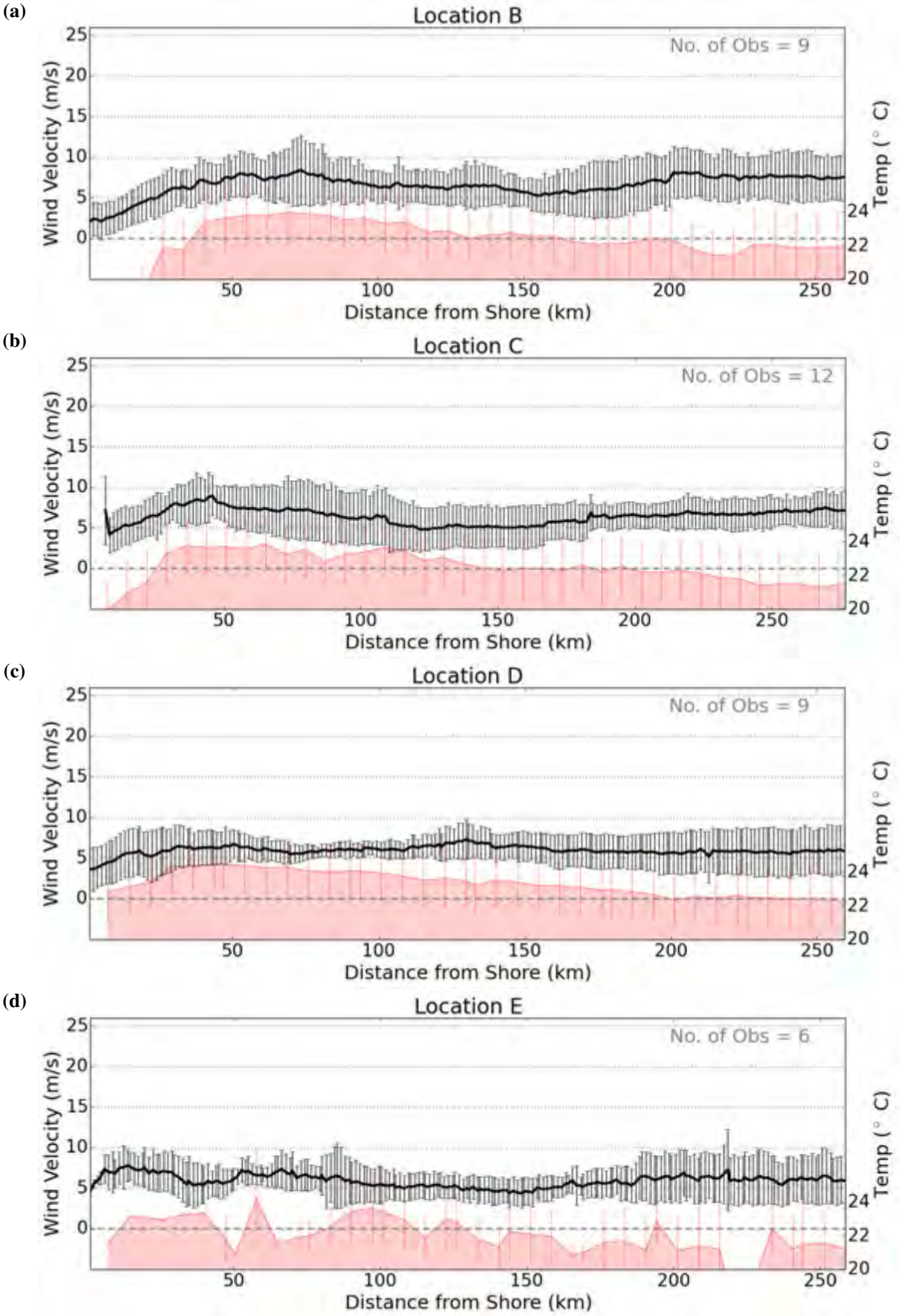


**Figure 4.10:** Mean crosscurrent west wind speed components plotted as perpendicular transects over the Agulhas Current for the locations B (a), C (b), D (c) and E (d). Data is co-plotted with the underlying SEVIRI SST (Red) as a representation of the location of the core of the Agulhas Current. Error bars show the standard deviations of each dataset along the transect.

Locations B (Figure 4.10a) exhibits the greatest increase in wind speed from the shore at $5m/s$ with the peak wind speeds located at $70km$ offshore. The increase in wind speed does appear to follow the sharp increases in SST of nearly $4°C$ from $20km$ to $55km$ offshore as well. However, further offshore, away from the current core, from $150km$ the wind speeds appear to separate from the SST pattern and increase in magnitude above a decrease in SST values.

Location C (Figure 4.10b) exhibits a similar pattern to that of Location B (Figure 4.10a) with an increase of $5m/s$ from the coast to approximately $50km$ offshore and a corresponding SST increase of $3.5°C$ over the same distance. Again, the wind speed values appear to follow a similar pattern to the SST values until around $150km$ offshore where they begin to increase and the SSTs begin to decrease.

Locations D (Figure 4.10c) and E (Figure 4.10d) do not appear to have any discernible increase pattern and are irregular in shape. Although there does appear to be a relationship between the irregularity of the SST pattern and that of the wind speed increase no conclusive pattern can be identified. The sharp inshore decrease and lowest wind speed values are still evident as they were in both of the alongcurrent regimes albeit much less prominent, especially in location E.

Finally, the variation in wind speed intensity throughout each location is much smaller than both alongcurrent regimes although it is not as regular. The mean variance for each location approximately ranges between $1m/s$ and $5m/s$.

The crosscurrent west mean wind speeds has delivered a similar wind speed pattern to that of the case studies in that there are minor increases in speed evident which doe appear to be related to the underlying changes in SSTs, however, much like the individual case studies as well, not all cases have provided reliable results. Locations D and E did not show any real noticeable influence from their corresponding SST values.

#### 4.3.2.4 Crosscurrent East

Only one of the transects for the crosscurrent-east regime showed any discernible pattern of wind speed increase over the location of the current. Location D (Figure 4.11) displayed a moderate increase in wind speeds along the current. The pattern of increase is similar to that of the downcurrent regimes, except that the peak wind speeds are even further offshore. Wind speed changes are highly irregular and unpredictable in locations E but appear to be fairly constant in locations B and C. The number of observations per location for the crosscurrent-east regime is near negligible. The two locations with the smoothest, least erratic wind variations are locations B and C which are comprised of 5 and 9 observations whereas locations D and E contain 3 and 2 observations respectively.

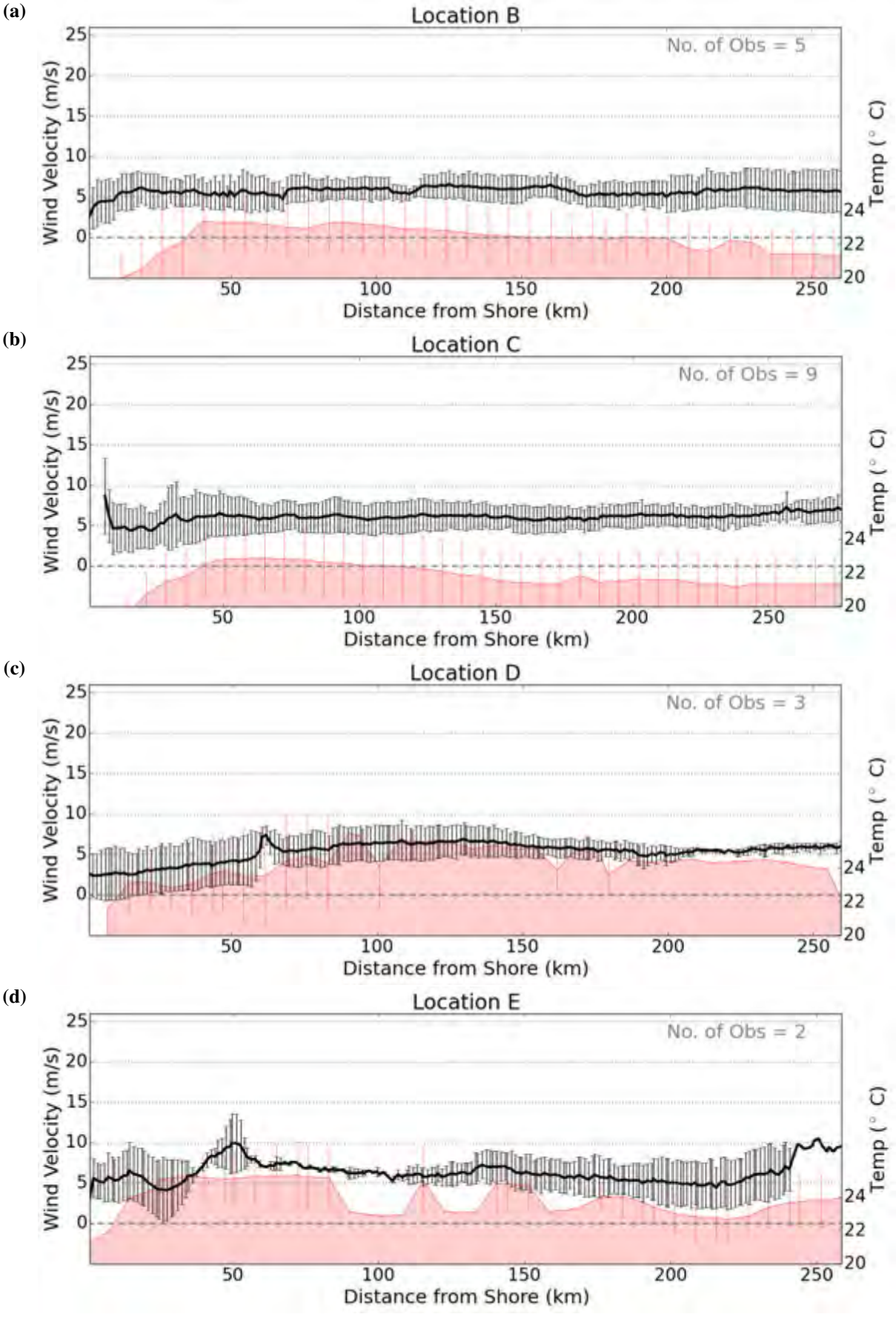


**Figure 4.11:** Mean crosscurrent east wind speed components plotted as perpendicular transects over the Agulhas Current for the locations B (a), C (b), D (c) and E (d). Data is co-plotted with the underlying SEVIRI SST (Red) as a representation of the location of the core of the Agulhas Current. Error bars show the standard deviations of each dataset along the transect.

The low wind speed values and sharp increase gradient that was evident in all other regimes, and highly prominent in the upcurrent regime is no longer visible. Conversely, location C exhibits a decrease in wind speed upon moving away from the coast and the lowest wind speed values occur approximately $10-20km$ offshore. The standard deviation in along-transect wind speeds is furthermore relatively low in all location with the exception of location E which exhibits a highly erratic pattern.

The mean wind speed changes for each of the wind direction direction regimes have shown similar results to that of their corresponding individual case studies. For the upcurrent regime, the characteristic wind speed peak was evident for all of the locations of interest The likewise characteristic dome-like shaped increase in wind speeds in the downcurrent direction regime was also evident. Both of the crosscurrent regimes did not display much evidence of wind speed increases as a result of SST changes or the relative motion of the Agulhas, much like their case studies. The different wind speed increase shapes for each of the direction regimes and their varying relationships to the SST and current data are of great importance. The large standard deviation for all direction regimes and locations of interest needs to be further investigated in order to determine the possible causes of such a high variability and whether it impacts the resulting mean wind speed increase shapes. Thus in section 4.4 the influence of varying wind speed intensities in the relative wind speed increases is further investigated.

## 4.4 Influence of Variable Wind Intensity

The variation in the mean relative wind speed increase in relation to the overall wind intensity of an event is best illustrated by the upcurrent wind speed regimes for locations B and C.

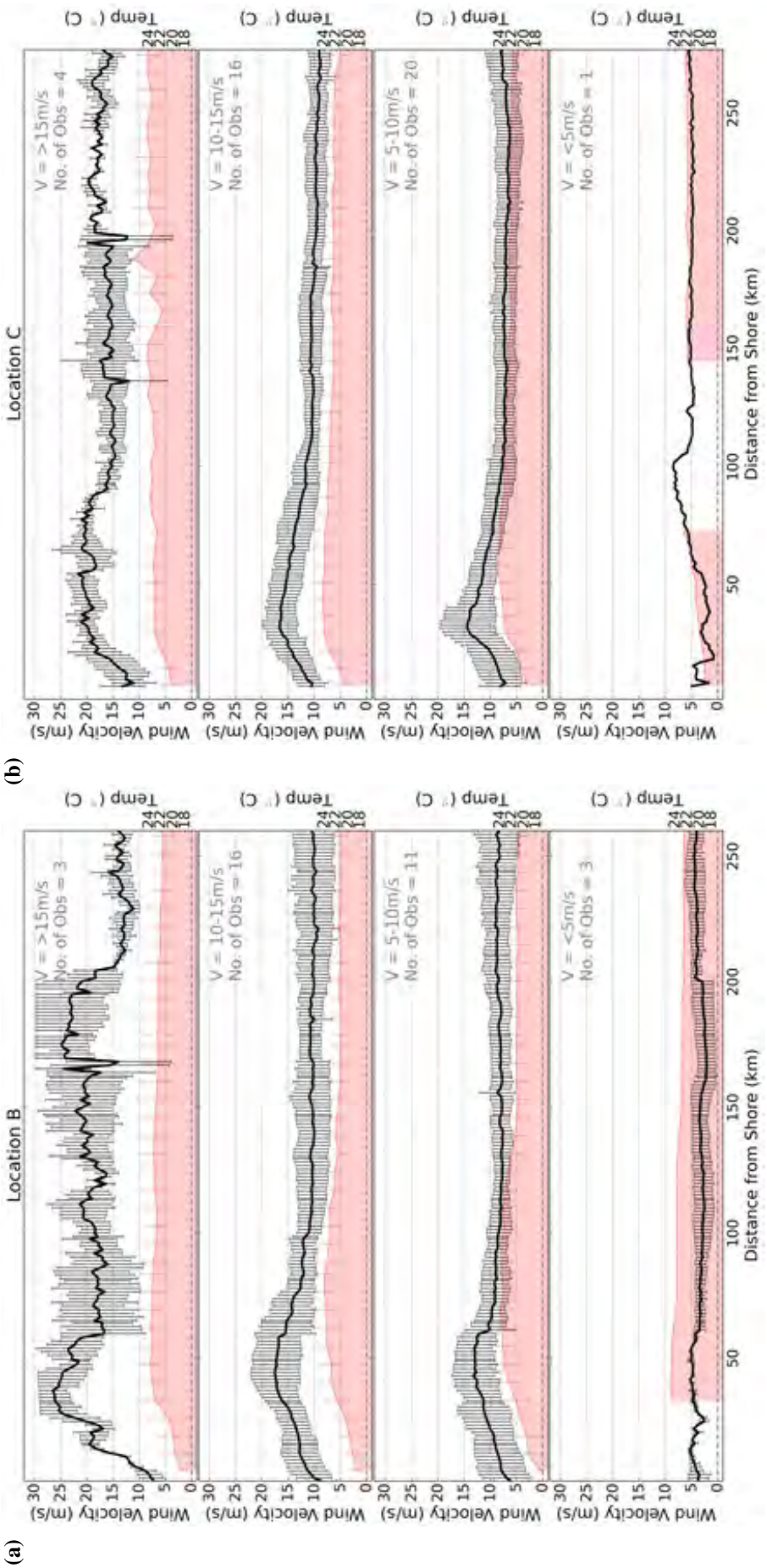


**Figure 4.12:** Individual Upcurrent wind speed components over locations B (a) and C (b), grouped into 4 brackets of wind speed. Brackets are: < 5; 5 - 10; 10 - 15;> 15m/s. Data is co-plotted with the underlying SEVIRI SST. Black line is the mean wind speeds and error bars show the standard deviation of wind speed along the transect.

For both location B (Figure 4.12a) and C (Figure 4.12b), the characteristic wind speed peaks over the core of the current, as exhibited in the overall upcurrent means for the same locations in subsection 4.3.2, are most evident in the $5-10m/s$ and $10-15m/s$ wind speed brackets. The $5-10m/s$ wind speed bracket appears to exhibit the largest increase in wind speed for Location C at $8m/s$ with the sharpest gradient. This is followed by the $10-15m/s$ bracket with an increase if $6.5m/s$. For Location B, the largest increase in wind speed is displayed by the $10-15m/s$ intensity bracket with an increase of $8m/s$. The $5-10m/s$ is close, however, at a $7m/s$ increase. Both intensity brackets also appear to show a good relation to SST for both locations as the peak in wind speed values corresponds to the inshore SST gradient of the current. The number of observations for both the $5-10m/s$ and $10-15m/s$ brackets are moderate at in between 10 and 20 observations.

The highest wind speed intensity bracket, the $>15m/s$ bracket, does not appear to show any meaningful pattern or relationship for neither location B nor C. Rather, the wind speed changes are intense, numerous and irregular with a significant range throughout the length of the transects. There appears to be no relationship between wind speed and temperature gradients for either location. The number of observations is relatively low at 3 and 4 observations respectively.

The lowest intensity bracket, $<5m/s$, does not appear to exhibit any meaningful changes in wind speed nor correlation to SST. The number of observations is also close to zero at 3 and 1 for the locations B and C respectively.

The wind speed standard deviation for the moderate ($5-10m/s$ and $10-15m/s$) wind speeds along the transect is reduced in comparison the that of the overall mean in Figures 4.8a and b at approximately$0-2m/s$ for both locations. This in stark contrast with the $>15m/s$ intensity bracket which exhibits both a much higher as well as spatially more irregular variability than the overall mean. The standard deviation does not appear to follow any recognisable patterns or signatures. Finally the standard deviation in the lowest intensity bracket is virtually nonexistent due to the low number of observations. In fact for location C, there is no standard deviation as there is only a single observation for the transect.

It is clear to see that the presence of an increase in wind speed over the Agulhas Current is still evident in the majority of moderate wind speed events, however in extreme wind events the wind speed increase become obscured by the intense variation across the current. In low wind speeds, there is not enough initial wind speed to be able to conclusively refer a wind speed increase. The increase in wind speed for the moderate events does appear to be related to the initial wind speed.

# Chapter 5

# Discussion

## 5.1 Difference between ASAR, CFS and ASCAT

As previously discussed in section 2.1.2 the northeast-southwest polarity in wind direction over the Agulhas is as a result of the influence of the Indian Ocean High Pressure (IOHP). The IOHP is an anticyclonic circulation over the Southern Indian Ocean that shifts north and south with the seasons (Ffield et al., 1997; Grundlingh and Largier, 1991; Matano et al., 2002; van Heerden and Taljaard, 1998). This northeast-southwest wind direction polarity implies that winds over the Agulhas Current are predominantly aligned with Agulhas Current. This wind configuration in turn predisposes the Agulhas Current to greater current-relative wind effects.

The most noticeable difference between the ASAR wind speeds and both the CFS and ASCAT data is that the ASAR dataset exhibits a greater frequency of more intense events (Illustrated in Figure 4.2). In the CFS and ASCAT data, few events with wind speed intensities above $18m/s$ were recorded. In the ASAR dataset however, all 6 locations (Figure 4.2) experienced wind speeds above $18m/s$ with the majority of the locations experiencing strong wind events more than 5% of the time. What is most unusual however is the fact that the ASCAT wind dataset presented the lowest frequency of high intensity events whereas ASAR presented the highest frequency. This is unusual because the ASAR and ASCAT operate using the same principles and the winds were even derived using the same CMOD5.n GMF. Thus the results derived for the two satellite products should be show closer agreement in wind magnitudes and frequencies in comparison to the CFS data. The difference in wind speed intensities between the ASCAT and CFS datasets cannot be attributed to spatial resolution differences as both datasets are provided at a spatial resolution of about ~25km (See sections 3.1.3 and 3.1.4). (Chelton et al., 2004; Liu, 2002; Park et al., 2006; Saha, 2009; Saha et al., 2010). Unlike the ASCAT dataset which merges observations from

multiple scatterometers, The CFS dataset, assimilates wind observations from both scatterometers (QuikSCAT) and SARs (ERS) as well as a multitude of supplementary wind speed measurements used to correct for biases in the satellite data (Saha et al., 2010, 2014). It is possible that the higher intensity winds from the CFS data is because of higher resolution SAR observations as well as bias correction using the supplementary data in the CFS model. Another possibility for the difference in intensity frequencies could be due to the difference sampling frequency in between the ASCAT and the CFS datasets. The CFS reanalysis is provided at an hourly temporal resolution (see section 3.1.3), whereas the ASCAT dataset is only available at daily time interval. In the ASCAT dataset, twice-daily wind observations are averaged to provide a daily composite (see section 3.1.4). Averaging wind observations to a daily time interval would lead to lower wind speeds as the mean is always lower than the peak in any dataset. All of these factors would contribute to lower wind speeds in the ASCAT dataset when compared to the CFS dataset.

In their observational case study investigation, Jury and Courtney (1991) noted wind speeds in excess of $20m/s$ directly over the Agulhas while Rouault et al. (2000), also measured wind speed of about $14m/s$ over the current. Both the ASCAT and CFS winds over the current are more in the range of between $3-9m/s$ each whereas the ASAR tends to have a higher percentage of wind speeds between $9-12m/s$ than either other dataset. . This suggests that the ASAR data is capturing a more accurate wind speed over the current. ASAR has a resolution that is over 25 times greater than that of ASCAT and CFS (Desnos et al., 2000; Figa-Saldaña et al., 2002). Because the Agulhas current is only about $150km-200km$ wide (Beal et al., 2015), the $0.25°$resolution of the ASCAT and the $0.2°-0.3°$resolution of the CFS data means that there is substantially less capability for detecting the sharp, small scale changes in wind speed that could occur over the width of the Agulhas Current. The decreased resolution of the ASCAT and the CFS models could lead to a smoothed signal and weaker wind speeds.

In the ASAR wind datasets, the strongest wind events were observed when wind directions were aligned along a NW-SE axis for all locations (Figure 4.1). This points towards the greatest differences in wind speed between ASAR, and the CFS and ASCAT datasets occurring when winds are blowing in the mean direction of the Agulhas Current flow. Along-front winds drive the strongest changes in relative wind speeds and based on the findings of Kelly et al. (2001, 2005) and Plagge et al. (2012), one would expect stronger ASAR winds in an upcurrent wind regime and weaker ASAR velocity in a downcurrent wind regime. What is surprising however is that when compared to the CFS and ASCAT dataset, the ASAR wind velocities, are stronger both in upcurrent (northeasterly) and in downcurrent (southwesterly) wind regimes. The larger proportion of strong winds in both the upcurrent and downcurrent

direction regime may imply that in addition to intrinsic sensor and resolutions differences between the ASCAT, ASAR and CFS datasets, the ASAR dataset might be able to better capture localised wind speed increases over the Agulhas Current not induced by the relative wind effect. As previously stated, wind speed increases over the Agulhas Current could also occur through geophysical roughness modifying forces such as turbulence inducing friction at the boundaries of the current, or a physical increase in wind speed over the current due to ocean-atmosphere interactions as documented by Lee-Thorp et al. (1998); Rouault et al. (2000) and Jury and Courtney (1991).

In the following 2 sections, we reflect on the two distinct major influences of the Agulhas Current on satellite-derived wind speeds, namely 1) the current relative effect and 2) the influence of SST on the overlying atmospheric marine boundary layer.

## 5.2 Current Relative Wind Speed Changes over the Agulhas Current

For both the individual case studies and the regime means, the strongest impact of the Agulhas Current on wind speeds is seen in the upcurrent wind regime (Figures 4.4 and 4.8): the regime where the wind is blowing in an opposite direction to the flow of the Agulhas Current. According to the relative wind theory, when the wind direction is in the opposite direction to that of the current flow, the speed of the wind relative to the motion of ocean should theoretically appear faster than the true wind speed (Kelly et al., 2001). The increase found was, however much greater than previously reported. Our analyses showed that on average, wind speed differences between the wind speed maxima and winds away from the current were in the $5-7m/s$ $(50-70\%)$ for all of the selected locations. Such increases in wind speeds over the current are $10-20\%$ greater than previously reported by Kelly et al. (2001, 2005) and Plagge et al. (2012).Case studies presented in Figure 4.4 , show even greater changes over the Agulhas Current with wind speeds increasing from $5m/s$ to $12m/s$ in Figure 4.4b or even as much as from $5m/s$ and $15m/s$ (Figure 4.4c) over the current. This represents an over 200% increase in the extreme cases. One reason our observations show much larger wind speed increases over the Agulhas Current compared to previous studies in an upcurrent regime could be due to the fact that the Agulhas is a much more intense ocean current on a whole than the ocean currents previously investigated in current-relative wind speed research. In his investigations by Plagge et al. (2012), for example focused in regions of predominantly tidal flows (with the addition of minor wind-driven coastal flows) where the average near surface current velocity was $0.4m/s$ with absolute maximum velocity of up

to $1.2m/s$. By comparison, the Agulhas current has a mean flow of approximately $1.5m/s$ and maximum speeds often in excess of $2.0m/s$ (Beal et al., 2015; Bryden et al., 2005). The Agulhas Current would thus, theoretically induce a greater relative wind speed increase in upcurrent winds than previously reported. The relative wind effect does not, however, completely explain the much greater wind speed increases detected in the ASAR dataset over the Agulhas. If the ratio of wind increase to current speed were the same as those calculated by Kelly et al. (2001, 2005) and Plagge et al. (2012) the wind increase should only be as great as $5m/s$ maximum. Therefore there is still a further 50% increase in the mean wind speeds which is unaccounted for.

The previous results such as those from Kelly et al. (2001, 2005) and Plagge et al. (2012) were also obtained using ASCAT scatterometry data which appears to underestimate small scale wind speeds, as previously discussed in section 5.1. Above the Agulhas, the greatest change in wind speeds occur over a distance of approximately $100km$ for all of the zones of interest, with the steepest wind speeds increases observed over distances of about 30km. For the scatterometers and CFS models, which have a resolution range from $0.2^\circ - 0.3^\circ$ that translates to approximately $22 - 33km$, these high resolution wind speed changes would be poorly resolved. In their investigation, Plagge et al. (2012) observed relative wind speed differences over the Gulf of Maine in a region where spatial variations in currents occurred over short distances of $20 - 40km$. Thus the same resolution issue would have prevented them adequately resolving small spatial scale increases in wind speed. On the note of mean current speeds, one must be reminded that the current speeds and gradient of change used in the case study transects are themselves not a true representation of the Agulhas Current's structure and speed. As stated in section 3.1.6, the true current speeds could be as much as $1m/s$ faster than those depicted in the case studies (Bryden et al., 2005; Danielson et al., 2014). The current speed variations along the transects away from the core of the current are also steeper and more asymmetrical than what is represented in the data used. The Agulhas Current has a much sharper, inshore speed gradient and a more gradual offshore gradient (Bryden et al., 2005) in comparisons to the Globcurrent ocean current product. Thus the current data can only be used as a much more general indication of the location of the current and its core rather than for an exact comparison.

## 5.3 SST Driven Wind Changes

As previously noted in Section 2.1.3, the sharp change in ocean temperature between the warm Agulhas Current waters and colder waters away from the current core has been shown to influence the overlying atmosphere in such a way as to increase the mean wind speeds

over the warmer current core. This is due to the transfer of heat from the ocean to the atmosphere which results in uplift and an unstable MABL.

### 5.3.1 SST Driven Changes in the Downcurrent Regime

The effects of ocean-atmosphere heat transfer related wind increases are best illustrated by selected case studies of downcurrent events (Figure 4.5). According to the current relative theory postulated by Kelly et al. (2001), if the direction of the wind is parallel to the flow of the current, and in the same direction of flow, the relative motion of the current to the wind *should* result in an apparent decrease in satellite derived wind speeds. The mean downcurrent (Figure 4.9) wind speeds corroborate the evidence in the case studies of an influence on wind speeds from the SST gradients, much like the upcurrent regime does with the current relative effect. The results retrieved for the downcurrent direction regime from the ASAR data are, strangely, contradictory to this theory. For the downcurrent regimes, we still observe an increase in wind speed over the Agulhas Current in the ASAR derived dataset. The increase in wind speed is neither as distinct nor as large as the increases in wind speed observed in an upcurrent regime, but it is still notable and persistent at between $5-7m/s$ in some cases. A similar pattern of increase was found in many different individual case studies. The wind speed changes do not appear to be related to the location of the core of the current at all, as there is no real change of wind speeds near to where the current speeds are greatest. A relationship which is evident though, is the relationship between the sharpest changes in SST values, and the changing wind speeds. It is clear in both Figures 4.5a and b that there is an obvious relationship between wind speeds and the location of two distinct temperature fronts on the inshore and offshore boundaries of the Agulhas. In these frontal regions, SSTs can increase by as much as $2-3^{\circ}C$ over a short distance, and wind speeds can increase by up to $5m/s$ (An approximately 50% increase or an increase ratio of approximate $2.5m/s$ per $^{\circ}C$). Notably, after rapidly changing speed over these temperature fronts, the wind speeds remain relatively constant above the rest of the current, oscillating by approximately only $2m/s$. This is much like the underlying SSTs which do not stray more than approximately $1^{\circ}C$ between the fronts.

The wind speed patterns in Figures 4.5a and b are similar to those observed by Park et al. (2006); Rouault et al. (2000) and Jury and Courtney (1991) in their individual studies. Both Jury and Courtney (1991) and Rouault et al. (2000) noted the increase and decrease of the physical wind speed over the temperature boundaries of the Agulhas Current. Rouault et al. (2000) noted that in moderate wind speed conditions of approximately $10m/s$, the wind speed above the core of the Agulhas Current increased by as much as $4m/s$. The wind speed increases corresponded with an increase of sea surface temperatures of between

$4-5°C$ (nearly $1m/s$ per $°C$) with the greatest change in wind speed occurring directly over the sharpest SST gradients. This pattern and relation is nearly identical to that of Figures 4.5a and b. Jury and Courtney (1991), did not record as great an increase in wind speeds over the current with only increases of approximately $3m/s$ (from $17m/s$ to $20m/s$) over SST differences of as great as $6.5°C$ (less than $0.5m/s$ per $°C$). However, the wind events that Jury and Courtney (1991) recorded were not strictly parallel to the current but more diagonally crosscurrent. This suggests that wind speed events which contain a crosscurrent component might be less affected by the changing SST values and resulting atmospheric boundary layer heating than would be expected

The mean downcurrent effect (Figure 4.9) shows no evidence of a sharp peak in wind speeds like that of the upcurrent regime, but rather a smaller, more gradual increase of only up to $4m/s$ from $7-8m/s$ with more constant wind speeds over the entire width of the current. The shape of the increase follows a more symmetrical shape. The shape is however not so much like a table top as the case studies, but more dome like in structure. The speed maxima, although not as clearly visible, are still closer toward the core of the current and the peak SST values. In the case of Location E (Figure 4.9d), the wind speed increase is virtually nonexistent. This is mostly likely due to the widening and shoreward shift of the current further north (See section 5.3.5)

The percentage increase of between $40-50\%$ as a result of SST influences is still over triple that of the mean wind speed changes found by Park et al. (2006) and over a lower SST gradient of only $0.86°C$ per $10km$ in the inshore boundary. Park et al. (2006) used scatterometer data in conjunction with SSTs in a study on eddies from the gulf stream to show that wind speeds can be altered by $10-15\%$ over an SST gradient of $1.5°C$ per $10km$. This discrepancy is most likely as a result of the averaging in Park et al. (2006)'s study, as well as the resolution difference between ASAR and ASCAT as discussed in section 5.1 but it is possible that other, eddy specific factors may be at play.

Although Figure 4.5c does not exhibit the characteristic plateau of wind speeds and SSTs displayed in the other cases studies and the means, the results further boost the evidence of an influence of SST changes on the atmosphere over the relevant motion of the current. This is because the wind speeds and SST fluctuate in the same manner. Over the core of the current, where the SSTs are high, so are the wind speeds. And when the SSTs decrease again, the wind speeds decrease accordingly. An anomaly in the relation is the much greater increase in wind speed between the coast and $50km$ offshore. This increase is unusually high and does not increase in the same way as other downcurrent wind speed events over the inshore boundary of the Agulhas. The spatial gradients in SST are also much less than those observed in Figures 4.5a and b and there is no characteristic steep temperature front. This

could mean that the high SST values could be acting in combination with other unknown geophysical forcings. This, coupled with the fact that the mean wind speed values also tend to follow the SST changes, reaffirms the conclusion that there are differences in the wind speed change forcing at play between the upcurrent and downcurrent regimes. The downcurrent regime better reveals changes in wind speed due to the changing SST values than the relative motion of the current.

In the upcurrent case studies, there are some interesting anomalies which offer insight into SST-driven wind speed modifications. Figures 4.4b and c display an interesting anomaly whereby the wind speed increase over the inshore core of the Agulhas has a clear relationship to the current speed data. Further offshore however, when the current velocities lessen to almost $0m/s$, the wind speed does not drop by a corresponding factor, but rather remains anomalously high with a gradual decrease in wind speed. There is even a minor increase over $200km$ from shore in Figure 4.4b. In both instances, the SST values further offshore remain relatively high in comparison to the current speed values and away from the main current flow. In Figure 4.4c the wind speed can especially be seen to closely follow the pattern of decrease in SST values further offshore. This apparent relationship indicates that, although the current relative wind speed effect has the largest, most notable effect on wind speed changes, there is a definite increase in wind speed over the Agulhas Current. This is as a result of differential heating of the atmospheric boundary layer from the changing SSTs (Jury and Courtney, 1991; Rouault et al., 2000).

### 5.3.2 Wind modifications in Crosscurrent Wind Regimes

When looking at both of the crosscurrent regimes, a caveat to consider is that there are far fewer events recorded in comparison to the along current events. This means that the case studies selected might not be ideal and thus there could be external influences such as synoptic conditions or other anomalies which would influence the results and cannot otherwise be explained. This particularly becomes a problem when the synoptic conditions for an event cause a major change in direction along the transect. As discussed below, this can result in the transect registering a decrease or increase in wind speed which might not be true.

Of the two crosscurrent regimes, the crosscurrent west is the regime which showed the strongest wind speed increase in relation to the current (Figure 4.6). The increases for all three of the transects are however somewhat different from each other. The most noteworthy transect is Figure 4.6b, as the transect appears to display an increase in speed as the winds come into contact with the offshore boundary of the current from the oceanward side (Note: For the crosscurrent west regime, the winds in the transects are travelling parallel to the

transect, from east to west and not perpendicular like those in the alongcurrent regimes). The increase is neither as great nor as sharp as the downcurrent regime. Our results are in agreement with those of Jury and Courtney (1991) who found that the wind speed increases in a cross current regime are not as great as those observed in an alongcurrent regime. The shallower gradient of speed increase is also explained by the results found by Park et al. (2006) whereby wind speed changes for wind flowing perpendicularly over a current were found to have a response time scale in the order of an hour which results in a spatial change in the order of tens of kilometres. In a crosscurrent transect situation this means that the response time is slower along the transect as the wind speeds are parallel to the transect and perpendicular to the SST fronts. They do not experience as rapid a change in SST because the direction of SST change is parallel their direction of flow and the winds flow too quickly over the gradient and do not have as much time to be affect by it. Similar results can be seen in the other two transects, Figures 4.6a and c, where a small wind speed increase and delayed response time can be noted. An anomaly that is difficult to explain, is the appearance of a peak in wind speed increase in Figure 4.6b which is reminiscent of those seen in the upcurrent regimes. This is unusual as the current relative effect, postulated by Kelly et al. (2001), can only work for along current winds due to the physical principals of vector addition upon which it is based (Knight et al., 2015). Thus the increases seen in the two transects may be as a result of some other roughness modification on the inshore boundary of the current. One explanation could be a general increase in turbulence of the current due to its interaction with the Agulhas Bank. The interaction between the Agulhas Current and the Agulhas Bank has been previously shown to induce inshore eddies and shear in the waters inshore of the Agulhas which might, in turn be associated with high turbulence (Speich et al., 2006). The two transects which show an increase are from location B which is situated right at the point where the Agulhas comes into contact with the Agulhas bank.

The crosscurrent east regime (Figure 4.7) is the only regime to display little to no increase in wind speeds over the Agulhas Current. Figure 4.7b does not appear to exhibit an increase in wind speed at all; Figure 4.7c shows a minor increase, and Figure 4.7a shows a decrease in wind speed over the current and increases further offshore. However if one were to look at the accompanying map plots of the speed and direction for each case study, one can see that the transects experience a change in wind speed which is not represented in the scalar wind speeds of the map plots. In fact where Figure 4.7c decreases in wind speed on the transect, an increase in wind speed is seen on the map. So a disparity in scalar wind speeds is apparent. This is important, because the regimes for the transects are calculated using the vector components of the wind events which are parallel to the regime, as described in section 3.2.2. The problem arises when a major change in wind direction

occurs along the transect. The nature of vector components means that the magnitudes of a vector are the sum of its two perpendicular components. Thus a change in direction of the wind vector without a change in the speed would result in a decrease in the magnitude of the component parallel to the regime and an increase in the component perpendicular to the regime. Thus, because only the vector parallel to the regime is used, a change in direction of the wind would result in a decrease in the magnitude of the component which is being utilised and an increase in the non-utilised component without an actual change in the wind speed. This can be seen in Figure 4.7c where the transect shows a decrease in the wind speed component further offshore but the map plots shows an increase in the scalar wind speed. As mentioned above, this problem was not experienced in our analysis of all of the other wind regimes because we selected conditions with little to no variation in the wind direction along the transect from a much larger data pool. However it is still evident in the three case studies that there is little to no influence of the current or changing SST values on the wind speed (See accompanying map plots from Figure 4.7). One possible reason for this could be the fact that the air which is flowing over the current in the crosscurrent east regime is coming from land which is relatively much warmer than the ocean during the day. Thus the boundary layer may already be relatively unstable due to heating from the land.

The crosscurrent west regime (Figure 4.10), which represents a wind direction towards the coast, does exhibit an apparent minor increase in mean wind speed over the inshore boundary of the current for the two more southerly locations (Figures 4.10a and b). Surprisingly these increases show minor peaks in wind speed over the inshore edge of the current which were evident in some of the case studies (Figures 4.6). This may mean that the increase in wind speed is a result of some particular geophysical forcing, but it is unclear what that may be. The increases do also appear to follow the changes in SST to some degree however, as with the case studies, the relationship is not as clear as that in the alongcurrent regimes. The more northerly locations (Figures 4.10c and d) do not appear to show any noticeable increase or significant pattern in relation to SST changes.

Unfortunately, as stated in the evaluation of the case studies (above), due to NE-SW polarity of the wind regimes over the Agulhas region, the infrequent occurrence of crosscurrent wind events means that hardly any conclusion can be deduced from the available data. Too few events occur for each regime in order to consider the calculated means a “mean state”. This is particularly true of the crosscurrent east regime (Figure 4.11)

### 5.3.3 Anomalous Spike in Windspeeds

A feature present in many of the wind speed transects which cannot be explained is that of the anomalous increase in wind speed magnitude on the inshore edge of the Agulhas

Current. The best examples can bee seen in Figures, 4.4c, 4.10b and in the Upcurrent means (Figure 4.8).This anomalous increase in wind speeds appears to be much greater than what would be expected from Kelly et al. (2001, 2005)'s relative wind effect, SST influences or a combination of both. A possible influence could be that of surface roughness modulations in the current as a result of unknown influences similar to the likes which have been noted by Rascle et al. (2014) and Kudryavtsev (2005). Kudryavtsev (2005) noted that breaking waves and their resulting roughness scatter radio waves and therefore can directly effect the NRCS signature. Rascle et al. (2014), on the other hand, noted that convergent and divergent current structures in relation to wind direction, may also have an effect on the signatures NRCS derived by SAR. It is very difficult, however, to identify these effects in the studies conducted within this investigation as further study and evidence is required.

### 5.3.4 Sharp Decrease in Wind Speed at the Coast

An interesting feature present in the regimes for all directions (The best examples can be seen in Figures 4.4c,4.5c and 4.8a), is the presence of a sharp decrease in wind speed at the coast which often results in the lowest wind speed values along the transect regardless of the wind direction. The dramatic drop in wind speeds do appear to follow the similar patterns of change of the SSTs although some cases better than others.Many factors could cause lower wind speeds at the coast. Not least of which could be the effects of the coastal orography (in the form of wind shadows or the like), differential heating between the land and the ocean (causing a change in the atmospheric pressure differences and a resulting change in wind speed and direction). No compelling evidence for either of these effects is present in the ASAR data, however.

It has been shown in previous research that the CFS model used in the ASAR wind speed derivations does battle to resolve small scale features close to the coast due to parameterisations as well as its much lower resolution than ASAR (Saha et al., 2010, 2014), but this would mostly effect the ASAR wind directions and not the ASAR wind speeds in the transects. There is also a probability that the NRCS collected by the ASAR may be subject to a power loss due to irregularities in the return signal close to the coast which has also been postulated (HORSTMANN et al., 2014). These derived wind speed decreases might actually be as a result of a genuine decrease in wind speeds at the coast as has been found by Rouault et al. (2000) and Jury and Courtney (1991) who both described decreases in the order of $1-4m/s$. These decreases in wind speed were generally attributed to the sharp changes in SSTs at the coast. However, the wind speed decreases presented by Rouault et al. (2000) and Jury and Courtney (1991) did not drop much lower than what the mean wind speeds were further offshore, away from the current and in the open ocean. They were

not nearly as dramatic as some of those captured in the ASAR dataset. The SST values close to the coast in the transects can, themselves not be considered completely accurate either. Coastal waters are characterised by highly variable, sub-mesoscale circulations and interactions which would not be properly resolved by SST datasets such as SEVIRI or OSTIA, or even the higher resolution MODIS dataset. Other issues such as errors in processing techniques, flagging techniques can also lead to SST errors at the coast. In fact, Dufois et al. (2012) and Smit et al. (2013) both showed that satellite derived SST data from sensors such as MODIS Terra and Pathfinder can display a positive temperature bias of between $3-6°C$ at the coast. This would mean that the temperature gradient might be stronger than shown, and the drop in wind speeds might be more affected by the corresponding drop in SSTs at the coast. Some other, unknown factor would then have to account for the anomalously low wind speeds. Thus, although the derived wind speeds may be an accurate representation of the true wind speeds at the coast, there is simply too much uncertainty to draw a solid conclusion from.

### 5.3.5 Coastward Shift of Peak Wind Speeds Further North

Interestingly, for both the mean upcurrent and mean downcurrent regimes, in the locations further north ( Figures 4.8c and d and 4.9c and d.), the peak wind increase appears to move closer to the shoreline along with the peak SST. The peak wind speeds are also slightly lower than that of locations further south (Figures 4.8a and b and 4.9a and b). This coastward shift is most likely be attributed to the fact that the continental shelf begins to widen further south (Close to locations B and C) as it transitions into the Agulhas Bank. A widening in the continental shelf causes a change in the structure of the current as it moves further south, narrows and becomes more defined (Bryden et al., 2005; Lutjeharms, 2006b; Rouault et al., 2010). Thus the wider current further north could be spreading the effect on the winds over a larger area. This does however reaffirm that the wind speed increases over the current are a consistent, mean effect. They are due to an interaction of the atmosphere with the current and an altering of the surface roughness, and not merely a coincidental change in synoptic conditions over the current for individual events.

## 5.4 Effect of Event Intensity on Wind Speed increase

Due to the highly variable nature of wind speeds in the investigation, it stands to reason that different wind speed intensities might be more or less affected by current relative or SST driven wind speed changes. Thus in order to study the effect that wind intensity has on wind

speed increases, the wind direction regimes were categorised into 4 intensity brackets as described in section 3.2.6

For this investigation only the two best locations of interest, for only the upcurrent regime (Figures 4.12a and b), were necessary for presentation as the remaining locations produced a similar result.

On first assessment it is clear that all of the notable features and the pattern of increase are only visible in the two moderate wind speed intensity brackets ($5-10m/s$ and $10-15m/s$). Both brackets appear to resemble the shape of their full dataset means with location C (Figure 4.12b) exhibiting a slightly sharper, more distinct peak in the maximum wind speeds than location B (Figure 4.12a) especially in the $5-10m/s$ bracket but the peak remains on the inshore boundary of the current.

For the mean wind speeds greater than $15m/s$, the wind speed changes are far more chaotic and do not necessarily correspond to the location of the current or SST features. For both of the regimes presented, there does appear to be a wind speed increase over the location of the current but it is mired by other wind speed increases and changes further offshore where there is no current present or significant change in SST. The standard deviation in wind speed is also much higher and far more chaotic than that of the moderate wind speed regimes. This standard deviation suggests that there is a much greater amount of random wind speed changes along the transect which cannot be accounted for by the relative motion of the current or ocean-atmosphere heat exchange influences. The chaotic nature of the wind speeds greater than $15m/s$ is most likely due to the sheer intensity of the wind speeds overriding any other wind altering influences that may be occurring. A wind speed that is 15m/s or greater would be travelling in the order of 10 times faster than the flow of the Agulhas and thus the impact of the relative motion would be lessened (Hersbach, 2010). Additionally, in much greater wind speed, the presence of breaking waves would play a key role in the derived wind speed. Breaking waves have been proven to both scatter radio waves more effectively which means that less of a return signal would be recorded (Kudryavtsev, 2005). They have also been shown to physically dissipate wind energy thus meaning that sharp changes in wind speed could result due to breaking waves (Kudryavtsev, 2005). Finally, they can also generate additional short surface waves through energy dissipation which would thus result in an inaccurate NRCS measurement through ASAR and resulting wind speed derivation (Kudryavtsev, 2005). It is also worth noting that the number of observations for the $>15m/s$ intensity brackets are lower than the other intensity brakcets. Locations B (Figure 4.12a) and C (Figure 4.12b) have 3 and 4 observations above $15m/s$ respectively, thus the results obtained could be inaccurate and not representative of a mean effect.

The intensity brackets for wind speed less than 5m/s also do not appear to display any noticeable influence from the motion of the ocean current, nor from SST differences across the transect. This is most likely due to the fact that the wind speeds are so close to the lower threshold of wind speeds for which the CMOD5.n GMF can still be applied Hersbach (2008). In order for there to be a relative wind speed increase over the current, a sufficient initial wind speed is required. In the case of the <5m/s bracket, it's most likely that the wind speed is insufficient in order to exhibit a true wind speed increase.

The result that the greatest wind speed changes occur for moderate wind speed corroborates the result presented by Plagge et al. (2012) in which they concluded that the greatest effect of current-relative wind speeds is on moderate wind speeds. Plagge et al. (2012) do not however take into account the effects that might occur due to ocean-atmosphere heat exchange.

## 5.5 Impact of mesoscale features

The results discussed above are for ideal situations where the wind directions are well defined and categorised into highly specific directions regimes. Our analysis shows that on some occasions, ocean mesoscale variability can induce sudden changes in both wind direction and intensities. Agulhas Meanders are known to have strongly cyclonic flows and can result in a northward flow on the inshore edge of the Agulhas (Lutjeharms, 2006b; Rouault and Penven, 2011). For a wind direction that is downcurrent, a northward flow from the cyclonic circulation of an Agulhas Meander would result in the same effect as if the wind were blowing upcurrent (See section 5.2). In essence, the wind and current flow would be in opposite directions and a relative increase in wind speed such as that described by Kelly et al. (2001) should occur. Additionally, Agulhas meanders are a source of shear and upwelling as they propagate down the Agulhas Current (Bryden et al., 2005; Rouault and Penven, 2011). These shear related process would then affect the surface roughness of the ocean, which, in turn, would modify the derived wind speed. Lastly, Agulhas Meanders are also associated with changes in SSTs as they propagate down the Agulhas Current their cyclonic circulation is associated with upwelling on the inshore edges and coastal shelf. As discussed above in Section 5.3, SST gradients can have an effect on the overlying atmospheric boundary layer and result in wind substantial wind speed changes. Here we provide evidence of complex wind modifications induced by the presence of large Agulhas Current meanders

The appearance of the Natal Pulse-like features in Figure 4.3 suggests that there is indeed an influence of oceanic forcing on the surface roughness of the ocean and, in turn, an effect

on the NRCS signatures and resulting derived wind speeds. At first inspection, however it cannot be determined what drives the surface roughness, and hence wind speed changes. There are multiple factors which influence the surface roughness of the ocean and its NRCS signature. However when investigated individually and taking into account the direction of the wind as it flows over the current, conclusions can be made as to the possible underlying forces causing the apparent increase in wind speed. Firstly, in Figure 4.3a the increase in wind speed is from a crosscurrent wind direction, relative to the mean flow and secondly, the increase is not over the entire width of the current. The fact that the increase is not over the entire width of the current means that it is reasonable to assume that the increase in the SAR derived wind speed is most likely not due to SST induced modifications of the atmospheric marine boundary layer as suggested by Rouault et al. (2000) (Rouault et al. (2000) documented that the wind speed should increase uniformly over the current as a result of SST changes). The wind direction is also offshore and therefore across the flow of the current, not along current. This, therefore appears to rule out Kelly et al. (2001)'s relative effect. But upon closer inspection, it is possible that the meander in the current is causing the current to flow toward the shore on the more southerly side of the meander, thus resulting in an upcurrent-like flow over the meander - as discussed above - and an increase in wind speed.

Alternatively, the apparent increase in wind speed may not be an actual increase in wind speed but rather due to an increase in the surface roughness of the ocean due to frictional forces involved in the highly variable flow and changing vorticities of the meander (Lutjeharms, 2006b).

Figure 4.3b also presents a challenge upon first assessment. The predominant wind direction for this event is in fact southeasterly but over the inshore side of the current the wind shifts to a more southwesterly direction. Thus the wind direction over the current is actually upcurrent. More importantly, however, is the fact that the wind speed appears to increase as the wind flows in an upcurrent direction over the inshore boundary of the current. This is suggestive of a current relative wind influence such as those documented by Kelly et al. (2001, 2005) and Plagge et al. (2012). The localised wind speed increase over only the more intense inshore edge provides further evidence of a current relative wind effect. However, the effect of SSTs on the wind speed cannot be rejected as there does appear to be a general decrease in the wind speed as the wind flows over the cooler core of the Agulhas meander at 31.3°S. This uniform decrease in wind speed over the cooler SSTs is evidence of the atmospheric boundary layer adjusting to the changing surface temperatures of the underlying ocean. This is what Rouault et al. (2000) described. The fact that the wind changes direction over the current could also be evidence of the SST's influence on

the overlying boundary layer and resulting winds. It has been previously shown that high SSTs can alter the wind curl over western boundary currents such as the Gulf Stream (Park et al., 2006). The maximum change in wind direction previously recorded is only 15° (Park et al., 2006) though and the wind direction change over the Agulhas Current - in Figure 4.3b - is closer to 90°. Thus, although wind veering as a result of SST influence might be occurring, it cannot be said with any certainty whether the change in wind curl for this event is solely due to the influence of the SST changes rather that from external change in atmospheric synoptic circulation patterns.

The last case study selected (Figure 4.3c) displays the most interesting characteristics. It appears to exhibit wind speed changes due to combined effects of the current relative wind and the SSTs on the atmospheric boundary layer. The primary wind direction for the event is northeasterly and thus downcurrent. The apparent increase in wind speed due to SSTs altering the boundary layer is most obvious at first assessment as there is a uniform increase in wind speed over the entire width of the current, just as Rouault et al. (2000) described and the wind speed increase even appears to follow the meander of the current. However, the decrease in wind speed at the core of the meander exhibits a distinctly cyclonic looking feature. The comparative increase in wind speed over the inshore side of the meander coincides with where the meander's cyclonic nature and resulting instability would indicate the possibility of a slowing down in the current or even a weak northward flow. This means that a current direction which was in opposition to the wind direction and a resulting increase in wind speed due to the current relative effect postulated by Kelly et al. (2001). This suggests that, although the wind speed might have decreased over cooler water, the current relative effect could be overriding the effect on the inshore side where a net upcurrent flow is seen.

The evidence presented above is however not conclusive as there a few major caveats that must be considered when comparing the winds to the OSTIA data set. Because the OSTIA SSTs are an interpolated product from multiple assimilations of data, much of the small scale features and variation have been smoothed out in the process. Some of the features which are evident in the ASAR would not match up to those in the SST data, or even appear at all. The position of the Agulhas Meander and corresponding SST lows might also be skewed if smoothed. Secondly, the time difference between the datasets is an issue as ASAR has a collection process which is in the order of minutes per swath over the Agulhas Region and is, therefore, effectively a snapshot of the environmental conditions. It would therefore not match up to the OSTIA's daily mean.

Finally, the apparent increase in wind speed may well be as a result of a general increase in roughness of the ocean due to highly variable flow, as previously stated. Agulhas meanders are associated with major instabilities such as plumes and smaller frontal eddies

from conflicting flow directions and oscillations (Rouault and Penven, 2011). These features induce a roughness in the surface of the ocean which the ASAR sensor would detect (Johannessen et al., 2005). These roughness inducing features have not been fully investigated and, therefore may not be flagged during the wind speed derivation process. The evidence for this is however limited due to a lack of research.

Thus, due to the high level of uncertainty for each image, there is insufficient proof in the map plots in Figure 4.3 to suggest that either the relative influence of the current motion or the influence of SSTs which might be altering the ASAR derived wind speed. It is probable that both the change in SSTs along the current boundaries and the relative motion of the Agulhas Current in relation to the wind direction have a contributing effect on the derived wind speed to some degree but neither are singularly responsible.

# Chapter 6

# Conclusions

Satellite remotes sensing of wind fields has become an essential tool in the study of both global scale and high resolution wind research. This is especially true over the world's oceans where in situ measurements are too few and far between as a result of the difficulties in access and data collection. The data collected is not only invaluable in the study of wind dynamics and weather patterns as well as ocean-atmosphere interactions, it is also a source of assimilation data for numerical weather prediction models making it vital for industrial and civilian use. Synthetic Aperture Radar is one of the newest, most promising forms of wind measurement to date and has proven itself valuable on many occasions. Although not without its limitations, the benefits that can be had from the derivation of such high resolution wind fields are unmatched. A major caveat with satellite remote sensing in general, but especially with SAR due to its relatively recent development, is the need for validation of the derived products and the elimination of any errors that might occur as a result of the data collection process or the physical limitations of the satellites being so far away. There are still issues of error and inaccuracy in the data collection and wind derivation process of SAR which need to be addressed. Identification and elimination of these issues would help to produce a more accurate dataset which is compatible with other forms of wind speed measurement. A major issue that needs to be investigated is the influence that warm, strong western boundary currents such as the Agulhas Current have on the derived wind speed signature. The two primary effects investigated in this project are: The influence of the relative motion of the Agulhas current on the satellite detected, normalised radar cross section and the resulting derived wind speeds. Secondly, the influence of changing SST values on the overlying marine atmospheric boundary layer and the resulting wind speed changes.

At first assessment, these two influences appear to have the same effect on the derived wind speeds by causing changes in magnitude over the Agulhas, but due to the fact that they are governed by different physical properties, it is possible to differentiate between the

two influences and to, theoretically, quantify the effect that each influence has. Although previous research has shown separately that wind speed changes due to the current relative effect and changing SSTs do occur, there has been little to no research as yet of the combined effects over a narrow, intense and warm current such as the Agulhas using as high resolution data as from ASAR.

**Differences between ASAR Derived Wind Speeds and CFS and Scatterometry Data** The mean speed and direction distribution of the ASAR for 6 locations of interest over the Agulhas Current were compared to ASCAT and CFS data for the same location. Both the CFS and ASCAT dataset showed a strong polarity in the wind direction with winds aligned along a northeast-southwest axis, in agreement with the prevalent wind directions along the East Coast of South Africa and over the Agulhas. Thus the CFS data was deemed a suitable wind direction input in the derived ASAR dataset. ASAR derived wind speed exhibited an improved ability to record greater wind speeds in comparison to ASCAT and CFS wind speed in the alongcurrent wind events. This manifested in a greater frequency of high intensity wind events with a 5% increase in wind speed above $18m/s$ and a $2-3\%$ increase in wind speeds between $15-18m/s$. This increase is mostly attributed to ASAR's ability to resolve the higher resolution wind speed changes and thus retain data which would otherwise be lost to smoothing and interpolation. Surprisingly, no bias in wind speed increase towards the upcurrent regime was found, as was expected due to the current relative effect (Kelly et al., 2001). Instead the ASAR exhibited an even distribution of wind intensities between the upcurrent and downcurrent regimes.

**Identification of Different Influencing Factors on ASAR Derived Wind Fields** The research presented in this manuscript revealed that wind speed increases over the Agulhas Current in both the upcurrent and downcurrent direction regimes. This is a surprising result as previous studies have theorised that a wind travelling in a downcurrent direction should theoretically present a decreased wind speed due to the current relative effect (Kelly et al., 2001, 2005; Plagge et al., 2012). The current relative wind speed effect, as postulated by Kelly et al. (2001, 2005) and Plagge et al. (2012), does indeed affect the wind speeds over the Agulhas Current significantly for the upcurrent direction regime. In an upcurrent wind regime, winds speeds generally increased by between 50% and 100% over the current. These increases are over double those found by Plagge et al. (2012) but more similar to those reported by Kelly et al. (2005) who reported wind speed changes of up to 50%. It was also found that the greatest wind speed increase was not located directly over the core of the Agulhas Current, as thought, but on the inshore boundary of the current where the SST and

current speed gradients are steepest.

The current-relative wind effect is not the only effect causing the derived wind speed to increase over the current. A surprising increase in downcurrent wind speeds over the current of up to 40% (instead of the previously suggested decrease), as well as increases in upcurrent wind speeds as far as 100$km$ away from the current core, suggests that there are other derived wind speed modification factors at play. Wind speed and SST displayed similar modulations along the transects. For certain moderate wind events, it was also possible to collocate wind speed changes with the contours of oceanographic isotherms across the surface of the current, thus enabling mesoscale ocean phenomena such as Agulhas Meanders to be identified. The downcurrent wind speed increase is the strongest evidence of SST induced wind changes. The increase suggests that if the relative motion of the current is inducing a decrease in wind speeds, the effect is being overridden by the SST influences. The same argument can be made for the upcurrent regime where the SST influences and the relative current effect are compounding and generating greater wind speed increases greater than previously reported. This means that SST induced wind speed changes are a stronger influence than the current relative effect.

Interestingly, little evidence of SST induced wind speed changes were found in the crosscurrent wind data. This is surprising as it was expected that SST induced changes would have a greater if not the same effect on crosscurrent wind speeds due to the change in properties of the marine boundary layer as it flows over the current. However, it is difficult to draw conclusions based on results in a crosscurrent wind regime due to the limited number of observations available. A localized and strong wind speed increase was observed at the inshore front of the Agulhas Current, in the region of strongest SST gradient. This increase can not be due to SST because wind would adjust over much greater spatial scales than just in this narrow region. The increase of the wind at the AC front also can not be attributed to increases in current since the current maxima is located further offshore from the region of maximum SST gradient. The observed spike in the wind speed is therefore most likely as a result of surface roughness modulation through local modification of wave spectra by processes such as horizontal shear or divergence similarly to what has been reported by Rascle et al. (2014)

**The Effect of Event Intensity on Wind Speed Increase** The effect of the Agulhas Current on the satellite-derived wind speeds is found to be strongly dependent on the velocity of the initial wind event. The greatest effect is observed in moderate wind speeds, between $5-10m/s$ and $10-15m/s$, where the influence of the current drive a distinct increase in wind speeds. In the upcurrent regime, characteristic sharp peaks in wind speeds are ob-

served. Similarly in the downcurrent regime, the dome-like structure in the wind speeds clearly emerges. For wind intensities in the $5m/s$ to $15m/s$ range, wind speed differences over the Agulhas Current appear to be more affected by the structure of the current and the underlying SSTs. In stronger winds ( greater than $15m/s$), the influence of the current is difficult to determine due to the shear intensity of the winds which mask any signatures associated with the current relative effects or the influence of SSTs. Low radar backscatter in a weak wind regime ( below $5m/s$) prevent the identification of any Agulhas Current impact on the overlying winds. At speeds lower than $2-3m/s$, the CMOD5.n GMF is considered invalid as wind speeds at these magnitudes do not generate surface waves large enough for the ASAR sensor to detect.

**Caveats and Research Issues** The most important caveat to consider when assessing the wind speeds derived from Synthetic Aperture Radars, is the fact that to date there are no other wind datasets of equal resolution. Thus during the wind derivation process with the CMOD5.n GMF, a lower resolution model output which has been interpolated to a higher resolution had to be used. Errors in wind direction due to the model dynamics as well as the interpolation process might induce a secondary error in the wind speeds derived. Small scale, sharp wind direction changes which the model would not resolve, but the ASAR would, will result in an incorrect wind speed derivation. This problem is difficult to solve due to the lack of high resolution wind measurements and the limitation of currently available numerical models needed for processing and validation.

The CMOD5.n derivation model has, in itself an caveat for its use. As suggested in sections 2.2.2 and 3.1.2, the model is empirically derived using a statistical equilibrium between measured, in situ wind and wave data. Thus the CMOD5.n model itself may contain an inherent relative wind error which may skew the results. As mentioned in section 3.1.2, the model is also only valid between $2m/s$ and $35m/s$ do to a minimum return signal threshold required in order to gain a reading. This can be seen in the lover wind speed events in section 4.4.

Differences in spatial resolution between the dataset used in this study also introduce some complexity to the analysis of the results. The MODIS SST climatology, SEVIRI daily averaged SST, OSTIA SST products and the Globcurrent ocean velocities are all interpolated to some degree due to missing data in one form or another and have lower spatial resolution than ASAR dataset. Inadequate representation of the SST and current velocity fields make it hard to derive quantitative relationships between ocean temperature, current velocities and wind speeds. For example, the relative wind effect could not be accurately determined due to the lack of sufficiently high resolution ocean current velocities for the case

studies and an overall lack of data for the mean winds. The Globcurrent data product used is currently in development, and more data should be available in the years to come, and we expect that this could lead to better estimates of the mean relative wind speed effect. The quantifiable difference between the wind speeds and SST data could also not be established due to the difficulty in separating the wind speed increases as a result of the SST changes and other wind speed influences. SST changes are not the only influence on the near surface wind speed and direction. Further research needs to be conducted into identifying the exact wind speed changes due to the sole influence of SST changes.

**Implications of Findings** We hope that the results of this research help improve satellite derived wind observations of the ocean surface by highlighting the importance that strong boundary currents such as the Agulhas have on satellite wind products as well as increasing our understanding of SST driven changes on near surface wind speeds over the ocean. This study also further emphasises the limitation associated with routinely used scatterometers wind datasets which cannot resolve many of the small scale wind patterns and features. This inability to resolve these small scale wind patterns results in a large underestimation of wind speeds in areas of high wind variability. Thus, SAR derived wind speeds would be vital in supplementing scatterometer wind measurements and being assimilated into numerical weather prediction models. This would serve to improve the understanding of wind and weather patterns. As both SAR and it's product derivation processes develop over time, greater accuracy and understanding of the mechanics and physical processes involved in it's utilisation will lead to better and more accurate data collection across the board.

**Scope for Future Research and Development** It is at present challenging to separate the relative contributions of the ocean current and air-sea interaction processes to the wind speed increases over the Agulhas Current. Improved ocean currents products would certainly assist in this endeavour by allowing a better quantification of the ocean current speed contribution. Further research is still necessary to better understand the influence of sharp SST changes on near surface wind speed and the overlying marine atmospheric boundary layer. This would lead to these effects being eventually catered for in GMFs used for the wind speed derivation process. Two improvements that would be absolutely necessary for this to occur would be: The utilisation of higher resolution model data as a direction input in the wind speed derivation process. The low resolution model data used in this investigation had to be interpolated to a higher resolution which would have inevitably led to inaccuracies in the derived data. Especially in areas of small-scale variability and sharp gradients of change. Higher resolution model data would also enable a more thorough ap-

proach to be take in the investigation of the wind speed transects. The model and ASAR derived wind speed could be subtracted from each other in order to identify the differences between the two. The numerical model should theoretically not contain any signature of the relative wind effect. This is due to the fact that the wind speeds in the model are considered the true wind speed and not the wind speed relative to the motion of the ocean. Secondly the use of high resolution ocean current velocity data in order to complete a true vector sum of current-wind differences would help enable the quantification of the current-relative wind speed changes. Producing quantifiable differences would pave the way to the development of numerical predictions of wind speed changes for given wind and ocean current velocities and thus enable the neutralisation of the errors. Adding high resolution, more accurate SST data into ocean-atmosphere coupled numerical models (Such as the CFS model) or as a boundary condition for atmospheric models is also highly necessary, in order to cater for the influence that the underlying ocean has on the wind speeds above it. The addition of in situ wind speed measurements as a form of validation of the ASAR wind speed data is also a necessary undertaking. Although ideally in situ data of as high a resolution would be best, even eularian point measurements of the conditions over the Agulhas versus offshore conditions would serve to help validate that the wind speeds and directions derived from the ASAR data are correct for those specific locations.

# References


Lisa M Beal, Wilhelmus P M De Ruijter, Arne Biastoch, and Rainer Zahn.

Lisa M. Beal, Shane Elipot, Adam Houk, and Greta M. Leber. Capturing the Transport Variability of a Western Boundary Jet: Results from the Agulhas Current Time-Series Experiment (ACT). *Journal of Physical Oceanography*, 45(5):1302–1324, feb 2015. ISSN 0022-3670. doi: 10.1175/JPO-D-14-0119.1.

Abderrahim Bentamy and Denis Croize Fillon. Gridded surface wind fields from Metop/ASCAT measurements. *International Journal of Remote Sensing*, 33(6):1729–1754, 2012. ISSN 0143-1161. doi: 10.1080/01431161.2011.600348.

M a Bourassa, H Bonekamp, P Chang, D B Chelton, J Courtney, R Edson, J Figa, Y He, H Hersbach, K Hilburn, T Lee, W T Liu, D Long, K Kelly, R Knabb, E Lindstorm, W Perrie, M Portabella, M Powell, E Rodriguez, D Smith, a Stoffelen, V Swail, and F Wentz. Remotely sensed winds and wind stresses for marine forecasting and ocean modeling. *Proceedings of the OceanObs 09: Sustained Ocean Observations and Information for Society Conference*, 2(ESA Publication WPP-306. doi:10.5270/OceanObs09.cwp.08), 2010. doi: 10.5270/OceanObs09.cwp.08.

Harry L. Bryden, Lisa M. Beal, and Louise M. Duncan. Structure and transport of the Agulhas current and its temporal variability. *Journal of Oceanography*, 61(3):479–492, 2005. ISSN 09168370. doi: 10.1007/s10872-005-0057-8.

Tânia G D Cásal, Lisa M. Beal, Rick Lumpkin, and William E. Johns. Structure and downstream evolution of the Agulhas Current system during a quasi-synoptic survey in February-March 2003. *Journal of Geophysical Research: Oceans*, 114(3), 2009. ISSN 21699291. doi: 10.1029/2008JC004954.

Yee Kit Chan and Voon Chet Koo. an Introduction To Synthetic Aperture Radar (Sar). *Progress In Electromagnetics Research B*, 2:27–60, 2008. ISSN 19376472. doi: 10.2528/PIERB07110101.

Dudley Chelton and Shang-Ping Xie. Coupled Ocean-Atmosphere Interaction at Oceanic Mesoscales. *Oceanography*, 23(4):52–69, 2010. ISSN 10428275. doi: 10.5670/oceanog.2010.05.

Dudley B Chelton, Steven K Esbensen, Michael G Schlax, Nicolai Thum, Michael H Freilich, Frank J Wentz, Chelle L Gentemann, Michael J McPhaden, and Paul S Schopf. Observations of coupling between surface wind stress and sea surface temperature in the eastern tropical pacific. *Journal of Climate*, 14(7):1479–1498, 2001.

Dudley B Chelton, Michael G Schlax, Michael H Freilich, and Ralph F Milliff. Satellite measurements reveal persistent small-scale features in ocean winds. *Science (New York, N.Y.)*, 303(5660):978–983, 2004. ISSN 0036-8075. doi: 10.1126/science.1091901.

Fabrice Collard, Alexis Mouche, Bertrand Chapron, Johnny Johannessen, et al. Routine high resolution observation of selected major surface currents from space. 2008.

Knut-frode Dagestad, Jochen Horstmann, Alexis Mouche, William Perrie, and Hui Shen. Wind Retrieval From Synthetic Aperture Radar, an Overview. *Seasar 2012 Oceanography Workshop*, 4th, 2013.

R Danielson, J Johannessen, and C Donlon. GlobCurrent USER REQUIREMENTS DOCUMENT. Technical Report December 2014, 2014.

Wilhelmus P. M. de Ruijter, Peter Jan van Leeuwen, and Johann R. E. Lutjeharms. Generation and Evolution of Natal Pulses: Solitary Meanders in the Agulhas Current, 1999. ISSN 0022-3670.

Wilhelmus P M de Ruijter, Herman Ridderinkhof, and Mathijs W Schouten. Variability of the southwest Indian Ocean. *Philosophical transactions. Series A, Mathematical, physical, and engineering sciences*, 363(1826):63–76, 2005. ISSN 1364-503X. doi: 10.1098/rsta.2004.1478.

Y L Desnos, C Buck, J Guijarro, J L Suchail, R Torres, and E Attema. ASAR - Envisat's Advanced Synthetic Aperture Radar - Building on ERS achievements towards future earth watch missions. *ESA Bulletin*, (102):91–100, 2000.

Penny Driver. *Rainfall Variability over Southern Africa*. Phd, University of Cape Town, 2014.

François Dufois, Pierrick Penven, Christo Peter Whittle, and Jennifer Veitch. On the warm nearshore bias in Pathfinder monthly SST products over Eastern Boundary Upwelling

Systems. *Ocean Modelling*, 47:113–118, 2012. ISSN 14635003. doi: 10.1016/j.ocemod.2012.01.007.

Esa. European Space Agency - EnviSat ASAR Product Handbook. page 564, 2007.

Eumetsat. ASCAT Product Guide. *ASCAT Products Overview*, (v5):164, 2015. doi: EUM/OPS-EPS/MAN/04/0028.

Peter Falcon and Cornell Lewis. RapidScat, a.

Peter Falcon and Cornell Lewis. About Scatterometry, b.

Florence Fetterer, Denise Gineris, and Christopher C. Wackerman. Validating a scatterometer wind algorithm for ERS-1 SAR. *IEEE Transactions on Geoscience and Remote Sensing*, 36(2):479–492, 1998. ISSN 01962892. doi: 10.1109/36.662731.

Amy Ffield, John Toole, and Doug Wilson. Seasonal circulation in the south Indian Ocean. *Geophysical Research Letters*, 24(22):2773, 1997. ISSN 0094-8276. doi: 10.1029/97GL01253.

J. Figa-Saldaña, J. J W Wilson, E. Attema, R. Gelsthorpe, M. R. Drinkwater, and a. Stoffelen. The advanced scatterometer (ASCAT) on the meteorological operational (MetOp) platform: A follow on for European wind scatterometers. *Canadian Journal of Remote Sensing*, 28(3):404–412, 2002. ISSN 07038992. doi: 10.5589/m02-035.

T. W. Gerling. Structure of the surface wind field from the Seasat SAR. *Journal of Geophysical Research*, 91(C2):2308, 1986. ISSN 0148-0227. doi: 10.1029/JC091iC02p02308.

Arnold L. Gordon. Inter-ocean exchange of thermocline water. *Journal of Geophysical Research C: Oceans*, 91(C4):5037–5046, 1986. ISSN 0148-0227. doi: 10.1029/JC091iC04p05037.

M L Grundlingh and J L Largier. Physical oceanography of False Bay: a review. *Royal Society of South Africa. Transactions TRSAAC,*, 47(4/5), 1991.

Marten L. Gründlingh. On the Course of the Agulhas Current. *South African Geographical Journal*, 65(1):49–57, 1983. ISSN 0373-6245. doi: 10.1080/03736245.1983.10559671.

C Hall and J R E Lutjeharms.

Morten W. Hansen. Sea Surface Range Doppler Velocity Retrievals from Synthetic Aperture Radar. *Ph.D. Thesis in Physical Oceanography*, (August), 2011.

H Hersbach, A Stoffelen, and S De Haan. An improved Cband scatterometer ocean geophysical model function: CMOD5. *Journal of Geophysical Research: Oceans (1978 2012)*, 112(C3), 2007.

Hans Hersbach. *CMOD5. N: A C-band geophysical model function for equivalent neutral wind*. Number April. European Centre for Medium-Range Weather Forecasts, 2008.

Hans Hersbach. Comparison of C-Band scatterometer CMOD5.N equivalent neutral winds with ECMWF. *Journal of Atmospheric and Oceanic Technology*, 27(4):721–736, 2010. ISSN 07390572. doi: 10.1175/2009JTECHO698.1.

Hans Hersbach, a Stoffelen, and S De Haan. CMOD5: An improved geophysical model function for ERS C-band scatterometry. *Ecmwf*, (January):1–52, 2003.

Benjamin Holt. Chapter 2 . SAR Imaging of the Ocean Surface. *Synthetic Aperture Radar Marine Users Manual (NOAA)*, pages 25–79, 2004.

J. HORSTMANN, W. KOCH, W. ROSENTHAL, and S. LEHNER. Wind fields from ERS SAR, compared with a mesoscale atmospheric model near to the coast. *ESA SP*, pages 1205–1209, 2014. ISSN 0379-6566.

Ian T Hunter. Climate and weather off Natal. *Coastal Ocean Studies off Natal, South Africa*, pages 81–100, 1988.

Johnny a. Johannessen, Vladimir Kudryavtsev, Dmitry Akimov, T. Eldevik, N. Winther, and Bertrand Chapron. On radar imaging of current features: 2. Mesoscale eddy and current front detection. *Journal of Geophysical Research C: Oceans*, 110(7):1–14, 2005. ISSN 01480227. doi: 10.1029/2004JC002802.

Johnny A Johannessen, Bertrand Chapron, Fabrice Collard, Vladimir Kudryavtsev, Alexis Mouche, D Akimov, and K-F Dagestad. Direct ocean surface velocity measurements from space: Improved quantitative interpretation of envisat asar observations. *Geophysical Research Letters*, 35(22), 2008.

M. R. Jury and S. Courtney. A transition in weather over the Agulhas Current. *South African Journal of Marine Science*, 10(1):159–171, 1991. ISSN 0257-7615. doi: 10.2989/02577619109504629.

Mark R. Jury, Henry R. Valentine, and Johann R. E. Lutjeharms. Influence of the Agulhas Current on Summer Rainfall along the Southeast Coast of South Africa, 1993. ISSN 0894-8763.

Kathryn A Kelly, Suzanne Dickinson, Michael J McPhaden, and Gregory C Johnson. Ocean currents evident in satellite wind data. *Geophysical Research Letters*, 28(12):2469–2472, 2001.

Kathryn a. Kelly, Suzanne Dickinson, and Gregory C. Johnson. Comparisons of scatterometer and TAO winds reveal time-varying surface currents for the Tropical Pacific Ocean. *Journal of Atmospheric and Oceanic Technology*, 22(6):735–745, 2005. ISSN 07390572. doi: 10.1175/JTECH1738.1.

Robert Kistler, William Collins, Suranjana Saha, Glenn White, John Woollen, Eugenia Kalnay, Muthuvel Chelliah, Wesley Ebisuzaki, Masao Kanamitsu, Vernon Kousky, Huug van den Dool, Roy Jenne, and Michael Fiorino. The NCEP-NCAR 50-Year Reanalysis: Monthly Means CD-ROM and Documentation. *Bulletin of the American Meteorological Society*, 82(2):247–267, feb 2001. ISSN 0003-0007. doi: 10.1175/1520-0477(2001)082<0247:TNNYRM>2.3.CO;2.

Randall Knight, Brian Jones, and Stuart Field. *College Physics : A Strategic Approach*. Pearson, Boston, 3rd edition, 2015. ISBN 9781292057156.

Marjolaine Krug, Cipollini Paolo, and Dufois Francois. *Remote Sensing of the African Seas*. Springer, illustrate edition, 2014. ISBN 9789401780087.

V. Kudryavtsev. On radar imaging of current features: 1. Model and comparison with observations. *Journal of Geophysical Research*, 110(C7):1–27, 2005. ISSN 0148-0227. doi: 10.1029/2004JC002505.

A M Lee-Thorp, M Rouault, and J R E Lutjeharms. Cumulus cloud formation above the Agulhas Current. *South African Journal of Science*, 94(7):351–354, 1998.

W Timothy Liu. Progress in scatterometer application. *Journal of Oceanography*, 58(1):121–136, 2002.

David G Long, Mark R Drinkwater, Benjamin Holt, Sasan Saatchi, and Cheryl Bertoia. Global ice and land climate studies using scatterometer image data. *EOS Transactions Electronic Supplement, American Geophysical Union*, 82(43):503, 2001. ISSN 2324-9250. doi: 10.1029/01EO00303.

J. R. E. Lutjeharms. Three decades of research on the greater Agulhas Current, 2006a. ISSN 1812-0792.

J. R E Lutjeharms and J. Cooper. Interbasin leakage through Agulhas current filaments. *Deep-Sea Research Part I: Oceanographic Research Papers*, 43(2):213–238, 1996. ISSN 09670637. doi: 10.1016/0967-0637(96)00002-7.

J. R. E. Lutjeharms and R. C. Van Ballegooyen. The Retroflection of the Agulhas Current. *Journal of Physical Oceanography*, 18(11):1570–1583, 1988. ISSN 0022-3670. doi: 10.1175/1520-0485(1988)018<1570:TROTAC>2.0.CO;2.

Johann R. E. Lutjeharms. *The Agulhas Current*. Springer-Verlag, Wurzburg, Germany, 1st edition, 2006b. ISBN 10 3-540-42392-3.

Lijuan Ma, Tingjun Zhang, Qingxiang Li, Oliver W. Frauenfeld, and Dahe Qin. Evaluation of era-40, ncep-1, and ncep-2 reanalysis air temperatures with ground-based measurements in china. *Journal of Geophysical Research: Atmospheres*, 113(D15):n/a–n/a, 2008. ISSN 2156-2202. doi: 10.1029/2007JD009549. D15115.

Matthew Martin, Emma Fiedler, Jonah Roberts-Jones, Ed Blockley, and Alison Mclaren. For OSTIA Near Real Time Level 4 SST products over the global ocean. Technical Report 3.4, 2015.

S.J. Mason and M.R. Jury. Climatic variability and change over southern Africa: a reflection on underlying processes. *Progress in Physical Geography*, 21(1):23–50, 1997. ISSN 0309-1333. doi: 10.1177/030913339702100103.

R. P. Matano, E. J. Beier, P. T. Strub, and R. Tokmakian. Large-Scale Forcing of the Agulhas Variability: The Seasonal Cycle, 2002. ISSN 0022-3670.

Samuel W Walt Mccandless and Christopher R Jackson. Chapter 1 . Principles of Synthetic Aperture Radar. pages 1–23, 2004.

Rosemary D. Mey, Nan D. Walker, and Mark R. Jury. Surface heat fluxes and marine boundary layer modification in the Agulhas Retroflection region. *Journal of Geophysical Research*, 95(C9):15997, 1990. ISSN 0148-0227. doi: 10.1029/JC095iC09p15997.

Frank M Monaldo and Robert Beal. Chapter 13 . Wind Speed and Direction. pages 305–320, 2004.

Ocean Biology Processing Group NASA Goddard Space Flight Center, Ocean Ecology Laboratory.

NERSC, Ifremer, CLS, IsardSAT, PML, Oceandatalab, and University of Exeter. Globcurrent, 2013.

Larry W O'Neill, Dudley B Chelton, and Steven K Esbensen. Observations of sst-induced perturbations of the wind stress field over the southern ocean on seasonal timescales. *Surface Wind Modification Near Mid-Latitude Ocean Fronts: Observational and Dynamical Analysis*, page 9, 2003.

Larry W. O'Neill, Dudley B. Chelton, Steven K. Esbensen, and Frank J. Wentz. High-resolution satellite measurements of the atmospheric boundary layer response to SST variations along the Agulhas Return Current. *Journal of Climate*, 18(14):2706–2723, 2005. ISSN 08948755. doi: 10.1175/JCLI3415.1.

Kyung Ae Park, Peter Cornillon, and Daniel L. Codiga. Modification of surface winds near ocean fronts: Effects of Gulf Stream rings on scatterometer (QuikSCAT, NSCAT) wind observations. *Journal of Geophysical Research: Oceans*, 111(3):1–19, 2006. ISSN 21699291. doi: 10.1029/2005JC003016.

Amanda M. Plagge, Douglas Vandemark, and Bertrand Chapron. Examining the impact of surface currents on satellite scatterometer and altimeter ocean winds. *Journal of Atmospheric and Oceanic Technology*, 29(12):1776–1793, 2012. ISSN 07390572. doi: 10.1175/JTECH-D-12-00017.1.

Marcos Portabella and Ad Stoffelen. Scatterometer backscatter uncertainty due to wind variability. *Geoscience and Remote Sensing, IEEE Transactions on*, 44(11):3356–3362, 2006.

Nicolas Rascle, Bertrand Chapron, Aurélien Ponte, Fabrice Ardhuin, and Patrice Klein. Surface roughness imaging of currents shows divergence and strain in the wind direction. *Journal of Physical Oceanography*, 44(8):10, 2014. ISSN 0022-3670. doi: 10.1175/JPO-D-13-0278.1.

Craig M. Risien and Dudley B. Chelton. A Global Climatology of Surface Wind and Wind Stress Fields from Eight Years of QuikSCAT Scatterometer Data. *Journal of Physical Oceanography*, 38(11):2379–2413, 2008. ISSN 0022-3670. doi: 10.1175/2008JPO3881.1.

M. Rouault, a. M. Lee-Thorp, and J. R. E. Lutjeharms. The Atmospheric Boundary Layer above the Agulhas Current during Alongcurrent Winds. *Journal of Physical Oceanography*, 30(1):40–50, 2000. ISSN 0022-3670. doi: 10.1175/1520-0485(2000)030<0040:TABLAT>2.0.CO;2.

M. J. Rouault and Pierrick Penven. New perspectives on Natal Pulses from satellite observations. *Journal of Geophysical Research: Oceans (1978 2012)*, 116(C7):1–14, 2011. ISSN 21699291. doi: 10.1029/2010JC006866.

M. J. Rouault, a. Mouche, F. Collard, J. a. Johannessen, and B. Chapron. Mapping the Agulhas Current from space: An assessment of ASAR surface current velocities. *Journal of Geophysical Research: Oceans*, 115(10):1–14, 2010. ISSN 21699291. doi: 10.1029/2009JC006050.

Marjolaine Rouault. *Agulhas Current variability determined from space: a multi-sensor approach.* PhD thesis, University of Cape Town, 2011.

Sea Ice Saf. Algorithm Theoretical Basis Document for the OSI SAF wind products. (August):1–18, 2012.

Suranjana Saha. Documentation of the Hourly Time Series from the NCEP Climate Forecast System Reanalysis (1979-2009). pages 1–7, 2009.

Suranjana Saha, Shrinivas Moorthi, Hua Lu Pan, Xingren Wu, Jiande Wang, Sudhir Nadiga, Patrick Tripp, Robert Kistler, John Woollen, David Behringer, Haixia Liu, Diane Stokes, Robert Grumbine, George Gayno, Jun Wang, Yu Tai Hou, Hui Ya Chuang, Hann Ming H Juang, Joe Sela, Mark Iredell, Russ Treadon, Daryl Kleist, Paul Van Delst, Dennis Keyser, John Derber, Michael Ek, Jesse Meng, Helin Wei, Rongqian Yang, Stephen Lord, Huug Van Den Dool, Arun Kumar, Wanqiu Wang, Craig Long, Muthuvel Chelliah, Yan Xue, Boyin Huang, Jae Kyung Schemm, Wesley Ebisuzaki, Roger Lin, Pingping Xie, Mingyue Chen, Shuntai Zhou, Wayne Higgins, Cheng Zhi Zou, Quanhua Liu, Yong Chen, Yong Han, Lidia Cucurull, Richard W. Reynolds, Glenn Rutledge, and Mitch Goldberg. The NCEP climate forecast system reanalysis. *Bulletin of the American Meteorological Society*, 91(8):1015–1057, 2010. ISSN 00030007. doi: 10.1175/2010BAMS3001.1.

Suranjana Saha, Shrinivas Moorthi, Xingren Wu, Jiande Wang, Sudhir Nadiga, Patrick Tripp, David Behringer, Yu-Tai Hou, Hui-ya Chuang, Mark Iredell, Michael Ek, Jesse Meng, Rongqian Yang, Malaquías Peña Mendez, Huug van den Dool, Qin Zhang, Wanqiu Wang, Mingyue Chen, and Emily Becker. The NCEP Climate Forecast System Version 2. *Journal of Climate*, 27(6):2185–2208, 2014. ISSN 0894-8755. doi: 10.1175/JCLI-D-12-00823.1.

Mathijs W Schouten, Wilhelmus P M De Ruijter, and Peter Jan Van Leeuwen. Upstream control of Agulhas Ring shedding. 107(August), 2002.

Albertus J. Smit, Michael Roberts, Robert J. Anderson, Francois Dufois, Sheldon F. J. Dudley, Thomas G. Bornman, Jennifer Olbers, and John J. Bolton. A Coastal Seawater Temperature Dataset for Biogeographical Studies: Large Biases between In Situ and Remotely-Sensed Data Sets around the Coast of South Africa. *PLoS ONE*, 8(12):e81944, 2013. ISSN 1932-6203. doi: 10.1371/journal.pone.0081944.

S Speich, J R E Lutjeharms, P Penven, and B Blanke. Role of bathymetry in Agulhas Current configuration and behaviour. 33(December):2–6, 2006. doi: 10.1029/2006GL027157.

Robert H Stewart. Introduction to Physical Oceanography. *American Journal of Physics*, 65(10):1028, 1997. ISSN 00029505. doi: 10.1119/1.18716.

A Stoffelen and D L T Anderson. Wind retrieval and ERS-1 scatterometer radar backscatter measurements. *Advances in Space Research*, 13(5):53–60, 1993.

Ad Stoffelen and David Anderson. Scatterometer data interpretation: Estimation and validation of the transfer function CMOD4. *Journal of Geophysical Research*, 102(C3):5767, 1997. ISSN 0148-0227. doi: 10.1029/96JC02860.

Liba Taub. *Ancient Meteorolgy*. Routledge, 2004.

Kiyo Tomiyasu. Tutorial Review of Synthetic-Aperture Radar (Sar) With Applications To Imaging of the Ocean Surface. *Proceedings of the IEEE*, 66(5):563–583, 1978. ISSN 00189219. doi: 10.1109/PROC.1978.10961.

P W Vachon and F W Dobson. Validation of wind vector retrieval from ERS-1 SAR images over the ocean. *The Global Atmosphere and Ocean System*, 5(2):177–187, 1996.

P. C. F. van der Vaart and W. P. M. de Ruijter. Stability of Western Boundary Currents with an Application to Pulselike Behavior of the Agulhas Current, 2001. ISSN 0022-3670.

John van Heerden and J J Taljaard. Africa and surrounding waters. In *Meteorology of the Southern Hemisphere*, pages 141–174. Springer, 1998.

Gabriel A Vecchi, Shang-Ping Xie, and Albert S Fischer. Ocean-atmosphere covariability in the western arabian sea*. *Journal of climate*, 17(6):1213–1224, 2004.

Christopher C. Wackerman, Clifford L. Rufenach, Robert a. Shuchman, Johnny a. Johannessen, and Kenneth L. Davidson. Wind vector retrieval using ERS-1 synthetic aperture radar imagery. *IEEE Transactions on Geoscience and Remote Sensing*, 34(6):1343–1352, 1996. ISSN 01962892. doi: 10.1109/36.544558.

Frank J Wentz, Chelle Gentemann, Deborah Smith, and Dudley Chelton. Satellite measurements of sea surface temperature through clouds. *Science*, 288(5467):847–850, 2000.

Warren B White and Jeffrey L Annis. Coupling of extratropical mesoscale eddies in the ocean to westerly winds in the atmospheric boundary layer. *Journal of physical oceanography*, 33(5):1095–1107, 2003.

J Wright. Backscattering from capillary waves with application to sea clutter. *Antennas and Propagation, IEEE Transactions on*, 14(6):749–754, 1966. ISSN 0018-926X. doi: 10.1109/TAP.1966.1138799.

Shang-Ping Xie. Satellite Observations of Cool Ocean-Atmosphere Interaction. *Bulletin of the American Meteorological Society*, 85(2):195–208, 2004. ISSN 0003-0007. doi: 10.1175/BAMS-85-2-195.

Shang-Ping Xie, Masaki Ishiwatari, Hiroshi Hashizume, and Kensuke Takeuchi. Coupled ocean-atmospheric waves on the equatorial front. *Geophysical Research Letters*, 25(20): 3863–3866, 1998.

Shang-Ping Xie, W Timothy Liu, Qinyu Liu, and Masami Nonaka. Far-reaching effects of the hawaiian islands on the pacific ocean-atmosphere system. *Science*, 292(5524): 2057–2060, 2001.

Tao Xie, William Perrie, Wei Chen, Tao Xie, William Perrie, and Wei Chen. Gulf Stream thermal fronts detected by synthetic aperture radar. *Geophysical Research Letters*, 37(6): 2426–2427, 2010. ISSN 00948276. doi: 10.1109/IGARSS.2010.5651914.

# Appendix A

# Please see attached files for appendices

The Files can be found at this web address:
https://drive.google.com/folderview?id=0B4e4Z1OXWB0GRENoWWlZbndmSGc&usp=sharing